# Advanced Engineering Research

Theoretical and scientific-practical journal

Vol. 21
no. 4
2021

ISSN 2687-1653

1 Mechanics

2 Machine Building and Machine Science

3 Information Technology, Computer Science, and Management

DOI 10.23947/2687-1653

vestnik-donstu.ru

**Advanced Engineering Research**

**Vol. 21, no. 4**

**Theoretical and scientific-practical journal**

Published since 1999

Quarterly
October-December 2021

**ISSN 2687-1653**
**DOI: 10.23947/2687-1653**

***Founder and publisher – Federal State Budgetary Educational Institution of Higher Education Don State Technical University (DSTU)***

***The journal was known as Vestnik of Don State Technical University (until August 2020)***

***Included in the list of peer-reviewed scientific editions where the basic research results of doctoral, candidate's theses should be published (State Commission for Academic Degrees and Titles List) in the following research areas:***

*01.02.01 – Analytical Mechanics (Engineering Sciences)*
*01.02.04 –Deformable Solid Mechanics (Engineering Sciences)*
*01.02.04 –Deformable Solid Mechanics (Physicomathematical Sciences)*
*01.02.06 – Dynamics, Strength of Machines, Gear, and Equipment (Engineering Sciences)*
*05.02.02 – Engineering Science, Drive Systems and Machine Parts (Engineering Sciences)*
*05.02.04 –Machine Friction and Wrear (Engineering Sciences)*
*05.02.07 – Technology and Equipment of Mechanical and Physicotechnical Processing (Engineering Sciences)*
*05.02.08 – Engineering Technology (Engineering Sciences)*
*05.02.10 –Welding, Allied Processes and Technologies (Engineering Sciences)*
*05.02.11 – Testing Methods and Diagnosis in Machine Building (Engineering Sciences)*
*05.13.11 – Software and Mathematical Support of Machines, Complexes and Computer Networks (Engineering Sciences)*
*05.13.17 – Foundations of Information Science (Engineering Sciences)*
*05.13.18 –Mathematical Simulation, Numerical Methods and Program Systems (Engineering Sciences)*

***The journal is indexed and archived in the Russian Science Citation Index (RSCI), in the International Database EBSCO (Academic Search Ultimate Magazines and Journals), Dimensions, CyberLeninka, ROAD, GoogleScholar. The journal is a member of Directory of Open Access Journals (DOAJ), Association of Science Editors and Publishers (ASEP) and CrossRef.***

*Certificate of mass media registration ЭЛ № ФС 77 – 78854 of 07.08.2020 is issued by the Federal Service for Supervision of Communications, Information Technology, and Mass Media*

***The issue is prepared by:***

Inna V. Boyko, Gennady I. Rassokhin, Marina P. Smirnova (English version)

***Founder's, Publisher's and Printery Address:***

Gagarin Sq. 1, Rostov-on-Don, 344003, Russia. Phone: +7 (863) 2-738-372

E-mail: vestnik@donstu.ru http://vestnik-donstu.ru/

The content is available under Creative Commons Attribution 4.0 License

© Don State Technical University, 2021

**Editorial Board**

***Editor-in-Chief — Besarion Ch. Meskhi,*** *Dr.Sci. (Eng.), professor, Don State Technical University (Russian Federation);*

*deputy chief editor — Valery P. Dimitrov, Dr.Sci. (Eng.), professor, Don State Technical University (Russian Federation);*
*executive editor — Manana G. Komakhidze, Cand.Sci. (Chemistry), Don State Technical University (Russian Federation);*
*executive secretary — Nadezhda A. Shevchenko, Don State Technical University (Russian Federation);*

**Evgeny V. Ageev**, Dr.Sci. (Eng.), professor, South-Western State University (Russian Federation);
**Sergey M. Aizikovich**, Dr.Sci. (Phys.-Math.), professor, Don State Technical University (Russian Federation);
**Kamil S. Akhverdiev**, Dr.Sci. (Eng.), professor, Rostov State Transport University (Russian Federation);
**Vladimir I. Andreev**, member of RAACS, Dr.Sci. (Eng.), professor, National Research Moscow State University of Civil Engineering (Russian Federation);
**Imad R. Antipas**, Cand.Sci. (Eng.), Don State Technical University (Russian Federation);
**Hubert Anysz,** PhD (Eng.), assistant professor, Warsaw University of Technology (Warsaw, Poland);
**Ahilan Appathurai,** national junior research fellow, Anna University Chennai (India);
**Gultekin Basmaci,** professor (Eng.), Mehmet Akif Ersoy Üniversity (Burdur, Turkey);
**Torsten Bertram**, Dr.Sci. (Eng.), professor, TU Dortmund University (Germany);
**Dmitry A. Bezuglov**, Dr.Sci. (Eng.), professor, Rostov branch of Russian Customs Academy (Russian Federation);
**Larisa V. Cherkesova**, Dr.Sci. (Phys. -Math.), professor, Don State Technical University (Russian Federation);
**Alexandr N. Chukarin**, Dr.Sci. (Eng.), professor, Rostov State Transport University (Russian Federation);
**Oleg V. Dvornikov**, Dr.Sci. (Eng.), professor, Belarusian State University (Belarus);
**Karen O. Egiazaryan**, Dr.Sci. (Eng.), professor, Tampere University of Technology (Tampere, Finland);
**Victor A. Eremeev**, Dr.Sci. (Phys.-Math.), professor, Southern Scientific Center of RAS (Russian Federation);
**Mikhail B. Flek**, Dr.Sci. (Eng.), professor, "Rostvertol" JSC (Russian Federation);
**Nikolay E. Galushkin**, Dr.Sci. (Eng.), professor, Institute of Service and Business (DSTU branch) (Russian Federation);
**LaRoux K. Gillespie**, Dr.Sci. (Eng.), professor, President-elect of the Society of Manufacturing Engineers (USA);
**Ali M. Hasan,** PhD (Computer Engineering), Al Nahrain University (Baghdad, Iraq);
**Hamid A. Jalab,** PhD (Computer Science & IT), University of Malaya (Kuala Lumpur, Malaysia);
**Anatoly A. Korotkii**, Dr.Sci. (Eng.), professor, Don State Technical University (Russian Federation);
**Janusz Witalis Kozubal,** Dr.Sci.Tech, Wroclaw Polytechnic University (Republic of Poland);
**Victor M. Kureychik**, Dr.Sci. (Eng.), professor, Southern Federal University (Russian Federation);
**Geny V. Kuznetzov**, Dr.Sci. (Phys.-Math.), professor, Tomsk Polytechnic University (Russian Federation);
**Huchang Liao,** professor (Eng.), Sichuan University (Chengdu, China);
**Vladimir I. Lysak**, Dr.Sci. (Eng.), professor, Volgograd State Technical University, (Russian Federation);
**Vladimir I. Marchuk**, Dr.Sci. (Eng.), professor, Institute of Service and Business (DSTU branch) (Shakhty);
**Igor P. Miroshnichenko**, Cand.Sci. (Eng.), professor, Don State Technical University (Russian Federation);
**Vladimir G. Mokrozub**, Dr.Sci. (Eng.), associate professor, Rostov State Transport University (Russian Federation);
**Murman A. Mukutadze**, Cand.Sci. (Eng.), professor, Tambov State Technical University (Russian Federation);
**Nguyen Dong Ahn**, Dr.Sci. (Phys.-Math.), professor, Institute of Mechanics, Academy of Sciences and Technologies of Vietnam (Vietnam);
**Petr M. Ogar**, Dr.Sci. (Eng.), professor, Bratsk State University (Russian Federation);
**Gennady A. Ougolnitsky**, Dr.Sci. (Phys.-Math.), professor, Southern Federal University (Russian Federation);
**Sergey G. Parshin**, Dr.Sci. (Eng.), associate professor, St. Petersburg Polytechnic University (Russian Federation);
**Valentin L. Popov**, Dr.Sci. (Phys.-Math.), professor, Institute of Mechanics, Berlin University of Technology (Germany);
**Nikolay N. Prokopenko**, Dr.Sci. (Eng.), professor, Don State Technical University (Russian Federation);
**Muzafer H. Saračević,** full professor (Computer Sciences), International University of Novi Pazar (Serbia**);**
**Murat Tezer,** PhD (Math. & Computer Sciences), Yakin Doğu Üniversitesi (Nicosia, Turkey);
**Vladimir N. Sidorov**, Dr.Sci. (Eng.), Russian University of Transport (Russian Federation);
**Arkady N. Solovyev**, Dr.Sci. (Phys.-Math.), professor, Don State Technical University (Russian Federation);
**Alexandr I. Sukhinov**, Dr.Sci. (Phys.-Math.), professor, Don State Technical University (Russian Federation);
**Mikhail A. Tamarkin**, Dr.Sci. (Eng.), professor, Don State Technical University (Russian Federation);
**Ahmet Uyumaz,** associate professor (Eng.), Mehmet Akif Ersoy Üniversity (Burdur, Turkey);
**Valery N. Varavka**, Dr.Sci. (Eng.), professor, Don State Technical University (Russian Federation);
**Igor M. Verner,** Cand.Sci. (Eng.), Docent, Technion (Israel)
**Batyr M. Yazyev**, Dr.Sci. (Phys.-Math.), professor, Don State Technical University (Russian Federation);
**Vilor L. Zakovorotny**, Dr.Sci. (Eng.), professor, Don State Technical University (Russian Federation);

CONTENTS

**MECHANICS**

***Gaidzhurov P. P., Saveleva N. A., Trufanova E. V.*** Numerical simulation of the behavior of kinematically unstable slopes under dynamic influences ..... 300

**MACHINE BUILDING AND MACHINE SCIENCE**

***Molokov K. A., Novikov V. V.*** Evaluation of crack resistance of welded joints with soft interlayers ..... 308

***Antypas I. R., Dyachenko A. G., Saed Bakir Imad*** Liquid temperature effect on the hydraulic shock wave velocity in polyethylene pipes ..... 319

***Popov A. V., Samuylov A. O., Cherepanov I. S.*** Application and evaluation of the technical condition of composite materials in aircraft and unmanned aerial vehicles by acoustic emission method of nondestructive testing ..... 328

***Rybak A. T., Ivanovskaya A. V., Batura P. P., Pelipenko A. Yu.*** Synchronization in multi-motor hydromechanical systems ..... 337

**INFORMATION TECHNOLOGY, COMPUTER SCIENCE, AND MANAGEMENT**

***Hubert Anysz*** Machine Learning and data mining tools applied for databases of low number of records ..... 346

***Elshamy M. M. M., Tiraturyan A. N., Uglova E. V.*** Evaluation of the elastic modulus of pavement layers using different types of neural networks models ..... 364

***Glushko S. G., Lyapin A. A., Shatilov Yu. Yu., Cherpakov A. V., Haldkar R. K.*** Software Module Development for the Parametric Generation of Truss Structure Geometry in a Two-Dimensional Setting ..... 376

# MECHANICS

UDC 539.42 https://doi.org/10.23947/2687-1653-2021-21-4-300-307

## Numerical simulation of the behavior of kinematically unstable slopes under dynamic influences

**P. P. Gaidzhurov ✉, N. A. Saveleva, E. V. Trufanova**
Don State Technical University (Rostov-on-Don, Russian Federation)
✉ gpp-161@yandex.ru

***Introduction.*** The concept of estimating the dynamic parameters of the "base — weakened layer — block" system is proposed, taking into account the physical nonlinearity of the material and the kinematic method of excitation of vibrations. In accordance with this approach, the physical nonlinearity of the base and block material is considered using the Drucker-Prager model. The weakened layer is modeled by 3D spring finite elements. The verification procedure of the proposed methodology is carried out on the example of the dynamic calculation of the "base — weakened layer — slope" system.
***Materials and Methods.*** The computational experiments were performed using the ANSYS Mechanical software package in combination with a nonlinear solver based on the Newton-Raphson procedure. SOLID45 volumetric finite elements were used to discretize the computational domains. Combined elastic-viscous elements COMBIN14 were used to simulate the displacement of the block relative to the fixed base.
***Results.*** An engineering technique for the dynamic analysis of the stress-strain state of the "base — weakened layer — block" spatial system with kinematic method of excitation of vibrations is developed. The accuracy and convergence of the proposed method is investigated using specific numerical examples.
***Discussion and Conclusion.*** Based on the mathematic simulation performed, it is shown that the developed technique provides assessing the risks of the occurrence of real landslide processes caused by external non-stationary impacts.

***Keywords*:** finite element method, Drucker-Prager model, Newton-Raphson method, dynamic modeling, slope, landslide process.

***For citation:*** P. P. Gaidzhurov, N. A. Saveleva, E. V. Trufanova. Numerical simulation of the behavior of kinematically unstable slopes under dynamic influences. Advanced Engineering Research, 2021, vol. 21, no. 4, pp. 300–307. https://doi.org/10.23947/2687-1653-2021-21-4-300-307

*© Gaidzhurov P. P., Saveleva N. A., Trufanova E. V., 2021*

**Introduction**. In the 70s of the last century, the finite element method (FEM) began to be extensively used in the analysis of the static stability of slopes and flanks [1–3]. According to the practice of geotechnical calculations, FEM, in contrast to simplified methods, provided taking into account such important factors as the real geometry and layered structure of the objects under study, as well as the presence of anti-landslide structures and the physical nonlinearity of the material with a previously unknown area of plasticity [4]. Currently, many researchers start using FEM to analyze the dynamic stability of actual slopes, as well as forecasting the risks of rock falls in the underground workings and from slopes located along highways and railways. Also, one of the topical areas of mountain dynamics is finite element modeling of earthquake consequences, taking into account the kinematic instability of conglomerations [5]. Today, there are the following methods of dynamic calculations in the field of geotechnics:

1. SRM (strength reduction method) is a method of reducing strength [6, 7]. It is designed to calculate the safety margin of a mountain range in a physically nonlinear formulation. In SRM, the actual strength parameters of the soil are iteratively reduced through dividing by some factor greater than 1:

$$c' = \frac{c}{k_{SRM}}; \quad \phi' = arctan\left(\frac{tan\,\phi}{k_{SRM}}\right),$$

where $c$, $\phi$ — actual values of the adhesion and the angle of internal friction of the soil, respectively; $c'$, $\phi'$ — the adhesion and the angle of internal friction of the soil, respectively, after their reduction relative to the actual values; $k_{SRM}$ — the shear strength reduction factor. Value $k_{SRM}$, corresponding to the limiting state of the system, determines the lower limit of the strength parameters of the material.

2. LEM (limit equilibrium method) is a method of limiting kinetics based on D'Alembert's principle [8, 9]. It is focused on the analysis of dynamic stability of articulated rock massifs.

3. TLEM (thin layer element method of FEM) is a thin-layer finite element method [10] in which elastic-plastic elements of a thin layer are used to model the behavior of kinematically unstable structures.

Analysis of the results obtained using the SRM, LEM and TLEM methods showed that there is currently no unified vision of mathematical modeling of the behavior of structurally unstable geotechnical systems under nonstationary external influence. This determines the topicality of developing a methodology for dynamic analysis of systems of the "base — weakened layer — block" type in a finite element formulation through a new approach to simulating sliding planes.

**Materials and Methods**. The equation of motion of a mechanical system in a finite element formulation can be given as follows [11]:

$$[M]\{W''(t)\}+[C]\{W'(t)\}+[K]\{W(t)\} = \{F_0\}+\{F(t)\}, \quad (1)$$

where $[M]$, $[C]$, $[K]$ — matrices of masses, damping and stiffness of the ensemble of finite elements, respectively; $\{W''(t)\}$, $\{W'(t)\}$, $\{W(t)\}$ — vectors-columns, respectively, of nodal accelerations, velocities, displacements; $\{F_0\}$, $\{F(t)\}$ — vectors-columns of specified static and dynamic loads, respectively, at a time $t$. In the future, we assume that the matrices $[M]$ and $[K]$ are consistent.

For the numerical integration of equation (1), we use Newmark method [12]. Here, we assign the integration step along the time axis $\Delta t$ so that the contributions of physically significant proper pairs are considered with sufficient accuracy. In the future, we will consider the kinematic methods of excitation of vibrations, set using either model seismogram $\{\overline{W}(t)\}$, or model accelerogram $\{\overline{W''}(t)\}$. With this method of setting the dynamic effect, the second term of the right side of equation (1) will be zero: $\{F(t)\}=0$.

Consider the method of excitation of mechanical vibrations from a model seismogram. Function $\overline{W}(t)$ can be written as [13]:

$$\overline{W}(t) = A t e^{-\chi t} \sin(\theta t), \quad (2)$$

where $A$ — initial amplitude; $\chi$ — attenuation coefficient; $\theta$ — angular frequency of external influence. Figure 1 shows a graph of function $\overline{W}(t)$ for the values: $A$ = 0.01553 m; $\chi$ = 0.7143; $\theta$ = 5 s$^{-1}$.

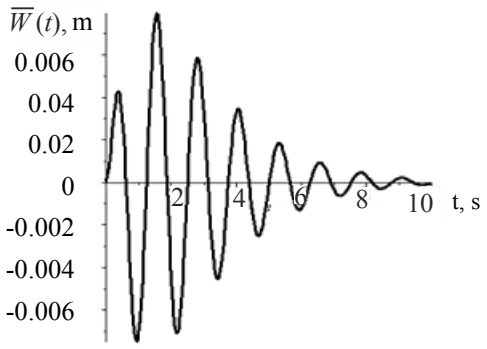


Fig. 1. Graph of the model seismogram

**Research Results**. As the first model example, consider the problem on forced vibrations of the slope located on the base (Fig. 2). The boundary conditions of the problem are shown in Figure 3, where letter *S* denotes the point under study.

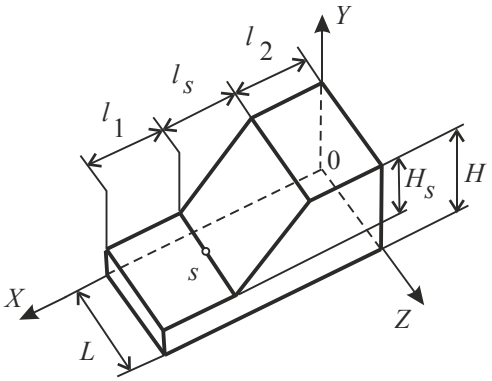


Fig. 2. Slope geometry

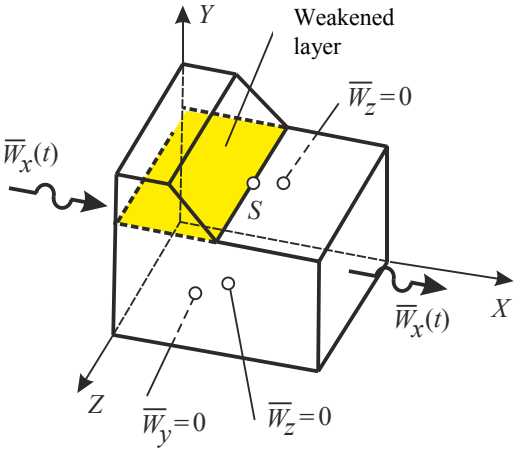


Fig. 3. Design scheme of the slope

Relationships between the geometric parameters of the slope and the base (Fig. 2) are presented in Table 1.

Table 1

Slope – Base Geometrics Relationship

| ***H*** | $l_1$ | $l_2$ | $l_2$ | ***L*** |
|---|---|---|---|---|
| $3.5H_s$ | $H_s$ | $(1.0-2.0)H_s$ | $H_s$ | $5H_s$ |

Mechanical characteristics of the slope and base material are ae follows: deformation modulus $E$ = 21 MPa; Poisson's ratio $\nu$ = 0.3; specific gravity $\gamma$ = 1702 kg/m$^3$; adhesion $c$ = 45 kPa; internal friction angle $\phi$ = 15°.

To model the slope and the base, we use SOLID45 volumetric finite elements of the ANSYS Mechanical software package. The finite element model for the variant with the parameters: $l_s = 2H_s$, $H_s$ = 10 m, assigned to the global Cartesian coordinate system, is shown in Figure 4.

The finite element grid is constructed so that on the contact surface, adjacent nodes of the base and slope have the same coordinates, but different numbers. This is done in order to arrange a weakened layer in this place. The kinematic effect in the form of a model seismogram (2) is set at each integration step $t_i$ in the form of nodal displacements $\overline{W}_x(t_i)$ on the end surfaces of the model with parameters: $X = 0$ and $X = l_1 + l_S + l_2$.

Modeling of the weakened layer (Fig. 4) is performed using elastic-viscous combined finite elements COMBIN14 [14]. The two-node element COMBIN14, consisting of a spring with stiffness $k$ and a liquid friction damper with a damping coefficient $c_v$, is shown in Figure 5. In the case under consideration, this element works only for tension-compression.

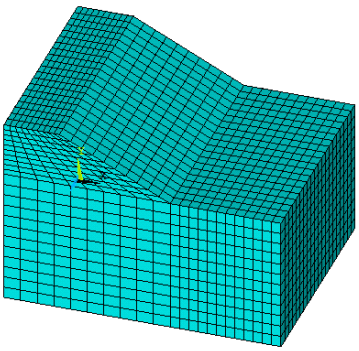

Fig. 4. Finite element model of the “base – slope” system

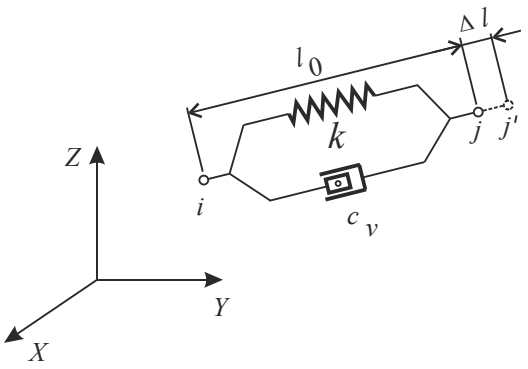


Fig. 5. Combined finite element COMBIN14

In each node of the contact surface (Fig. 4), along the global $X$, $Y$, $Z$ axes, we introduce elements of COMBIN14. Parameters of combined elements are:

$$k_x = 30 \text{ kN/m}; \; k_y = k_z = 9.44 \cdot 10^7 \text{ kN/m}; \; c_v = 0.5.$$

http://vestnik-donstu.ru

In this example, we further introduce the assumption of the natural undeformed state of the "base — weakened layer — slope" system. For calculations, we use the nonlinear solver of the ANSYS Mechanical complex.

The finite element modeling results in the form of visualization of the deformed state of the "base — slope" system with the account of the maximum horizontal displacement and the distribution of amplitude horizontal displacements $W_x(t)$ are shown in Figures 6 and 7. The integration step of equation (1) $\Delta t = 0.01$ s. As can be seen, the introduction of 3D elastic-viscous elements makes it possible to simulate the effect of kinematic instability of the "base — weakened layer — slope" mechanical system with the kinematic method of excitation of vibrations.

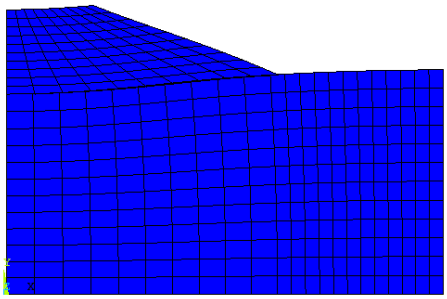

Fig. 6. Visualization of slope displacement regarding the base

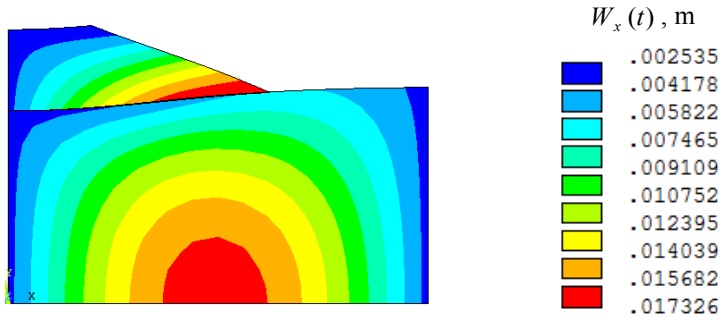


Fig. 7. Displacement distribution $W_x(t)$

The amplitude value of the displacement at point *S* was $W_{x_S\,\max} = 1.7$ cm. For the slope option $l_s = H_s$ (Fig. 2), $W_{x_S\,\max} = 1.1$ cm. The graphs of base and slope vibrations at the studied point *S* (Fig. 3) in the direction of *X*-axis are shown in Figure 8.

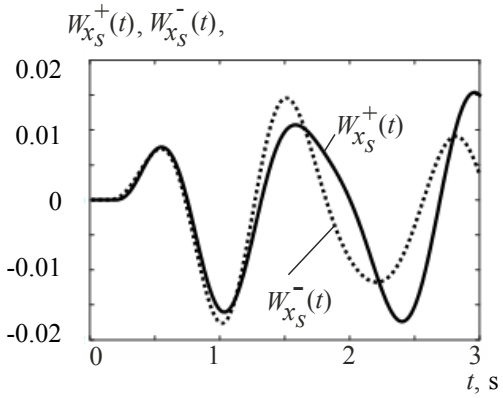


Fig. 8. Graphs of vibrations at point *S* of base $W_{x_S}^+(t)$ and slope $W_{x_S}^-(t)$ under kinematic excitation using a model seismogram

Based on the above graphs, it can be seen that starting from the moment of time $t > 1.5$ s, there is a mismatch of base and slope vibrations.

Let us consider the behavior of the "base — weakened layer — slope" system (Fig. 3) when vibrations are excited using a model accelerogram $\overline{W''}(t)$. To this end, we differentiate expression (2) twice. As a result, we get:

$$\overline{W''}(t) = Ae^{-\chi t}[\chi^2 \sin(\theta t)t - 2\chi\cos(\theta t)\theta t - \sin(\theta t)\theta^2 t - \\ -2\chi\sin(\theta t) + 2\cos(\theta t)\theta]. \quad (3)$$

Figure 9 shows the graph of function (3) for parameters: $A = 0.01553$ m; $\chi = 0.7143$; $\theta = 5$ s$^{-1}$.

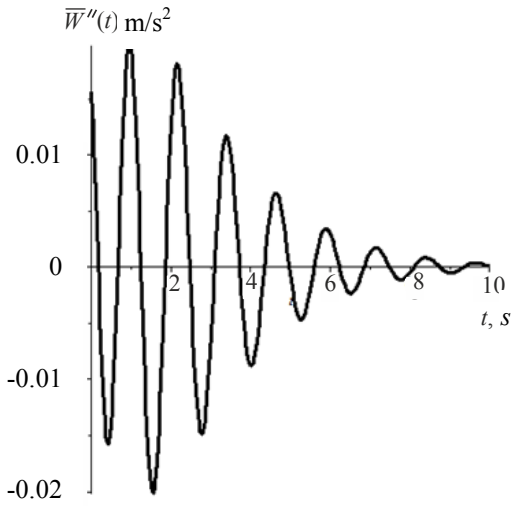


Fig. 9. Graph of the model accelerogram

The kinematic effect in the form of model accelerogram (3) , by analogy with seismogram (2), is set at each integration step $t_i$ in the form of nodal accelerations $\overline{W}_x''(t_i)$ on the end surfaces of the model with parameters: $X = 0$ and $X = l_1 + l_S + l_2$. Figure 10 shows the graphs of vibrations at the studied point *S* (Fig. 3) under kinematic action in the form of a model accelerogram. Comparing the vibration graphs shown in Figures 8 and 10, we establish that they almost coincide. This indicates the correctness of the developed finite element model, which allows describing the behavior of the "base — weakened layer — slope" system with various methods of unsteady kinematic action.

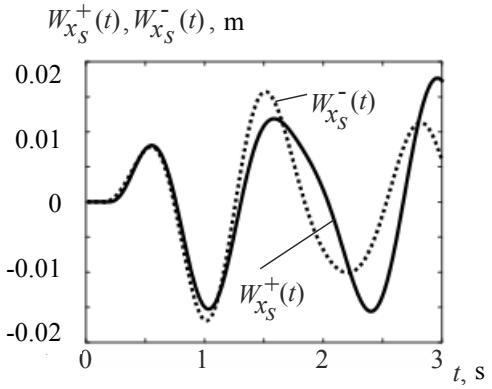


Fig. 10. Vibration graphs at point *S* of base $W_{x_S}^+(t)$ and slope $W_{x_S}^-(t)$ under kinematic excitation of vibrations using a model accelerogram

As a second model example, let us consider the problem on forced slope vibrations with a kinematically unstable wedge-shaped inclusion (Fig. 11). Due to the symmetry of the configuration, only 1/2 part of the slope and inclusions are taken into account in the computational scheme. The boundary conditions for the accepted design scheme are shown in Figure 12. Here, letter *S* denotes the point under study, which belongs simultaneously to the slope base and the wedge-shaped inclusion.

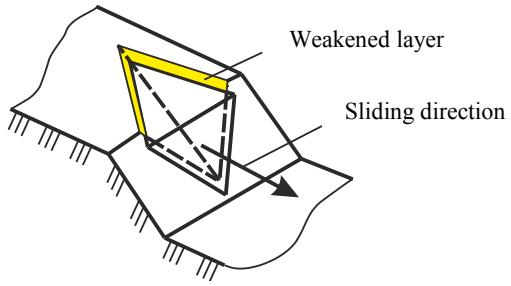


Fig. 11. Slope diagram with wedge -shaped inclusion

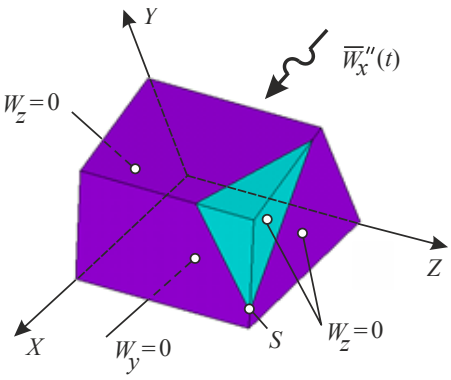


Fig. 12. Computational scheme for the "slope — wedge-shaped inclusion" problem

http://vestnik-donstu.ru

The finite element model of slope and wedge-shaped inclusion is shown in Figure 13. As in the previous example, in this case, we use SOLID45 and COMBIN14 elements with the same material characteristics.

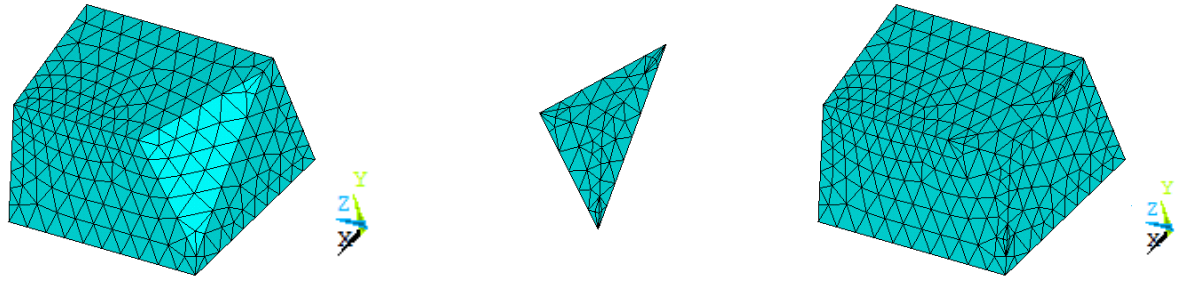

*a*) *b*) *c*)

Fig. 13. Finite element model: *a*) slope; *b*) wedge-shaped inclusion; *c*) slope with wedge-shaped inclusion

The function describing the model accelerogram has the form:

$$\overline{W}_x(t) = A \cdot \cos \theta t \,,$$

where $A$ — acceleration amplitude; $\theta$ — frequency of external influence. Figure 14 shows graph $\overline{W}_x(t)$ at $A$ = 2.5 m/s$^2$, $\theta$ = 2 Hz. The values of acceleration $\overline{W}_x(t_i)$ at the $i$-th step of integrating the equation of motion (1) are applied to the nodes of the model surface with coordinate $X$ = 0 (Fig. 12).

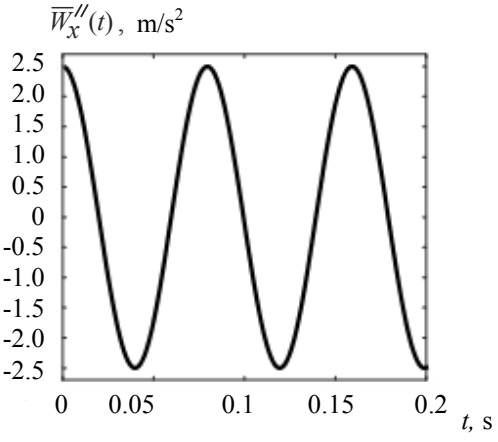


Fig. 14. Graph of the model accelerogram $\overline{W}_x(t)$

The simulation result in the form of a distribution of the amplitude values of displacements $W_x(t)$ is shown in Figure 15. Integration step $\Delta t$ = 0.01 s. Vibration graphs of the slope base and wedge-shaped inclusion at the studied point $S$ (Fig. 12) in the direction of $X$-axis are shown in Figure 16.

As can be seen from Figure 15, with a given kinematic effect, the continuity of the slope array breaks along the weakened layer, and the wedge-shaped inclusion shifts relative to the slope base along $X$-axis.

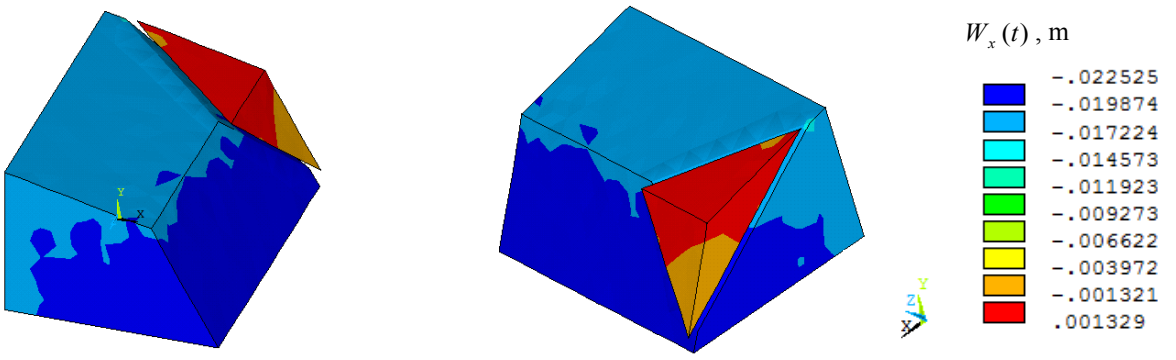


Fig. 15. Distributions $W_x(t)$ in 1/2 part of the slope with wedge-shaped inclusion

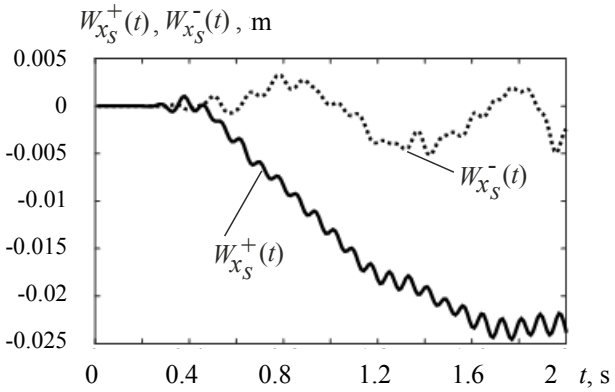


Fig. 16. Vibration graphs at point *S* of the slope base $W_{x_S}^+(t)$

and wedge-shaped inclusion $W_{x_S}^-(t)$ under kinematic excitation of vibrations using a model accelerogram

"Drift" $W_{x_S}^+(t)$ in Figure 16 is due to the fact that this finite element model has no connections that prevent displacements along *X*-axis. As shown in [11], it is possible to solve the "drift" problem by subtracting the displacement of the slope base, which represents the displacement "as a rigid whole", from the displacement values $W_{x_S}^+(t)$ and $W_{x_S}^-(t)$. It should be noted that the obtained amplitude values of the displacements provide evaluating the dynamic parameters of the "slope — weakened layer — wedge-shaped inclusion" system.

**Conclusion**. A finite element model has been developed and validated to study the dynamic behavior of kinematically unstable slopes in a three-dimensional formulation, taking into account the physical nonlinearity of the material.

**References**

1. Fadeev AB. Metod konechnykh ehlementov v geomekhanike. Moscow: Nedra; 1987. 221 p. (In Russ.)

2. Eberhardt E. Rock Slope Stability Analysis – Utilization of Advanced Numerical Techniques. Vancouver, Canada: Geological Engineering/Earth Ocean Sciences, UBS; 2003. 41 p.

3. Hoek H, Bray JW. Rock Slope Engineering. 3rd ed. London: The Institution of Mining and Metallurgy; 1981. 358 p.

4. Griffiths DV, Lane PA. Slope stability analysis by finite elements. Geotechnique. 1999;49:387–403. https://doi.org/10.1680/geot.1999.49.3.387

5. Stability Modeling with SLOPE/W. An Engineering Methodology. Alberta, Canada; 2015. 244 p.

6. Tamotsu Matsui, Ka-Ching San. Finite element slope stability analysis by shear strength reduction technique. Soils and Foundations. 1992;32:59–70. https://doi.org/10.3208/sandf1972.32.59

7. Griffiths DV, Marquez RM. Three-dimensional slope stability analysis by elasto-plastic finite elements. Geotechnique. 2007;57:537–546. https://doi.org/10.1680/geot.2007.57.6.537

8. Weida Ni, Huiming Tang, Xiao Liu, et al. Dynamic Stability Analysis of Wedge in Rock Slope Based on Kinetic Vector Method. Journal of Earth Science. 2014;25:749–756.

9. Md. Moniruzzaman Moni, Md. Mahmud Sazzad. Stability analysis of slopes with surcharge by LEM and FEM. International Journal of Advanced Structures and Geotechnical Engineering. 2015;4:216–225.

10. Tongchun Li, Jinwen He, Zhao Lanhao, et al. Strength Reduction Method for Stability Analysis of Local Discontinuous Rock Mass with Iterative Method of Partitioned Finite Element and Interface Boundary Element. Mathematical Problems in Engineering. 2015;2015:1–11. https://doi.org/10.1155/2015/872834

11. Gaydzhurov PP, Savelyeva NA, Sazonova AV. Modeling of dynamic response of the system "base – foundation – top structure" in various ways kinematic excitation of vibrations. University News. North-Caucasian Region. Technical Sciences Series. 2019;201:23–30. https://doi.org/10.17213/0321-2653-2019-1-23-30 (In Russ.)

12. Bate K, Vilson EM. Chislennye metody analiza i metod konechnykh ehlementov. Moscow: Stroiizdat; 1982. 448 p. (In Russ.)

13. Korchinskii IL, Borodin LA, Grossman AV, et al. Seismostoikoe stroitel'stvo zdanii. Moscow: Vysshaya shkola; 1971. 320 p. (In Russ.)

14. Gaidzhurov PP, Saveleva NA, Dyachenkov VA. Finite element modeling of the joint action of flow slide and protective structure. Advanced Engineering Research. 2021;21:133–142. https://doi.org/10.23947/2687-1653-2021-21-2-133-142 (In Russ.)

Received 27.09.2021
Revised 18.10.2021
Accepted 19.10.2021

*About the Authors:*

**Gaidzhurov, Petr P.,** professor of the Engineering Mechanics Department, Don State Technical University (1, Gagarin sq., Rostov-on-Don, 344003, RF), Dr.Sci. (Eng.), Scopus, ORCID, gpp-161@yandex.ru

**Saveleva, Nina A.,** senior lecturer of the Engineering Mechanics Department, Don State Technical University (1, Gagarin sq., Rostov-on-Don, 344003, RF), Scopus, ORCID, ninasav86@mail.ru

**Trufanova, Elena V.,** associate professor of the Engineering Mechanics Department, Don State Technical University (1, Gagarin sq., Rostov-on-Don, 344003, RF), Cand.Sci. (Eng.), Scopus, ORCID, el.trufanova@mail.ru

*Claimed contributorship:*

P. P. Gaidzhurov: task formulation; selection of solution methods; construction of mathematical and computer models; discussion of the results. N. A. Saveleva: performing review and calculations; discussion of the results. E.V. Trufanova: performing review and calculations; discussion of the results.

*All authors have read and approved the final manuscript.*

MACHINE BUILDING AND MACHINE SCIENCE

Check for updates

UDC 621.791.05:620.17 https://doi.org/10.23947/2687-1653-2021-21-4-308-318

# Evaluation of crack resistance of welded joints with soft interlayers

**K. A. Molokov**[1,2] ✉, **V. V. Novikov**[1]

[1]Far Eastern Federal University (Vladivostok, Russian Federation)

[2]Vladivostok State University of Economics and Service (Vladivostok, Russian Federation)

✉ Spektrum011277@gmail.com

***Introduction.*** Welded joints in large-sized metal structures (e.g., in the structures of ship hulls) subject to low-cycle fatigue are considered. The characteristic appearance of soft interlayers, which are significantly plastically deformed under working loads, was noted. Deformation of the metal structure with damage, especially in the form of cracks, reduces the strength and reliability of structural elements and joints. Pre-deformation negatively affects plasticity; therefore, much depends on the residual plasticity of the cracking material. At the same time, with a decrease in residual plasticity, such an important reliability indicator as the resistance of the material to crack propagation — the fracture toughness – decreases. The paper is devoted to the development of a model that includes analytical dependences for assessing the crack resistance of metal structures and their welded joints with soft interlayers according to the crack resistance limit for all crack sizes.

***Materials and Methods.*** The theory and methods of linear mechanics of materials destruction, structural-mechanical approach are used. The calculation results were analyzed and compared to the experimental data and other analytical solutions. The numerical experiment was performed for the ferrite-perlite steel grades of 10, 50, 22K, St3sp, etc., widely used in industry, as well as for alloy steels hardened to medium and high strength of 30KhGSA, 37KhN3A, etc.

***Results.*** Analytical dependences are obtained for calculating the relative crack resistance limit according to three main known mechanical characteristics of the state of the material of the soft interlayer of the welded joint.

***Discussion and Conclusions.*** The results obtained can be used to assess the crack resistance of pre-deformed structural elements and welded joints (including those with soft interlayers) operating under a transverse load. The results of experimental data and analytical calculations are shown in dimensionless form, which enables to obtain invariant results with respect to the fracture toughness limit.

***Keywords:*** weld joint, soft interlayer, mechanical inhomogeneity, deformation, crack resistance limit, crack length, contact hardening, elongation.

***For citation:*** K. A. Molokov, V. V. Novikov. Evaluation of crack resistance of welded joints with soft interlayers. Advanced Engineering Research, 2021, vol. 21, no. 4, p. 308–318. https://doi.org/10.23947/2687-1653-2021-21-4-308-318

*© Molokov K. A., Novikov V. V., 2021*

CC BY

**Introduction.** In welded joints subjected to cyclic loads, cracks often occur and develop, which can cause a dangerous condition of structures and their destruction. Examples of the formation of such cracks in the ship hulls are given in [1]. The kinetics of the formation of macrocracks in welds and their development depend on many factors, which requires comprehensive studies on the crack resistance of welded joints and the development of appropriate mathematical models.

The resistance of the metal to crack propagation is significantly affected by the so-called soft interlayers that appear after welding, which are subjected to plastic deformation. Different sections of the welded joint are characterized

by a greater or lesser degree of heterogeneity of the mechanical characteristics of the metal [2]. It depends on many initial conditions of the welding procedure. These include the cooling rate of welded joint zones and processing of welded steel, as well as the content of alloying elements, carbon, etc. O. A. Bakshi considered some problematic issues of viscous and brittle destruction of mechanically inhomogeneous welded joints, the influence of defects and microcracks on the processes occurring in the metal structure under loading, etc. The researchers solved a number of particular problems to increase the strength and durability of welded joints with interlayers [3–6].

In the steady-state welding mode, the width of the heat affected zone (HAZ) and mechanical properties of the metal vary slightly along the length of the welded joint. Therefore, it is advisable to consider the heterogeneity of characteristics in different zones in the welded joint under transverse load. For hardened or heat-treated (heat-strengthened) metals, the appearance of quenching structures or weakened zones, respectively, is characteristic. At the same time, depending on the properties of the steel in its initial state and the parameters of the process, soft zones may form. Here, yield strength $\sigma_{\text{т}}^{\text{м}}$ and tensile strength $\sigma_{\text{в}}^{\text{м}}$ of the metal are less than in the adjacent (so-called hard) zones $\sigma_{\text{т}}^{\text{т}}$ and $\sigma_{\text{в}}^{\text{т}}$. Thus, the soft zone will be involved in plastic deformation between areas with characteristics $\sigma_{\text{т}}^{\text{т}} > \sigma_{\text{т}}^{\text{м}}$, $\sigma_{\text{в}}^{\text{т}} > \sigma_{\text{в}}^{\text{м}}$ earlier than neighboring ones, and the degree of its influence on the strength of the joint will depend on the scheme of the applied load[1]. Deformation of the soft interlayer reduces the crack propagation resistance — the intensification of brittle fracture is initiated, in which the critical crack length will decrease dramatically [7].

The objective of this study is to develop analytical dependences and a mathematical model for assessing the crack resistance of welded joints with a soft interlayer as a result of its preliminary plastic deformation.

Assume that some limitation of the linear dimensions of the welded sample (except thickness) under transverse load does not noticeably affect the processes and phenomena considered in the metal structure (except for the formation of a soft interlayer) caused by the thermal welding cycle.

**Materials and Methods**

**Calculated prerequisites.** Consider the change in the physicomechanical characteristics of the metal of the soft interlayer when the butt joint is pulled across the seam of a sufficiently large range (Fig. 1).

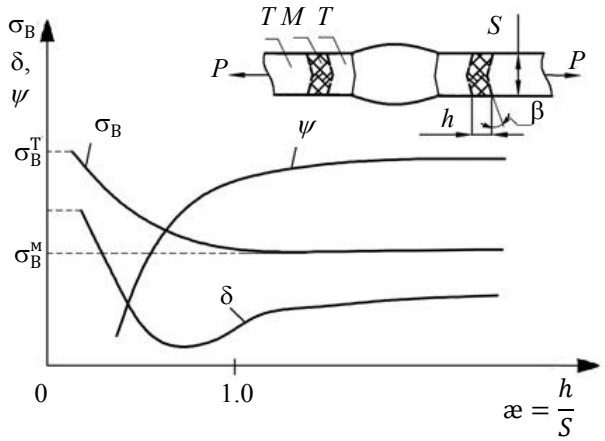


Fig. 1. Diagram of the dependence of characteristics $\sigma_{\text{в}}$ , δ and ψ on the relative thickness of the interlayer

In the elastic loading stage, the interlayer and adjacent sections of the considered region are deformed uniformly. When the stress level corresponding to yield strength $\sigma_{\text{т}}^{\text{м}}$ is reached, a plastic deformation is formed in it, and the adjacent sections remain in an elastic state. To simplify, we assume the angle of inclination of the face of the interlayer $\beta = 0$ (Fig. 1). With a further increase in load and deformation, the coefficient of transverse deformation μ

[1] Matokhin GV, Molokov KA. Prochnost' i nadezhnost' svarnykh soedinenii. Vladivostok: DVFU; 2019. 143 p. (In Russ.)

(Poisson's ratio) of the soft interlayer increases. As a result, it will be larger than that of the adjacent section of metal. As plastic deformation develops in the interlayer, $\mu \to 0.5$, and in the zone with an elastic state of metal, $\mu = 0.3$. Due to unequal transverse deformation, tangential stresses arise in the weld. Their maximum values are concentrated in the area of the separation planes of the soft interlayer and neighboring zones. Tangential stresses prevent transverse narrowing of the soft interlayer in the direction of the sheet thickness. The narrower the interlayer (i.e., the smaller the ratio $æ = h/s$, Fig. 1), the smaller the transverse constriction it receives at the time of the occurrence of true destructive stresses $\sigma_p$. This creates the effect of contact hardening, which provides an increase in load-bearing capacity.

The increase in destructive power has limits. The stronger zones adjacent to the soft interlayer will also be plastically deformed under certain conditions. The greater the strength of the adjacent zones and the smaller the relative thickness of interlayer æ, the more noticeable the effect of contact hardening. It is reinforced by harder interlayers located near relatively soft ones.

Relative transverse constriction ψ in the soft interlayer and the absolute elongation of sample δ depend on æ and the properties of metals in the compound. In wide interlayers, when there is no contact hardening yet, ψ remains constant with decreasing æ (see Fig. 1). And δ gradually decreases with decreasing æ in the total width of the welded sample. In the region of contact hardening, ψ decreases sharply, as transverse tangential stresses increase preventing the narrowing of the interlayers in the direction of the material thickness. In this case, the relative elongation of sample δ also first decreases. When a significant stiffness of the stress state in the soft interlayer is realized, δ increases, since the metal of the hard interlayer is involved in plastic deformation. Note that under welding heat-strengthened steels, $\delta_5^м$ of the soft interlayer turns out to be higher than $\delta_5^т$. But its plastic deformation is much greater, and the residual plasticity after loading to stresses $\sigma_в^м > \sigma > \sigma_т^м$ may become critical. As a result, the length of the critical crack is significantly reduced, which can occur under the influence of further cyclic operating stresses at the junction of soft and hard interlayers. At the same time, the risk of brittle fracture increases significantly, and its possibility should be assessed (crack resistance limit[2, 3] [8, 9]) in the area with a crack defect. This takes into account the conditions of plane deformation, contact hardening, and plastically deformed soft interlayer. According to the results of the study of the deformation of interlayers of composite material by the method of finite element modeling [3], it can be noted that the greatest deformation of the soft interlayer is formed near its junction with the hard interlayer. This is especially clear at the average values of the relative thickness of interlayer æ.

Sometimes, with static load, it is possible to find the optimal value of æ and achieve uniform strength of the connection. However, defects or discontinuities existing in the soft interlayer after some deformation may develop into cracks with a critical length, provided that the remaining part of the subcritical deformation is relatively small. The contact hardening degree in the case of plane deformation is determined from the formula[2] [2]:

$$K_æ = \frac{\pi + \frac{1}{æ}}{2\sqrt{3}}. \quad (1)$$

Tensile strength of a welded joint with a soft interlayer:

$$\sigma_в^{сс} = \sigma_в^м \cdot K_æ, \quad (2)$$

where $\sigma_в^м$ — tensile strength of soft interlayer.

http://vestnik-donstu.ru

[2] Matokhin GV, Molokov KA. Prochnost' i nadezhnost' svarnykh soedinenii. Vladivostok: DVFU; 2019. 143 p. (In Russ.)
[3] Goldstein RV, Morozov NF. Mekhanika deformiruemogo tverdogo tela: problemy i rezul'taty. In: Proc. All-Russian Conf. in memory of Academician L.I. Sedov on the centenary of his birth. Moscow: Torus Press; 2009. P. 121–166. (In Russ.)

Naturally, to provide equal strength under static load, at least the condition $\sigma_{в}^{сс} = \sigma_{в}^{т}$ is required to be fulfilled. In this case, the limit (minimum) value of the contact hardening coefficient is determined from the ratio of ultimate resistances:

$$K_{æпред} = \sigma_{в}^{т} / \sigma_{в}^{м}. \quad (3)$$

Using (1) and (2), we find the limit values of $æ_{пред}$, at which the equal strength of the joint is obtained under the conditions of plane deformation:

$$æ_{пред} = \frac{1}{\left(2\sqrt{3}\, K_{æпред} - \pi\right)}. \quad (4)$$

However, it must be borne in mind that the increase in the strength of the welded joint with a soft interlayer is limited by the true separation stresses for the soft metal.

When welding hardened steels, the width of the softened zone depends on the rate of energy input and is regulated by the selection of a suitable welding mode. For each metal thickness, welding method, and mode, there is a certain width of the softened section, at which the maximum possible contact hardening is provided, as well as equal strength of the welded joint and the base metal.

The study of the softening section under argon-arc and electron-beam welding of metal with a thickness of 4.5–8 mm shows:

— the hardness on it is determined only by the heating temperature;

— the strength of the joints does not depend on the hardness level of the softened section, but on its width $h$ (Fig. 1).

At the same time, it should be borne in mind that the softening section smoothly passes into harder sections of the heat affected zone.

The study of the kinetics and the mechanism of softening in HAZ allowed us to establish how the properties of the sections surrounding the soft interlayer affect the strength of welded joints.

A new criterion determining the temporary strength limit of the welded joint $\sigma_{вр}^{сс}$ is experimentally validated — this is the relative width of the soft interlayer $b_1/b_0$. The proposed empirical dependence has the form:

$$\sigma_{в}^{сс} = \sigma_{в}^{м} + 0.3\sigma_{в}^{м}\left(\frac{b_0}{b_1}\right) + 0.3\sigma_{в}^{м}\left(\frac{b_0}{b_1}\right)^2, \quad (5)$$

where $\sigma_{вр}^{сс}$ — the strength limit of the welded joint, MPa; $\sigma_{в}^{м}$ — the strength limit of the soft interlayer, MPa; $b_0$ — the width of the interlayer with equal strength of the welded joint and the base metal, m; $b_1$ — the current width of the interlayer, m.

It follows from the last equation that at $b_0 = b_1$, the soft interlayer is strengthened by a maximum of 60 %, i.e., $\sigma_{в}^{т} = 1.6\sigma_{в}^{м}$, since further hardening does not make sense.

The experimental results indicate a decrease in the endurance of welded joints with a soft interlayer formed after welding of heat-strengthened steels $U4$ and $U6$. This shows a significant reduction in load-bearing capacity [10]. In these steels, the endurance limits of welded samples without stress concentration almost coincide with the endurance limits of the same samples made of non-hardened steel. That is, despite the thermal hardening of steels (contributing to an increase in strength), the vibration strength of welded joints based on $10^6$ cycles, turns out to be almost the same. Consequently, it can be assumed that plastic deformation in soft interlayers causes early formation of a macrocrack, whose critical size $L_c$ is sharply limited by the plastic deformations that have occurred.

The crack resistance of a plastically deformed soft interlayer material up to the values of $\sigma < \sigma_{в}^{м}$ can be estimated by a two-parameter fracture criterion — the crack resistance limit, which is calculated according to the known analytical dependence[4] [2, 11]:

[4] Matokhin GV, Molokov KA. Ibid.

$$K_c = K_{1c}\sqrt{1-\left(\frac{\sigma_c}{\sigma_{\text{в}}^{\text{м}}}\right)^2}, \quad (6)$$

where $\sigma_c$ — gross critical fracture stress; $K_{1c}$ — critical stress intensity factor (the constant of the soft interlayer material).

After plastic deformation of the soft interlayer, $\sigma_c$ will depend on the characteristics of the defect. Assume that this characteristic is the critical length $L_c$ of the incipient crack. Then, $\sigma_c = K_c/\sqrt{\pi L_c}$. However, to use (6), it is necessary to know the degree of deformation of the interlayer, since $K_c$ will primarily depend on it. Value $L_c$ will be considered unknown. It must be determined depending on the deformation of the soft interlayer.

The authors[5] [11], investigating the structural parameter of fracture $d$ and determining it for a disc-shaped crack, come to an expression for estimating the crack resistance limit in one-dimensional form:

$$\frac{K_c}{K_{1c}} = \frac{\sqrt{2\eta(1-\eta)}}{\arccos(\eta)}, \quad (7)$$

where $\eta = a/(a+d)$ — dimensionless parameter specified by the range of variation $(0 \le \eta \le 1)$; $a$ — radius of the disk-shaped crack.

From the last equality, it follows that large cracks are characterized by a relatively small value of $d$, $a$. Destruction occurs with small plastic deformations in the net section, and $K_c \approx K_{1c}$. The reverse situation develops with relatively small cracks, if a large plastic deformation in the net section is required for destruction, and $\eta \approx 0$, $K_c \ll K_{1c}$.

Now imagine that the soft interlayer is subjected to cyclic loading. In this case, we use the concept of an effective threshold stress intensity factor $K_{th0}^e$[6] to calculate the limiting amplitude of the loading cycle $\sigma_{fr}$ at the level of average stresses $\sigma_{\text{в}}^{\text{м}} > \sigma_m + \sigma_{fr} > \sigma_{\text{т}}^{\text{м}}$. To this end, we calculate the length of the initial macrocrack $L$, corresponding to the limiting amplitude of stresses in a plastically deformed material up to $\sigma_m$:

$$L = \frac{K_{thr}^2}{\pi}\left(\frac{1}{\sigma_{fr}^2} - \frac{1-\mu+\mu^2}{\sigma_{fc}^2}\right) \quad (8)$$
$$\text{при } K_{th0} = K_{th0}^e, r = -1,$$

where $\sigma_{fr}$ — limiting stress amplitude; $\sigma_{fc}$ — cyclic yield strength; $r$ — cycle asymmetry coefficient; $\mu$ — Poisson's ratio.

The value of the length of the initial macrocrack $L$ should be substituted into the calculated dependence for determining the endurance limit [12]:

$$\sigma_{fr} = \sigma_{fc}\left[\pi L\left(\frac{\sigma_{fc}(1-r)}{\Delta K_{thr}}\right)^2 + 0.8\right]^{-0.5}. \quad (9)$$

The solution will be the desired values of the limiting amplitudes. The characteristics included in (9) are calculated according to [12] or[7]. Further, it is not difficult to determine the contribution of the preliminary plastic deformation of the soft interlayer to the equivalent damage with regard to estimating the length of the macrocrack.

**Research Results**

**Building a mathematical model.** We describe the proposed sequence of analytical dependences development. The remaining plastic properties of the structural element or part of it can be estimated by deformation using the

[5] Goldstein RV, Morozov NF. Ibid.
[6] Molokov KA. Otsenka povrezhdennosti ferrito-perlitnykh stalei v usloviyakh malotsiklovogo nagruzheniya. In: Proc. Conf. "Nauka. Innovatsii. Tekhnika i tekhnologii: problemy, dostizheniya i perspektivy". Komsomolsk-na-Amure: KnAGTU; 2015. P. 126–129. https://www.elibrary.ru/item.asp?id=25725387
[7] Ibid.

elongation for the material area. We assume that a uniform plastic deformation takes place on a small section of the soft interlayer. It is associated with the critical elongation to destruction $\delta_{5(10)}$ through the known dependence [13]:

$$e = \ln(1 + \delta_5). \tag{10}$$

Let us assume that the material of the soft interlayer is plastically deformed. Consider the case when plastic deformation occurs only in the first loading cycles. That is, the area of the soft interlayer is pulled plastically under the external transverse nominal load, and then it works under elastic cyclic stresses. This is how a fatigue crack develops. In a soft interlayer, it can be provoked by high plastic deformation and (or) a defect. Due to the reduction of the ultimate deformation of the soft interlayer material, preliminary plastic deformation causes a decrease in the critical opening at the crack tip. According to the results of work [14], it can be noted that the dependence of the critical crack tip opening $\delta_c$ (CCO) under the pulling deformation of steel is very close to linear. This fact is observed for both aluminum alloy and austenitic steel. The results of the mentioned experiments suggest that with the maximum uniform plastic deformation of these materials, $\delta_c = 0$.

The endurance limit depends significantly on the degree of pre-deformation. Such a dependence is difficult to obtain theoretically [15], because before the area of the average preliminary plastic deformation of the material, the endurance limit reaches a minimum, and after it increases and can reach the indicators of an undeformed material. Thus, the very fact of the crack appearance, apparently, plays a major role in fatigue. Non-propagating cracks, even with a large preliminary plastic deformation, cause destruction only in rare cases. This is evident from the examples of damage to ship structures given in [1].

We take into account that $\delta_c = 0$ in the limit of plastic deformation, and use a linear approximation of the dependence $\delta_{1c}(\varepsilon)$:

$$\delta(\varepsilon) = \delta_{1c} - \left(\frac{\delta_{1c}}{\varepsilon_{max}}\right)\varepsilon. \tag{11}$$

At the crack tip, the CCO is determined from the known dependence of linear fracture mechanics:

$$\delta_{1c} = \lambda\left(\frac{K_{1c}^2}{E\sigma_т}\right). \tag{12}$$

Coefficient λ [12] is found from the formula:

$$\lambda = \frac{(1-2\mu)^2 E}{1.24\pi\sigma_т}\left(\frac{q\sigma_т}{R_{mce}D}\right)^{\frac{1}{m}+1}. \tag{13}$$

Here, $E$ — modulus of elasticity of the material; $R_{mce}$ — micro-cleavage stress of deformed material; $D$ — coefficient taking into account the increase in the first principal stress component for the case of a complex state; $q$ — coefficient showing the ratio of the second principal stress component to the first one; $m$ — hardening coefficient.

For the specified characteristics and coefficients, there are well-defined design dependences on the basic mechanical characteristics of the material. The critical stress intensity coefficient in (12) is calculated from the formula:

$$K_{1c} = \sqrt{\left(\frac{R_{mce}D}{q\sigma_т}\right)^{\frac{1}{m}+1}\sigma_т \cdot 6.18\pi d_z}, \tag{14}$$

where $d_z$ — average grain diameter of the raw material of the soft interlayer. Substitute the last expression and (13) in (12). Make the necessary reductions. Note that in (12) and (11), a small component of elastic deformations can be neglected. As a result, we get:

$$\delta_{1c}(\varepsilon) = 5(1-2\mu)^2 d_z\left(1 - \frac{\varepsilon\sigma_в}{100}\right). \tag{15}$$

Deformation ε is calculated from dependence (10). Let us find dependence $K_{1c}(\varepsilon)$. From (12), we have $K_{1c}(\varepsilon) = \sqrt{E\sigma_т\delta_{1c}(\varepsilon)/\lambda}$. Substitute the known expressions and get:

$$K_{1c}(\varepsilon) = \sqrt{\left(\frac{R_{mce}D}{q\sigma_{т}}\right)^{\frac{1}{m}+1} 6.18\pi d_z \sigma_{т}^2 \left(1 - \frac{\varepsilon\sigma_{в}}{100}\right)} \quad (16)$$

or

$$K_{1c}(\delta) = \sqrt{\frac{0{,}618\pi d_z 2}{\sigma_{т}^{\frac{1}{m}-1}(1-2\mu)^2}\left(\frac{R_{mce}D}{q}\right)^{\frac{1}{m}+1} \cdot \left(1 - \frac{\sigma_{в}}{100}\ln(1+\delta)\right)}. \quad (17)$$

After reduction, it is possible to obtain a simple dependence of the critical stress intensity coefficient $K_{1c}$ on the current value δ of the soft interlayer pulling:

$$K_{1c}(\delta) = K_c = K_{1c}\sqrt{1 - \frac{\sigma_{в}}{100}\ln(1+\delta)}, \quad (18)$$

where δ — elongation (pulling) of the soft interlayer material, fractions.

In formula (18), $K_{1c}(\delta)$ — crack resistance limit $K_c$. Its relative value $K_{1c}(\delta)/K_{1c}$ shows how the decrease in the fracture toughness of the material depends on the elongation (pulling) of the elementary region of the soft interlayer. For simplicity of calculations, the averaged elongation of the soft interlayer under the payload can be used. Note that the locality of plastic elongation in the welded joint of a soft interlayer at $\Delta h$ relative to $h$ can significantly affect its fatigue strength. For the hardened base material, this effect, on the contrary, will be insignificant

At $\delta = \delta_5$, ratio $K_c/K_{1c}$ should give zero, so we equate (18) to zero and write down the following calculation formula relative to δ:

$$\delta_5 = \exp(100/\sigma_{в}) - 1. \quad (19)$$

Here, $\sigma_{в}$ is substituted in MPa.

**Analysis of the results and verification of the adequacy of the dependences obtained.** It is possible to recognize satisfactory results of verification of the coordination of the design characteristics according to the obtained analytical dependences with reference data of structural hypopearlitic steels in the state of delivery. We are talking about thin-sheet rolled steel St10, St50, 22K, St3sp, 37HN3A, 30HGSA, etc. (Table 1).

Table 1

Design and reference characteristics of steels

| **Steel** | $\sigma_{в}$, **MPa** | $\sigma_{т}$, **MPa** | $m$ | $d_z$, μm | $\varphi_k$ | $K_{1c}, MPa\sqrt{m}$ | $\delta_5^*$,% | $\delta_5$,% |
|---|---|---|---|---|---|---|---|---|
| St10 | 320 | 190 | 0.17 | 66 | 0.73 | 103.6 | 36.6 | > 31 |
| 15G | 410 | 245 | 0.148 | 94 | 0.55 | 104 | 26.4 | 26 |
| St3sp | 450 | 270 | 0.16 | 37 | 0.71 | 101 | 24.8 | 25 |
| 22K | 540 | 310 | 0.16 | 30 | 0.69 | 97 | 20.3 | 22 ... 26 |
| St50 | 680 | 350 | 0.16 | 25 | 0.62 | 78 | 15.8 | 17 |
| 10HSND | 540 | 390 | 0.132** | 27 | 0.71 | – | 20.3 | 19 |
| 37HNZA | 1014 | 743 | 0.12 | 7 | 0.6 | 73.8 | 10.3 | 10 |
| 30HGSA | 1750 | 1360 | 0.09 | 3 | 0.44 | 53.2*** | 6 | 7 |
| 30 HGSA | 1470 | 1080 | 0.12 | 4 | 0.6 | 58.5[2]*** | 7 | 7 |
| *Calculation by (19); **calculation by $m = \{0.75 \cdot lg[\sigma_{в}(1 + 1.4\varphi_{к})/\sigma_{0.2}]\}/lg\left[10^5 \cdot ln\left(\frac{1}{1-\varphi_{к}}\right)/(200 + 0.5\sigma_{0.2})\right]$ [15]; ***calculation by (14). | | | | | | | | |

The analysis performed earlier [12] confirms that coefficient λ calculated from (13) at the CCO at the tip $0.618d_z$, is consistent with the experimental data for steels 22K and St10. In the first case, λ is 0.22, in the second — 0.23.

Let us consider the preliminary deformation of thin sheets in a plane stress with the condition that the grain receives relative elongation $e_z$ in the longitudinal direction. In this case, its average diameter in the same direction will be larger by $(1 + e_z)$ times, and in the transverse direction, it will decrease by $\left(\sqrt{1 + e_z}\right)$. That is, if the average

http://vestnik-donstu.ru

diameter increases in the longitudinal direction by 2.618 times, then in the transverse direction, it will decrease by 1.618 times. Here, the transverse direction coincides with the direction of movement of the crack. It is easy to see the linearity of the dependence from which the increase in the average grain diameter is determined. It follows, that with uniform uniaxial plastic deformation, the critical opening at the crack tip should also decrease linearly, depending on the relative elongation $e_z$. When rolling steel sheets, such a pronounced linear relationship is not detected. Obviously, this is due to transverse deformations, which are characterized by flattened grains.

Diagrams of the change of $K_{1c}$ as a function of δ for steels (Table 1) are shown in Fig. 2.

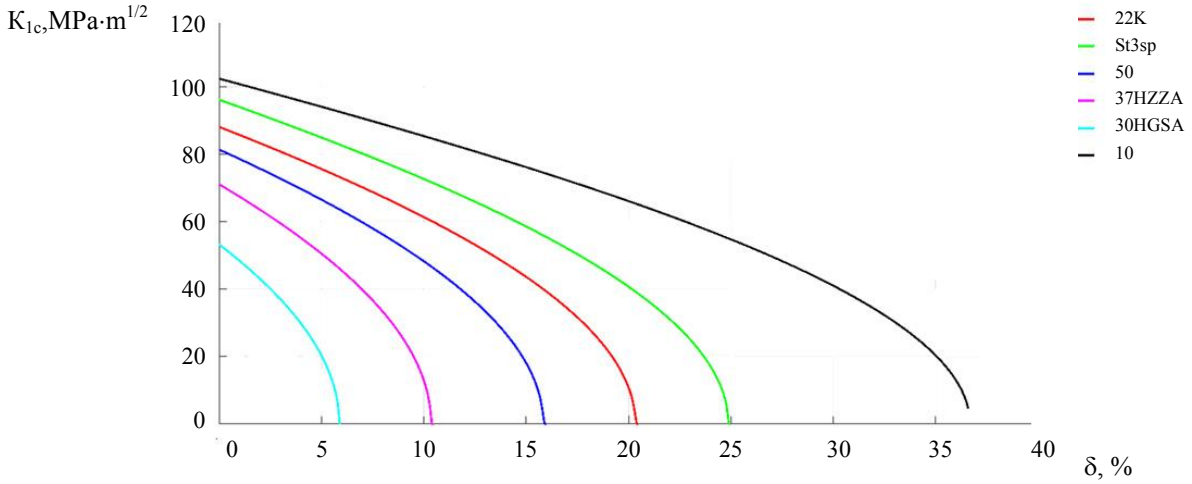


Fig. 2. Change in crack resistance depending on the preliminary elongation of steels

The critical intensity coefficient is calculated from (14) using the data in Table 1. This enables to determine the level of $K_{1c}$ under plastic deformation through pulling and compare it to the values of other steels. Thus, the comparison of 30HGSA steel treated to yield strength $\sigma_т = 1360$ MPa, and steel 10 shows that when using low-strength steel 10, level $K_{1c}$ can be reduced only with large elongation deformations (about 25 %). In practice, this happens quite rarely in constructions. However, with targeted pulling or cold rolling, a significant decrease in $K_{1c}$, is possible, and this should be taken into account.

If to rank steels according to the ultimate plasticity and compare maximum values of $K_{1c}$ for them, it turns out that plasticity decreases from one steel grade to another much faster than the critical stress intensity coefficient changes. So, $K_{1c}$ for 30HGSA and 10 steels, in the initial state of delivery differs by ~2 times, and relative elongation δ — by ~5 times. The appearance of plasticity in the tops of various stress concentrators is inevitable, therefore, to provide the necessary reliability of elements made of 30HGSA steel, it is advisable to control plastic deformations in the structure ~5 times more precisely. In addition, it should be taken into account that a decrease in viscosity by ~2 times will cause a decrease in the critical crack length by ~4 times. The reason is the low viscosity and ductility of 30HGSA steel, for whose operation it will be required to increase the safety factor by ~5 times. The latter does not mean that high-strength steels as a structural material are worse than medium-strength steels. The problem is in selecting the optimal combination of viscosity, ductility, and strength. The calculated dependences obtained in this analysis make it possible to evaluate these characteristics by calculation. This is important for the rational choice of material at the design stage, determining the optimal welding and heat treatment modes.

Let us compare the results of calculations according to (18) with the known dependence (7)[8] (fig. 2). The first function depends on the remaining ductility of the steel, and the second — on the relative length of the crack in the concept of the structural element. To conveniently present the results for their comparison, we introduce a

[8] Goldstein RV, Morozov NF. Ibid.

dimensionless parameter:

$$\eta^* = 1 - a/(a + d). \tag{20}$$

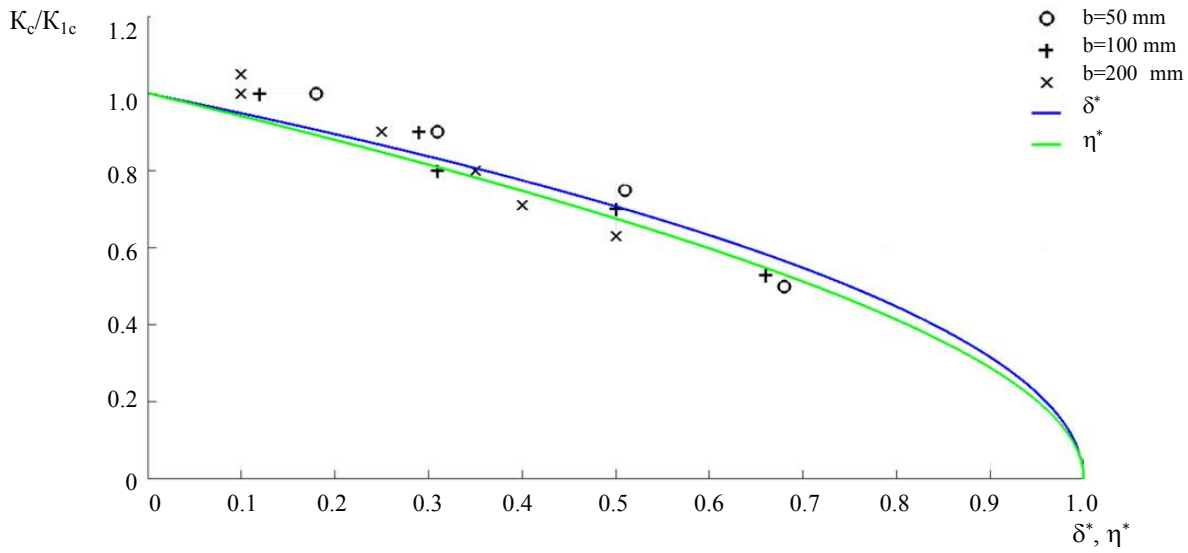


Fig. 3. Dependences of the relative crack resistance limit on the dimensionless parameter of the disc-shaped crack $\eta^*$ and on the dimensionless parameter of the preliminary uniform elongation of the material $\delta^*$. Lines are analytical dependences (7), (18). Markers are experimental data for compact sample[9] [11, 16] with dimensions $b$

After substituting (20) into (7), we obtain an invariant expression for the mean value. If we know $\eta^*$, then we can find the relation $a/(a + d)$ from (20). The comparison results show that the functions are almost the same. In relative coordinates, they are characterized by invariance with good approximation. Both functions well approximate the experimental data of the crack resistance limit obtained on the samples with characteristic dimensions $b$ [13].

Consider the conditions of plane deformation at the known critical crack length $L_c$. For hypopearlitic steels with $\sigma_т < 400$ MPa, it can be estimated approximately as $L_c = 2K_{1c}^2/\pi/\sigma_т^2$ , and it is easy to find the critical voltage of the external load $\sigma_c = K_c/\sqrt{\pi L_c}$:

$$\sigma_c = \sigma_т \sqrt{\frac{1}{2} - \frac{\sigma_в}{200}\ln(1 + \delta)}. \tag{21}$$

The equation reflects the law of reduction of critical stresses $\sigma_c$ below the value of the endurance limit of a material with crack length $L_c$ depending on the amount of preliminary elongation of the material. In the same formulation, the decrease in the critical crack length in the pre-deformed soft interlayer material can be estimated from the dependence:

$$L = \frac{1}{\pi}\left(\frac{K_{1c}}{\sigma}\right)^2 \left(1 - \frac{\sigma_в}{100}\ln(1 + \delta)\right), \tag{22}$$

where $L$ — half the length for through crack; $\sigma$ — critical stress for catastrophic crack propagation with length $L$.

At $\sigma = \sigma_{-1}$, it follows from (22) that length $L$ of the catastrophic crack propagation is directly proportional to the value $\left(1 - \frac{\sigma_в}{100}\ln(1 + \delta)\right)$ and the constant of the soft interlayer material $L_c$.

The obtained dependences in the system aggregate represent the proposed mathematical model for assessing the crack resistance of welded joints with soft interlayers.

**Discussion and Conclusions.** When welding heat-strengthened steels for hull and other sheet structures, soft interlayers are formed, the metal of which is plastically deformed in the first loading cycles. Numerical analysis

http://vestnik-donstu.ru



[9] Matokhin GV, Molokov KA. Ibid.

methods using CAE tools[10] can determine deformations or an increase in the width of the soft interlayer of the welded joint under the action of workloads. The reliability of the connection with a soft layer depends on the degree of plastic deformation, its hardening, stiffness of stress state with account of the boundary zones of the hard layers, and when a crack appears — on its critical length $L$. When pulling the soft interlayer, $L$ decreases in direct proportion to the constant of the soft interlayer material $L_c$ and the expression depending on the degree of pulling δ, i.e., on the relative pre-elongation.

A simple analytical dependence of the critical elongation to fracture is obtained (19). It provides calculation results that are in satisfactory agreement with experimental data for most structural steels (as of delivery). The formula provides estimating the reference characteristic $\delta_5$ of the sample by the only known parameter — the ultimate limit of strength. This dependence is characterized by a theoretical regularity that is in good agreement with the parameters of structural steels. However, in some cases (special heat treatment or tempering modes), it can give a relative error up to $\sim 30 - 40$ %.

Analytical dependence of the change in the crack resistance limit of a soft interlayer on its preliminary plastic deformation is proposed. Compared:

— calculated values of the crack resistance limit;

— experimental data obtained on compact test samples;

— earlier analytical solutions.

The comparison results convincingly prove the applicability of the proposed analytical solution. The effect of the law of reducing the crack resistance limit with relative preliminary plastic elongation up to destruction ($\delta_5$) and a change in parameter ($\eta^*$) of a pregrown crack in the material up to $L_c$ are studied. For this case, invariance in relative coordinates is established under the condition of plane deformation and the absence of the influence of the limited size of the sample or structure. Consideration of the limited size of samples and different loading schemes significantly changes the mentioned dependence[11] [13, 17].

The method proposed for estimating the crack resistance limit of welded elements with soft interlayers can be used in engineering calculations to minimize metal consumption, as well as for ship structures subjected to low-cycle fatigue.

**References**

1. Novikov VV, Turmov GP, Surov OE, et al. Povrezhdeniya i raschetnyi analiz prochnosti korabel'nykh konstruktsii. Vladivostok: DVFU; 2020. 266 p. (In Russ.)

2. Makhutov NA. Deformatsionnye kriterii razrusheniya i raschet ehlementov konstruktsii na prochnost'. Moscow: Mashinostroenie; 1981. 272 p. (In Russ.)

3. Gurevich LM, Trykov YuP, Ponomareva IA, et al. Komp'yuternoe modelirovanie kontaktnogo uprochneniya alyuminievoi prosloiki magnievo-alyuminievykh tsilindricheskikh sosudov. Vestnik SibGIU. 2015;14:12–16. (In Russ.)

4. Aymetov SF, Aymetov FG. The strength of butt joints weakened by soft interlayer under bending load. Bulletin of the South Ural State University. Series “Metallurgy”. 2015;15:107–112. (In Russ.)

5. Berg VI, Chekardovskiy MN, Yakubovskaya SV, et al. Influence of heterogeneity of mechanical properties of various zones of the welded butt joints work connections in elastic-plastic deformation stage. Modern Problems of Science and Education. 2015;2/3:28. URL: http://www.science-education.ru/ru/article/view?id=23518 (accessed: 11.02.2021). (In Russ.)

6. Kuliev VD, Zaitsev YV, Sultygova PS. Destruction laminates with a fatigue crack. News of the Kazan State University of Architecture and Engineering. 2014;29:162–166. (In Russ.)

[10]CAE (computer-aided engineering). This is the name of programs and software systems for solving engineering problems.

[11] Goldstein RV, Morozov NF. Ibid.

7. Molokov KA, Novikov VV, Turmov GP, et al. Estimation of reliability of ship structures with microcracks and residual welding stresses. Marine Intellectual Technologies. 2018;41:45–54. (In Russ.)

8. Molokov KA, Slavgorodskaya AV. The estimation of hypopearlitic steel damage under overloading. Marine Intellectual Technologies. 2013;2:56–58. (In Russ.)

9. Birdegulov LR, Shipachev AM. Research of crack resistance metals. Juvenis scientia. 2016;2:28–32. (In Russ.)

10. Asnis AE. Dinamicheskaya prochnost' svarnykh soedinenii iz malouglerodistoi i nizkolegirovannoi stalei. Moscow; Kiev: Mashgiz; 1962. 171 p. (In Russ.)

11. Matvienko YuG. Dvukhparametricheskaya mekhanika razrusheniya. Moscow: Fizmatlit; 2021. 208 p. (In Russ.)

12. Matokhin GV. Otsenka resursa svarnykh konstruktsii iz ferrito-perlitnykh stalei. Vladivostok: DVGTU; 2001. 202 p. (In Russ.)

13. Makhutov NA, ed. Prochnost', resurs, zhivuchest' i bezopasnost' mashin. Moscow: Librokom; 2008. 576 p. (In Russ.)

14. Gol'tsev VYu, Zelenskii AV, Kudryavtsev OG, et al. Zony lokalizatsii plasticheskoi deformatsii v predvaritel'no deformirovannykh tonkolistovykh plastichnykh materialakh. In: Issledovanie prochnosti materialov i konstruktsii atomnoi tekhniki. Moscow: Ehnergoatomizdat; 1984. P. 68–73. (In Russ.)

15. Makhutov NA, Frolov KV, Gadenin MM, et al. Nauchnye osnovy povysheniya malotsiklovoi prochnosti. Makhutov NA, ed. Moscow: Nauka; 2006. 623 p. (In Russ.)

16. Sosnovskii LA, Bogdanovich AV. Treshchinostoikost'. Gomel: BeLGUT; 2011. 366 p. (In Russ.)

17. Molokov KA, Novikov VV, Turmov GP, et al. Matematicheskie modeli otsenki ehkspluatatsionnogo resursa i rabotosposobnosti sudovykh svarnykh konstruktsii. Vladivostok: Far Eastern Federal University; 2021. 240 p. (In Russ.)

Received 20.09.2021
Revised 27.10.2021
Accepted 27.10.2021

*About the Authors:*

**Molokov, Konstantin A.,** associate professor of the Department of Industrial Safety, Polytechnic Institute, Far Eastern Federal University (8, Sukhanova St., Vladivostok, 690090, RF), associate professor of the Department of Information Technologies and Systems, Vladivostok State University of Economics and Service (41, Gogolya St., Vladivostok, 690014, RF), Cand.Sci. (Eng.), Scopus, ORCID, Researcher, Spektrum011277@gmail.com.

**Novikov, Valerii V.,** associate professor of the Department of Marine Engineering and Transport, Polytechnic Institute, Far Eastern Federal University (8, Sukhanova St., Vladivostok, 690090, RF), Cand.Sci. (Eng.), Scopus, ORCID, leka1551@rambler.ru.

*Claimed contributorship*

K. A. Molokov: basic concept formulation; research objectives and tasks; computational analysis; text preparation; formulation of conclusions. V. V. Novikov: academic advising; analysis of the research results; revision of the conclusions; correction of the text.

*All authors have read and approved the final manuscript.*

# MACHINE BUILDING AND MACHINE SCIENCE

UDC 678.549

https://doi.org/10.23947/2687-1653-2021-21-4-319-327

## Liquid temperature effect on the hydraulic shock wave velocity in polyethylene pipes

**I. R. Antypas**[1], **A.G. Dyachenko**[1], **Saed Bakir Imad**[2]

[1] Don State Technical University (Rostov-on-Don, Russian Federation)

[2] University of Aleppo (Aleppo, Syria)

✉ Imad.antypas@mail.ru

***Introduction.*** Providing people with high quality drinking water has always come first. However, its transportation through pipeline systems was often associated with some problems, such as the temperature of the water and the environment, as well as the possibility of water hammer on certain pipe sections. This was especially true for systems that use polyethylene pipes. Temperature is a key factor affecting the flexibility properties of polyethylene pipes, and it affects not only the design, but also the investment in the development of water supply networks. The purpose of these studies was to study the effect of water and ambient temperature on the density, properties of the pipe material and the speed of propagation of a hydraulic shock wave in polyethylene pipes.

***Materials and Methods.*** In the experiments performed, the method of field research was used, when tests are carried out on specialized equipment on samples specially made for the pursued purposes. Here, samples of high-density polyethylene pipes were used, which were subjected to tensile tests on a tensile testing machine, and each experiment was carried out three times.

In the course of the experiments, the samples were exposed to certain temperature regimes (both external and internal), while the influence of the hydrodynamic pressure of the liquid in the pipe was also investigated, as a result of the change in time of the liquid velocity in its sections. To do this, the samples were supplied with liquid under a certain pressure in order to find out the influence on the pipes of an effect known as water hammer.

***Results.*** In the course of the research, it was found that the value of the elastic modulus of high-density polyethylene PE100 decreases with increasing water temperature, and the decrease at a temperature of 60° C reaches 60.21 % compared to its value at a water temperature of +4° C. Based on the results of experiments to determine the effect of the elastic modulus of polyethylene with increasing temperature, an exponential equation was derived to calculate the value of the polyethylene coefficient as a function of time $E = 1.312e^{-0,01t}$ with the correlation coefficient $R^2 = 0.988$; and based on the results of the studies carried out to calculate the value of the propagation velocity of a hydraulic shock wave, an exponential equation was derived as a function of time $C = 275.9e^{-0,01t}$ with the coefficient correlation $R^2 = 0.987$.

***Discussion and Conclusions.*** In the course of the research, it was found that such a phenomenon as water hammer has a harmful effect on the pipe walls, which, if possible, should be avoided even at the design stage of the water supply network. During the experiments, it was found that with an increase in temperature, the values of the elastic modulus of polyethylene decreased with a simultaneous decrease in the values of the propagation velocity of the hydraulic shock wave.

***Keywords:*** polyethylene pipes, temperature range, water hammer.

***For citation:*** I. R. Antypas, A. G. Dyachenko, Saed Bakir Imad. Liquid temperature effect on the hydraulic shock wave velocity in polyethylene pipes. Advanced Engineering Research, 2021, vol. 21, no. 4, pp. 319–327. https://doi.org/10.23947/2687-1653-2021-21-4-319-327

*© Antypas I. R., Dyachenko A.G., Saed Bakir Imad, 2021*

**Introduction.** The temperature of the liquid flow and the ambient temperature have a significant impact on the properties of the material of pipes made of high-density polyethylene. As the temperature increases, the pipe material becomes more flexible, which causes a decrease in the hydraulic shock wave propagation velocity, and hence, a decrease in pressure. Manufactured polyethylene pipes made of PE100 (HDPE) are thermoplastics since their plasticity varies within the appropriate limits depending on the operating conditions. These plastics have a number of advantages, including a relatively small specific gravity, they make it possible to work at low temperatures, are able to withstand moderate pressure, have high corrosion resistance (specifically, to acids and alkalis), good electrical insulation properties, are easily painted, and easy to install. They are made immediately in large lengths which reduces the number of connecting elements during their laying; these elements are considered expensive and fragile and cause problems associated with leaks [1–6]. Polyethylene pipes are hydraulically smooth pipes in which the loss of friction energy during the liquid flow is much less than in metal pipes, which leads to saving pumping energy. These pipes are characterized by a very small roughness range (k=0.001-0.008 mm), which is 3-20 times less than the roughness of new steel pipes. Temperature is one of the most important factors affecting the flexibility properties of polyethylene pipes, and this factor not only affects the design and investment in various drinking water supply networks with flow stability, but also causes its unstable flow in the form of a water hammer in polyethylene pipes [7–10]. International standards define the properties of polyethylene pipes in drinking water supply networks at a temperature of 20-23 °C, while the European standards define them at a temperature of 10 °C. At low flow temperatures, the elastic modulus of polyethylene pipes is relatively large compared to high flow temperatures in case of the water hammer phenomenon, which can have a significant impact on the walls of polyethylene pipes in drinking water supply networks [11–14]. The objective of these studies is to explore the influence of liquid temperature and air temperature surrounding polyethylene pipes on the density, other properties of the pipe material, and on the hydraulic shock wave propagation velocity in them.

**Research methods and materials. Water hammer.** A water hammer is an increase or decrease in the hydrodynamic pressure of a liquid in a pipe as a result of a change in the liquid velocity in its section. This impact can create high pressure, which must be taken into account when calculating the wall thickness of the pipe. The liquid compressibility and the tendency of pipe walls to deform give the water hammer elasticity, since it is presented as pressure waves propagating through the pipe in an unstable flow. There are two types of water hammer:

1. Direct water hammer is dangerous and occurs when the stopping time is less than the hydraulic wave period, $t_C < t_0$.

2. Indirect water hammer, which is not dangerous and is triggered when the shutdown time is longer than the hydraulic wave period, $t_C > t_0$:

http://vestnik-donstu.ru

$$t_0 = 2L / C_j, \quad (1)$$

where $t_0$ — the hydraulic wave period, s; $L$ — the pipe length, m; $C_j$ — the hydraulic shock wave propagation velocity, m/s; $t_C$ — the valve closing or opening time, s.

Direct water hammer occurs when a valve connected to the wide surface of the tank suddenly opens or closes at the end of the pipe, or the power supply to the pumping station suddenly stops. The pressure change as a result of direct water hammer is determined from the Joukowski-Levy ratio:

$$\Delta P_{\max} = \rho_j \cdot C_j \cdot V_0, \quad (2)$$

where $\Delta P_{\max}$ — variation value of high or low pressure, N/m$^2$;

$\rho_j$ — liquid density at steady flow rate, kg/m$^3$;

$C_j$ — hydraulic shock wave propagation velocity, m/s;

$V_0$ — steady-state velocity of liquid flow in the pipe, m/s.

As for indirect water hammer, it occurs when the valve is slowly opened or closed at the end of the pipe connected to the wide surface of the tank, or when the shutdown time of the pumping group at the pumping station increases. The variation value of the pressure as a result of indirect water hammer is determined from the following ratio:

$$\Delta P_{\max} = 2\rho_j \cdot L \cdot V_0 / RT_c. \quad (3)$$

Value $C_j$ is determined from the following ratio of the hydraulic shock wave propagation velocity in polyethylene pipes:

$$C_j = \frac{\sqrt{\frac{E_{0j}}{\rho_j}}}{\sqrt{1 + \frac{D}{e} \cdot \frac{E_{0j}}{E_j} M}}, \quad (4)$$

where $M$ — constant consolidation at $D/e > 40$

— for support on one side of the pipe

$M = 1.25 - \mu$,

$M = 1 - \mu / 2$;

— to support the entire pipe

$M = 1 - \mu^2$;

— for pipes without support (expansion joints)

$M = 1$,

where $\mu$ — Poisson's modulus is 0.45 for HDPE pipes [3–4]; $E_{0j}$ — water elasticity coefficient, N/m$^2$; $\rho_j$ — water density, kg/m$^3$; $D$ — pipe inner diameter, m.

The hydraulic shock wave propagation velocity in polyethylene pipes is in the range of 180–370 m/s [1, 9]. Table 1 presents data on the physical properties of water at atmospheric pressure on its surface. Figure 1 shows a

decrease in the water density with an increase in temperature, and Figure 2 shows an increase in the value of the elastic modulus of water with an increase in its temperature.

Table 1

Physical properties of water at atmospheric pressure on its surface

| **Temperature, °C** | **0** | **4** | **10** | **20** | **30** | **40** | **50** | **60** |
|---|---|---|---|---|---|---|---|---|
| Water density, kg/m$^3$ | 999.8 | 1000 | 999.7 | 998.2 | 995.7 | 992.2 | 988 | 983.2 |
| Modulus of elasticity of water, GN/m$^2$ | 2.02 | 2.06 | 2.1 | 2.18 | 2.25 | 2.28 | 2.29 | 2.28 |

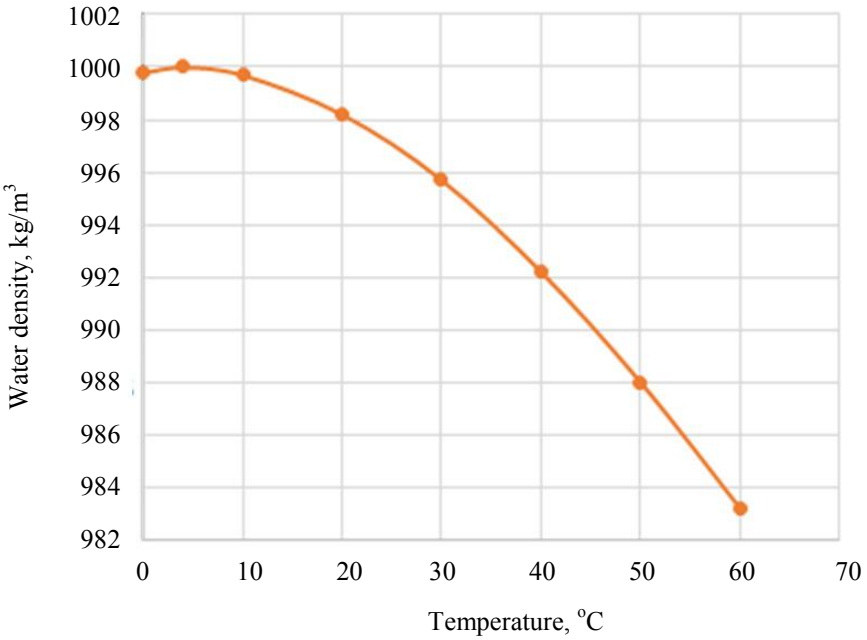


Fig. 1. Change in water density with increasing temperature

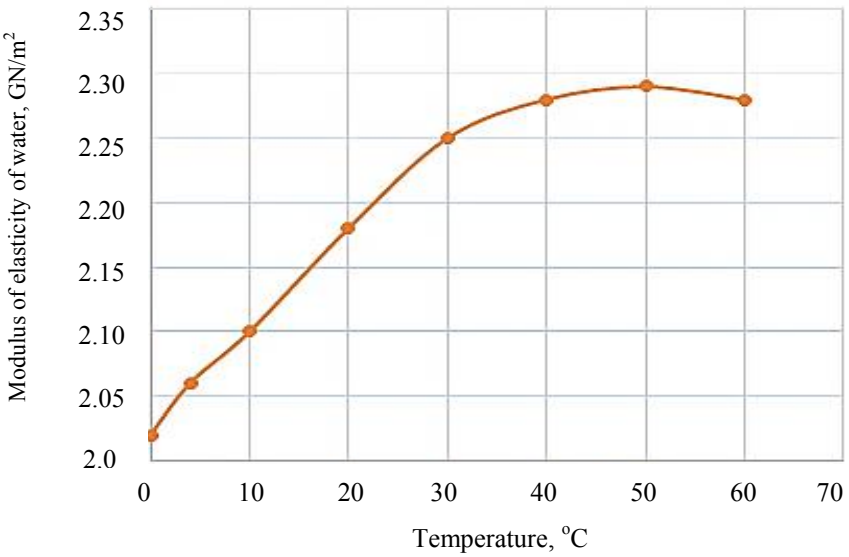


Fig. 2. Dependence of the water elastic modulus values on temperature

Table 2 shows the elastic modulus of the polyethylene pipe material at 16 °C [2, 10].

http://vestnik-donstu.ru

Table 2

Elastic modulus of the polyethylene pipe material at 16 °C

| **Elastic modulus of polyethylene, lb/in$^2$** | **Elastic modulus of polyethylene, MN/m$^2$** | **Elastic modulus of polyethylene, lb/ft$^2$** |
|---|---|---|
| 150,000 | 1,030 | 22,000,000 |

**Laboratory experiments.** 21 samples in the form of pipes were obtained from one large high-density HDPE polyethylene pipe, some of the characteristics of which are given in Table 3.

Table 3

Specifications of HDPE pipes

| **D, mm** | **$e_{min}$, mm** | **$e_{max}$, mm** | **PE** | **SDR** | **PN, MPa** |
|---|---|---|---|---|---|
| 110 | 6.6 | 7.4 | 100 | 17 | 1 |

To conduct the research, the following actions were performed:

— for each of the specified temperatures, three tensile samples (type 1) were used, and their average value was taken;

— temperature range in 4, 10, 20, 30, 40, 50, 60 °C was accepted;

— the tensile samples were heated in accordance with the temperature for one hour in a digital electric furnace, they were then stretched using a special device, the results are shown in Table 4 and in Fig. 3;

— a plastic tube with a diameter of 10 mm was injected with water, whose temperature corresponded to previously specified range, up to the point of rupture, and then relative deformation $\varepsilon = \Delta D / D$ was measured, the results are shown in Table 4.

The results of polyethylene samples were taken for a year for a pipe with an external diameter of 110 mm at a nominal pressure of 10 Bar. The results obtained were constantly compared to changes in laboratory temperatures during a year. They are presented in Table 5 and in Fig. 4.

Table 4

Maximum values of elastic tensile stresses and relative deformation of polyethylene samples in accordance with specified temperatures

| **Temperature,$^0$C** | **4** | **10** | **20** | **30** | **40** | **50** | **60** |
|---|---|---|---|---|---|---|---|
| Average values of elastic stresses, MPa | 29.576 | 26.074 | 23.656 | 22.340 | 19.716 | 18.426 | 17.229 |
| Relative deformation $\varepsilon = \Delta D / D$ | 0.0218 | 0.0226 | 0.0256 | 0.0275 | 0.0293 | 0.0306 | 0.0319 |

Table 5

Maximum variation values of elastic tensile stresses for polyethylene samples depending on temperature variation during the year

| **Months** | **January** | **February** | **March** | **April** | **May** | **June** |
|---|---|---|---|---|---|---|
| Elastic stresses, MPa | 28.16 | 31.30 | 26.49 | 26.01 | 24.71 | 24.64 |
| Months | July | August | September | October | November | December |
| Elastic stresses, MPa | 23.32 | 22.02 | 24.20 | 24.27 | 25.40 | 27.57 |

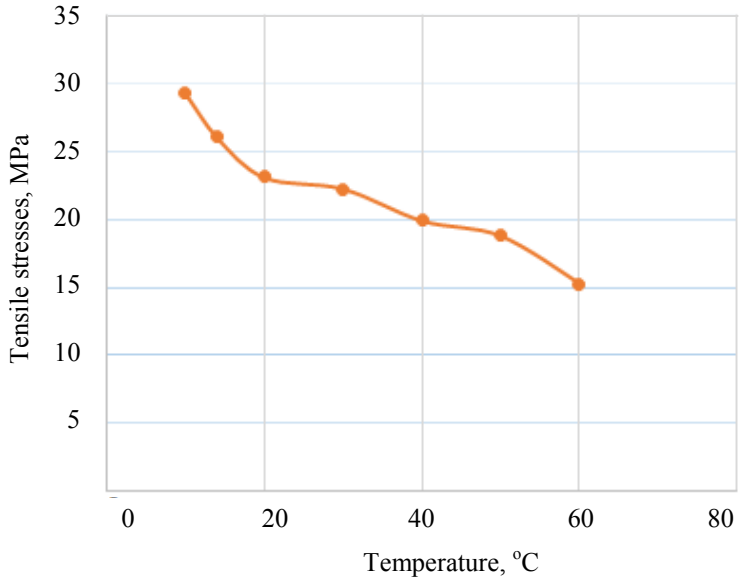


Fig. 3. Tensile stresses of polyethylene with increasing temperature

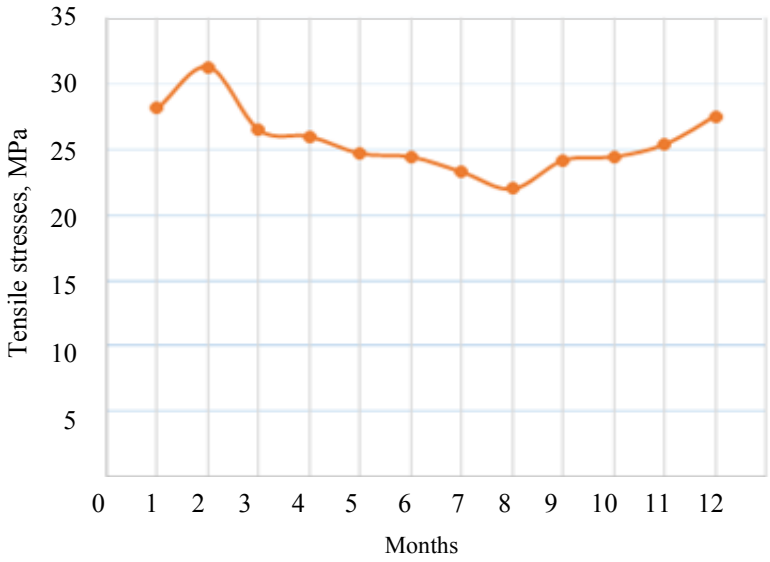


Fig. 4. Tensile stress values of polyethylene samples during the year

**Results.** The results were processed according to Hooke 's law as follows:

$$\varepsilon = \Delta D / D = \sigma / E , \quad (5)$$

where $\sigma$ — tensile stress in the pipe wall, MPa; $D$ — pipe diameter, mm; $\Delta D$ — change in pipe diameter, mm; $E$ — pipe material elasticity expressed by Young's modulus, MPa; $\varepsilon$ — relative deformation.

Table 6 shows the elastic modulus values of PE 100 polyethylene and the hydraulic shock wave propagation velocity at the specified temperatures.

Figure 5 shows a decrease in the value of the elastic modulus of polyethylene with an increase in temperature, and Figure 6 shows a decrease in the value of the hydraulic shock wave propagation velocity with an increase in temperature.

http://vestnik-donstu.ru

Table 6

Values of elastic modulus of PE 100 polyethylene and hydraulic shock wave propagation velocity at specified temperatures

| **Temperature (°C)** | **4** | **10** | **20** | **30** | **40** | **50** | **60** |
|---|---|---|---|---|---|---|---|
| Elastic modulus, E (MPa) | 1,357 | 1,154 | 924 | 812 | 673 | 602 | 540 |
| Hydraulic shock wave propagation velocity, C (m/s) | 280 | 259 | 233 | 219 | 200 | 190 | 180 |

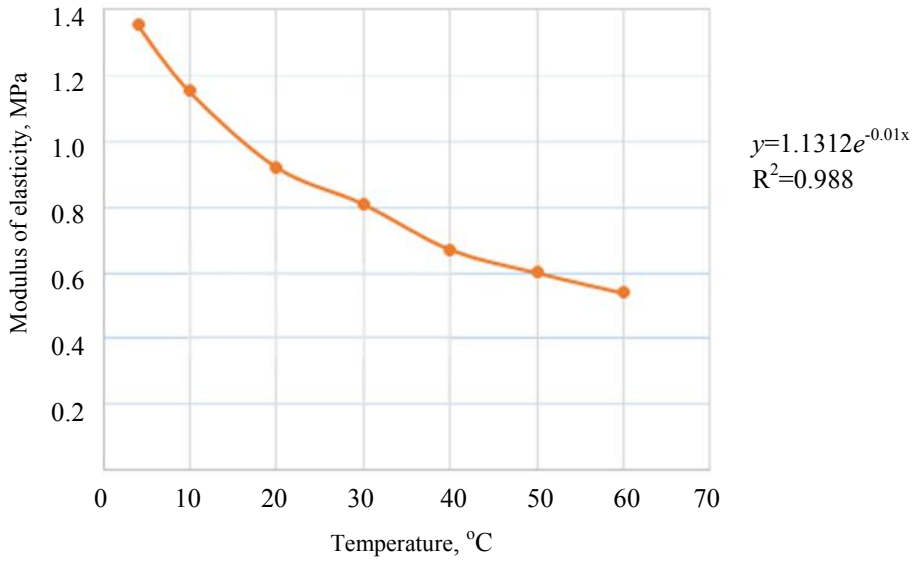


Fig. 5. Values of the elastic modulus of polyethylene with increasing temperature

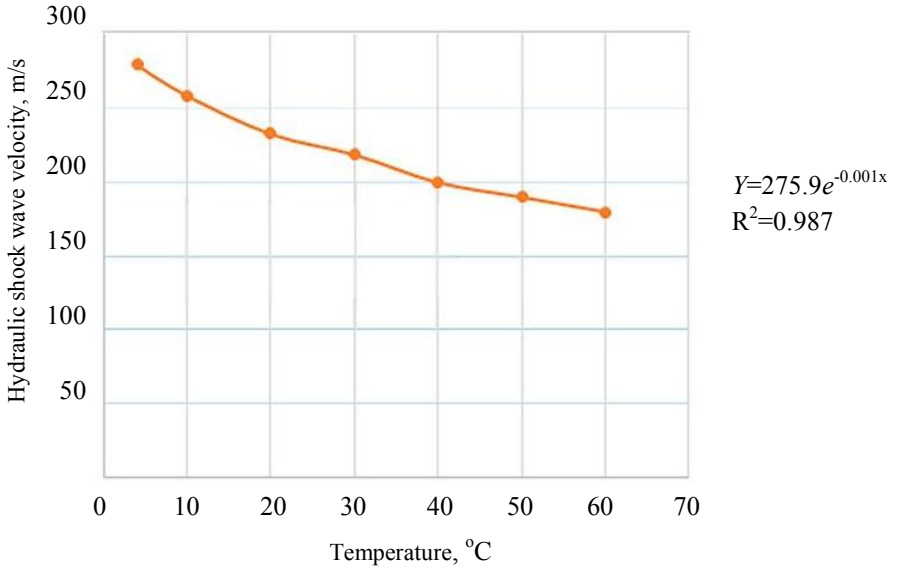


Fig. 6. Values of the hydraulic shock wave propagation velocity with increasing temperature

**Discussion and Conclusions.** After analyzing the results obtained in the course of research, we can draw the following conclusions:

— high water temperature has a significant impact on the properties of the material of pipes made of high-density polyethylene PE 100 and on the hydraulic properties of the hydraulic shock wave;

— the value of the elastic modulus of high-density polyethylene PE 100 decreases with increasing water temperature, and the value of the decrease at a temperature of 60 °C reaches 60.21% compared to its value at a water temperature of +4 °C. This decrease is relatively large and causes a significant decrease in the values of the hydraulic

shock wave propagation velocity, and the magnitude of the decrease reaches 35.71% compared to its value at a water temperature of +4 °C, which leads to a noticeable decrease in the value of the maximum pressure change as a result of water hammer, taking into account the density of water and its elasticity coefficient depending on temperature. When calculating the value of the hydraulic shock wave propagation velocity, the ratings of the maximum pressure change is also taken into account;

— based on the data obtained (shown in Fig. 5), an exponential equation was derived to calculate the value of the polyethylene coefficient as a function of time $E = 1.312e^{-0.01t}$ with correlation coefficient $R^2 = 0.988$;

— according to the data given in Figure 6, an exponential equation was derived to calculate the value of the hydraulic shock wave propagation velocity as a function of time $C = 275.9e^{-0.01t}$ with correlation coefficient $R^2 = 0.987$.

**References**

1. Li Chao, Wang Yan Jun, Qin Ke, et al. The Research Status of the Wetting of Metal/Ceramic in the High Temperature Self-Lubricating Materials. International Journal of Materials Science and Applications. 2016;5:108–112. http://dx.doi.org/10.11648/j.ijmsa.20160502.22

2. Amer Karnoub, Hajian Huang, Imad Antypas. Investigation of the impact behavior for composite materials reinforced by glass fibers. Journal of Physics: Conference Series. Engineering and Innovative Technologies. 2020;1515:042081. http://dx.doi.org/10.1088/1742-6596/1515/4/042081

3. Antypas IR. The influence of polyethylene processing on the plastic containers blowing. Journal of Physics: Conference Series. 2020;1515:042042. https://doi.org/10.1088/1742-6596/1515/4/042042

4. Qingquan Lai, Lei Zhang, Eustathopoulos N. Enhanced wetting of dual-phase metallic solids by liquid metals: A new effect of interfacial reaction. Acta Materialia. 2013;61:4127–4134. http://dx.doi.org/10.1016/j.actamat.2013.03.039

5. Alfons Buekens, Jie Yang. Recycling of WEEE plastics: a review. Journal of Material Cycle and Waste Management. 201;16:415−434.

6. Antypas IR. Improvement of mechanical behavior of neoprene rubber by means of glass fiber. Journal of Physics: Conference Series. Engineering and Innovative Technologies. 2021;1889:042007.

7. Wuyi Wan, Wenrui Huang, Cong Li. Sensitivity analysis for the resistance on the performance of a pressure vessel for water hammer protection. Journal of Pressure Vessel Technology. 2014;136:011303. https://doi.org/10.1115/1.4025829

8. Yan Gao, Fusheng Sui, Jennifer M. Muggleton, et al. Simplified dispersion relationships for fluid-dominated axisymmetric wave motion in buried fluid-filled pipes. Journal of Sound and Vibration. 2016;375:386–402. https://doi.org/10.1016/j.jsv.2016.04.012

9. Jinzhe Gong, Martin F. Lambert, Si T. N. Nguyen, et al. Detecting thinner-walled pipe sections using a spark transient pressure wave generator. Journal of Hydraulic Engineering. 2018;144:1–8. 10.1061/(ASCE)HY.1943-7900.0001409

10. Lars-Eric Janson. Plastics pipes for water supply and sewage disposal. Stockholm: Borealis; 2003. 404 p.

11. John Twyman. Wave Speed Calculation For Water Hammer Analysis. Obras y Proyectos. 2016;20:86-92.

12. Espinoza-Moreno G, Begovich O. Effect of the Temperature in Negative Pressure Wave Methods for Real Time Leak Location Applied to Plastic Water Pipelines. In: Memorias del XVI Congreso Latinoamericano de Control Automático, CLCA. Mexico: Cancún, Quintana Roo; 2014. P. 564–569.

13. Andrew Chadwick, John Morfett, Martin Borthwick. Hydraulics in civil and environmental engineering. CRC Press, 2021. 652 p. http://dx.doi.org/10.1061/(ASCE)0733-9429(2000)126:9(724)

14. Wei-Li Wu, Yi-Wen Wang. High density polyethylene film toughened with polypropylene and linear low density polyethylene. Materials Letters. 2019;257:126689. https://doi.org/10.1016/j.matlet.2019.126689

Received 04.10.2021
Revised 25.10.2021
Accepted 26.10.2021

*About the Authors:*

**Antypas, Imad Rizakalla,** associate professor of the Machine Design Principles Department, Don State Technical University (1, Gagarin sq., Rostov-on-Don, 344003, RF), Cand.Sci. (Eng.), associate professor, Scopus, Researcher, ORCID, imad.antypas@mail.ru

**Dyachenko, Alexey G.,** associate professor of the Machine Design Principles Department, Don State Technical University (1, Gagarin sq., Rostov-on-Don, 344003, RF), Cand.Sci. (Eng.), Scopus, ORCID, alexey-a2@mail.ru

**Saed Bakir Imad,** associate professor of the Agricultural Engineering Department, University of Aleppo (Mouhafaza, Aleppo, Syrian Arab Republic), Dr.Sci. (Eng.), associate professor, ORCID, bakir-111@mail.ru

*Claimed contributorship*

I. R. Antypas and Saed Bakir Imad: academic advising; problem statement; definition of research methodology; collection and analysis of analytical and practical materials on the research topic; critical analysis and finalization of the solution; computer implementation of the problem solution. A. G. Dyachenko: analysis of scientific sources on the research topic; critical analysis and revision of the text.

*All authors have read and approved the final manuscript*.

# MACHINE BUILDING AND MACHINE SCIENCE

UDC 620.179.17 https://doi.org/10.23947/2687-1653-2021-21-4-328-336

## Application and evaluation of the technical condition of composite materials in aircraft and unmanned aerial vehicles by acoustic emission method of nondestructive testing

**A. V. Popov** ✉, **A. O. Samuylov**, **I. S. Cherepanov**
Military Educational and Scientific Center of the Air Force "N.E. Zhukovsky and Y.A. Gagarin Air Force Academy" (Voronezh, Russian Federation)
✉ veselova.27@icloud.com

***Introduction.*** The paper analyzes the application of composite materials as the main determining method of reducing the mass of the airframe and an unmanned aerial vehicle. Advanced nondestructive testing methods provide assessing the technical condition of these materials, as well as determining stress concentrators on the airframe and an unmanned aerial vehicle with high accuracy in order to make a decision on the further operation of this object under control. The objective of the work was to increase the accuracy and efficiency of the assessment of crack resistance of composite materials through the acoustic emission control.

***Materials and Methods.*** This paper presents the nomenclature of composite materials used in the construction of various aircraft, including unmanned aerial vehicles. The most possible probable defects of these materials due to the influence of operational factors are presented. The applied methods of nondestructive testing of composite material and selection of the most suitable one according to specific advantages were compared. An experiment was carried out to determine the strength limits of carbon fiber using a hardware and software complex by acoustic emission method. The research results are presented in the form of drawings projected by the hardware and software complex.

***Results.*** The application of the acoustic-emission method of composite material control is described.

***Discussion and Conclusions.*** The results obtained experimentally can be used in the process of determining the strength limits of various composite materials by the acoustic emission method of nondestructive testing to assess the technical condition in mechanical engineering, shipbuilding, and aircraft construction. The paper is recommended to researchers involved in the design of aircraft and unmanned aerial vehicles.

***Keywords***: composite material, fiberglass, boron-fiber reinforced plastic, carbon fiber, organoplastics, aircraft, unmanned aerial vehicle, non-destructive testing, acoustic emission control, X-ray control, thermal control.

***For citation:*** A. V. Popov, A. O. Samuylov, I. S. Cherepanov. Application and evaluation of the technical condition of composite materials in aircraft and unmanned aerial vehicles by acoustic emission method of nondestructive testing. Advanced Engineering Research, 2021, vol. 21, no. 4, pp. 328–336. https://doi.org/10.23947/2687-1653-2021-21-4-328-336

*© Popov A. V., Samuylov A. O., Cherepanov I. S., 2021*

**Introduction.** The development of modern aviation technology (AT) is accompanied by the creation of new structural composite materials (CM) with promising mechanical and physical properties. Reducing the takeoff weight is an essential task for the aviation industry. The airframe design of most modern aircraft is made by 53 % of CM, and unmanned aerial vehicles (UAV) — by 90 %. Based on this, there is a need to assess the CM technical condition of the

airframe by radiation, thermal, acoustic emission (AE) methods of the nondestructive testing (NDT). A specific feature of the acoustic emission method is the ability to assess the development of various defects.

The objective of the study was to increase the accuracy and efficiency of the assessment of crack resistance of composite materials through the acoustic emission control.

Composite material is man-made material obtained through combining heterogeneous components into one structure, and characterized by better properties compared to the properties of each of the components.

CM has the following distinctive features:

– projected composition and shape;

– absence of analogue in nature;

– the composition is specified by a set of *n* components;

– CM properties are determined by the properties of the components;

– "service properties" — each separate component does not have such properties;

– microscale heterogeneity;

– macroscale heterogeneity.

Major advantages and disadvantages of CM are given in Table 1:

Table 1

**Major advantages and disadvantages of CM**

| No. | Advantages | Disadvantages |
|---|---|---|
| 1 | Low density (ρ = 1.35–4.8 g/cm$^3$) | Complex technology of obtaining |
| 2 | High strength ( $\sigma_в$ = 1,750 MPa) | High cost |
| 3 | High stiffness (E = 270,000 MPa) | Low bond strength of fibers with matrix |
| 4 | Heat resistance | Low erosion resistance and destruction |
| 5 | Thermal stability | |

Figure 1 shows the main materials used in the aircraft industry [1].

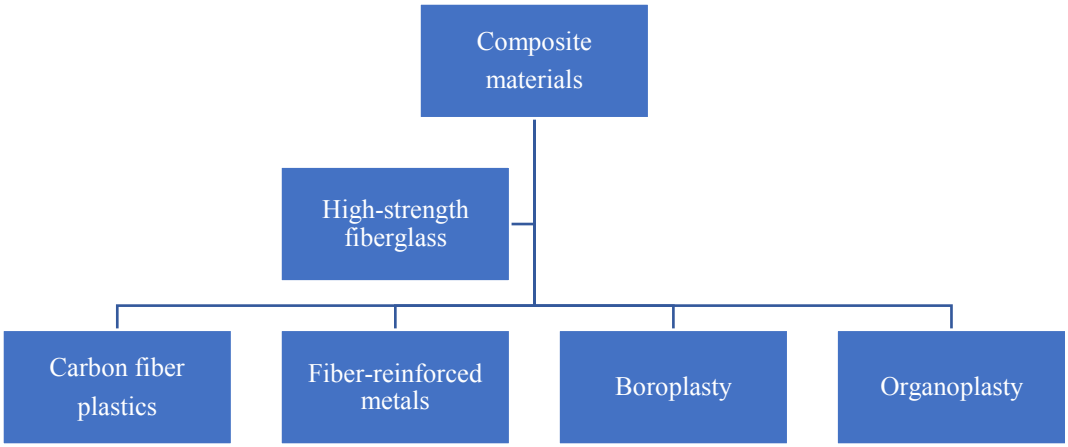


Fig. 1. CM classification

**Materials and Methods**

*High-strength fiberglass*

Fiberglass is CM consisting of a polymer matrix and a fiberglass filler, in which gaseous inclusions are present. The application of fiberglass for various purposes is increasing. This is due to the low cost and availability of raw materials, low energy consumption of glass fiber production, versatility, the possibility of regulation within a wide range of physical and mechanical properties, the possibility of creating hybrid materials and structures based on them. Fiberglass products can undergo all types of mechanical processing. The main examples of fiberglass used in the

creation of aircraft and UAV include CAST-V sheet, VFT-S, ST-911-1A, SK-9FA, STM-F sealed, VPS-19M sealed [2, 3].

*Carbon fiber plastics*

Carbon fiber plastics are CM consisting of a binder and hardeners in the form of carbon fibers, threads, bundles, tapes, or fabrics. Various epoxy or phenol-formaldehyde resins act as binders. The main brands of carbon fiber plastics are CMU-1, CMU-1U, CMU-1B, CMU-1L, CMU-2L, CMU-3L, CMU-3, CMU-4L, CMU-4E, CMU-6-41.

*Boroplasty*

Boron-fiber reinforced plastic is CM that consists of a polymer binder and a hardener — boron fibers. Epoxy and polyamide binders are used as a matrix, and boron filaments or complex boron fiberglass threads are used as hardeners. The use of boron fiberglass threads facilitates the technological process of manufacturing boroplasty. These include CMB-1, CM-1M, CM-1K, MB-2K, MB-3K.

*Organoplastics*

Organoplastics are CM in which fibrous fillers act as a reinforcing filler. Synthetic fibers have good textile properties. A wide range of various structures can be obtained from them: threads, bundles, ribbons, combined fabrics. Synthetic fibers have a light loss of strength under textile processing. They are insensitive to damage. Examples of organoplastics include 7T, 7T0, 5T, 9T, 6 TKS, 6 TKB, 7 TKS, 8 TKS.

*Fiber-reinforced metals*

Fiber-reinforced metals are CM in which boron fibers, carbon fibers, and filamentous crystals of refractory compounds act as a hardener. Various metals and alloys with characteristic plasticity are used as a matrix.

Examples of such materials include aluminum-boron fiber (VCA-1A), aluminum-carbon fiber (VCU-1), magnesium-boron fiber (VCM-1), magnesium-carbon fiber, nickel-tungsten wire (VCN-1).

The volumes of CM used in the airframe design of an advanced aircraft are different, and they are: wing — 80%, tail — 81%, fuselage — 31%, pylon — 34%, landing gear — 23%. The controls of Il-96-300 aircraft, the rotor blades of Mi-28 helicopter, the airframe of MS-21 aircraft are partially made of CM.

The volume of CM of the UAV airframe reaches 90%. Vivid examples are “Krunk”, “Dozor-600”, “Inokhodets”.

The use of CM in the airframe of aircraft and UAV can significantly lighten their weight. According to formulas (1), (2), it is possible to determine the change in the airframe mass when using CM in it:

$$\Delta m_{\text{пл}} = m_{\text{пл}}^{\text{т}} - m_{\text{пл}}^{\text{к}} = \left(\sum_{i=1}^{n} m_{\text{пл}_i}^{\text{т}} + \Delta m\right) - \left(\sum_{i=1}^{n} m_{\text{пл}_i}^{\text{т}} - \sum_{i=1}^{n} \varphi_i(1-\varepsilon_i)\right) m_{\text{пл}_i}^{\text{т}} + \Delta m \quad (1)$$

$$\Delta m_{\text{пл}} = \sum_{i=1}^{n} \varphi_i(1-\varepsilon_i)\, m_{\text{пл}_i}^{\text{т}} \quad (2)$$

where $m_{\text{пл}}^{\text{т}}$ — mass of the i-th part of the airframe made of traditional materials; $m_{\text{пл}}^{\text{к}}$ — mass of the i-th part of the airframe made of composite materials; $m$ — mass of traditional materials; $\varphi_i$ — coefficient considering the ratio of the masses of traditional and composite materials whose values lie in the range $0 \le \varphi_i \le 1$; $\varepsilon_i$ — coefficient of the mass denomination of the CM, equal to the ratio of the mass of the elements of the i-th part of the airframe made of CM to the mass of the i-th part of traditional materials ($\varepsilon_i = \frac{m_{\text{пл}_i}^{\text{к}}}{m_{\text{пл}_i}^{\text{т}}}$).

If $\Delta m_n > 0$, then $m_{\text{пл}}^{\text{к}} < m_{\text{пл}}^{\text{т}}$ — the airframe made of CM is lighter than an airframe made of traditional materials. Using formulas (1) and (2), it is possible to reduce the airframe weight by 28%, and the UAV — by 60%.

Due to the influence of operational factors (Fig. 2), the following defects may occur in the CM (Table 2 [1]).

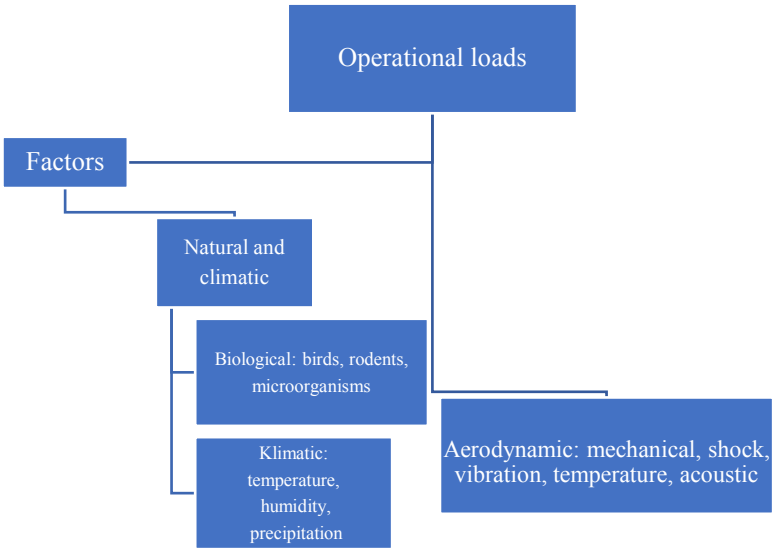


Fig. 2. Classification of operational factors affecting the CM structure [1]

Table 2

**Classification and characterization of CM defects**

| Name of the defect | Defect Image | Causes of the defect |
|---|---|---|
| surface crack<br>internal crack<br>through crack | 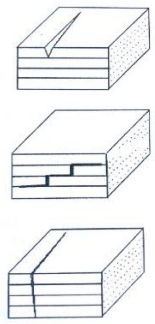 | High speed cooling, exceeding the permissible mechanical stress, transportation |
| Shell | 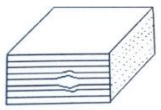 | An increase in the volatile content in the prepreg, a change in the heating rate, an increase in the time and magnitude of the pressure application |
| Surface foreign inclusion | 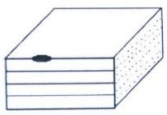 | Ingress of foreign materials in the manufacture of prepreg during its splitting and laying |

These defects can be diagnosed through the nondestructive testing that provides determining the technical condition of the airframe of an aircraft or UAV without reducing their suitability for use.

These NDT methods include:

– X-ray method;

– thermal treatment;

– ultrasonic method;

– acoustic emission method (AE).

*X-ray method*

The X-ray method is based on the reception and analysis of penetrating the ionizing radiation after interaction with a controlled object. The intensity of the radiation varies depending on the density of the material, its thickness, and the presence of defects[1]. To register the transmitted radiation, X-ray films of the selected variational sensitivity, fluorescent screens, and television installations are used. Part of the airframe design of an aircraft or UAV is placed in the X-ray installation "SaFair" for monitoring. The result of X-ray radiation is projected on a film in which the defect will be depicted in a color paler than the background of the entire structure. The major disadvantage of the X-ray method is a harmful effect on the object and subject of control [4, 5].

*Thermal method*

The thermal method is based on receiving data on changes in the thermal temperature fields of controlled objects caused by defects. This method is carried out through the use of thermal imagers and aviation heat guns.

Initially, 1/3 of the UAV airframe is heated using an aviation heat gun. At the intermolecular level, energy is transferred from the more heated part of the airframe to the colder one. We observe the process of energy flow using a thermal imager. The coloring of the defect differs from the process described above (Fig. 3) [6–8].

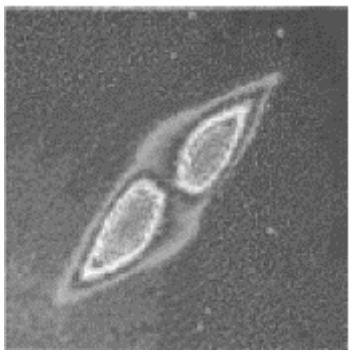

Fig. 3. Image of the UAV airframe defect through applying the thermal method

The disadvantage of this method is the inability to carry out control in unheated rooms.

*Ultrasonic method*

The ultrasonic method is based on the registration of elastic waves created in the controlled part. Flaw detectors UD2V-P, UDT-40, USD-50 allow detecting cracks of the order of 0.5–1 mm. To carry out control, it is required to establish a contact medium between the controlled part of the airframe of the aircraft or UAV and the receiver-converter of the flaw detector [9–11]. The major disadvantage is a harmful effect on the subject of control.

*Acoustic emission method (AE)*

The AE method is based on the emission of acoustic waves in the process of restructuring of the material. This method is passive since it is based on the registration of low-frequency pulses of defects of parts under loading. The AE method, in comparison to the traditional NDT methods, can detect deep-lying cracks in the structure of the material (Table 3).

Table 3

**Comparison of NDT methods**

| NDT method | Detected crack length, mm |
|---|---|
| Ultrasonic | 0.5–1 |
| X-ray | 2–3 |
| AE | 0.000001 |
| Thermal | 0.01–0.001 |

For control, a prototype of the AE diagnostics hardware and software complex was created, which provides real-time recording of developing CM defects in the low-frequency range (Fig. 4). To improve the efficiency of AE

[1]Ferrozondovyi metod nerazrushayushchego kontrolya detalei vagonov. Rukovodyashchii dokument RD 32.149. Moscow: Federal Agency for Technical Regulation and Metrology; 2008. 163 p. (In Russ.)

http://vestnik-donstu.ru

control, experts of the Military Educational and Scientific Center of the Air Force "N.E. Zhukovsky and Y.A. Gagarin Air Force Academy", among whom was the author of this paper, A.V. Popov, have developed a theoretical and probabilistic approach to the assessment of informative emission parameters. It is established that at early stages of deformation, the flow of CM AE signals from microdefects, randomly distributed over the volume of the aircraft, has a Poisson pattern. With an increase in the load, the integration of microdefects into the CM crack violates the Poisson distribution. The estimation method developed by the experts of the Center for the processes of accumulation of CM damage in aircraft and UAVs is based on the assessment of the change in the distributions of the number of AE acts at the fixed time intervals during the CM deformation. The CM deformation causes the formation of a macrodefect, the characteristics of the pulse flow become dependent. Combining microdefects of the OC destroys the hypothesis of the Poisson distribution. This phenomenon makes it possible to construct parametric invariants that are valid for the Poisson pattern, and, on this basis, to estimate the deviation of the analyzed process from the Poisson one (3):

$$I_1 = \frac{m[x^3]}{m^2[x^3]} - 3m^2[x] - m^4[x] \ = 1 \tag{3}$$

Based on equation (3), we obtain several expressions for determining the degree of deviation of the AE pulse flow from the Poisson one (4)–(7):

$$I_2 = m[x^3] * m^2[x] - 3m^4[x] - m^6[x] - m^2[x] \ = 1 \tag{4}$$

$$I_3 = m[x^3] - 3m^2[x] - m^4[x] - 1 = 0 \tag{5}$$

$$I_4 = m[x^3] * m^2[x](3 - \ m^2[x]) \ = 1 \tag{6}$$

$$I_5 = \frac{m[x^5]-1}{m^2[x]} + m^2[x] \ = 3 \tag{7}$$

The construction of invariant dependences based on formulas (3)–(7) is produced by an experimentally developed hardware-software complex (HSC) (Fig. 4), which provides multi-channel registration, processing and analysis of the values of loads and deformations; video surveillance and recording of the test process and the readings of analog devices using video cameras.

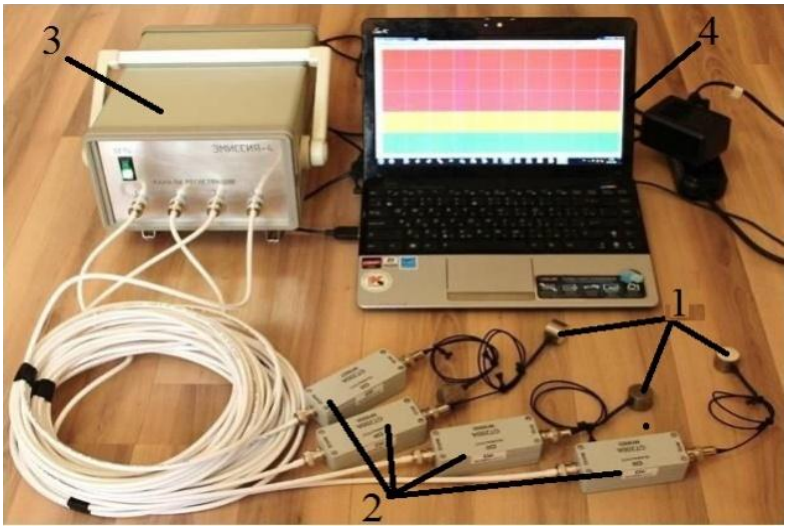


Fig. 4. Hardware-software complex of acoustic-emission diagnostics:
1 — highly sensitive piezoelectric sensor GT-300; 2 — vibroacoustic signal preamplifiers;
3 — analog-to-digital converter; 4 — PC for data processing

Highly sensitive piezoelectric sensors GT-300 are installed on the controlled surface of the CM. Informative parameters on the state of the CM from piezoelectric sensors are transmitted to the preamps of the vibroacoustic signal[2]. After amplification, the signal is sent to an analog-to-digital converter, in which it is converted from mechanical to electrical work. The PC is used for clustering and processing of received data.

**Research Results.** With the help of the HSC and RM-1 tensile testing machine, CMU-1 carbon fiber used in the production of the IL-96-300 aircraft and the Orion UAV was monitored at the Centre. The major characteristics of CMU-1 are given in Table 4.

[2]Popov AV. Sposob otsenki protsessov razrusheniya konstruktsii pri akustiko-ehmissionnom kontrole. RF patent no. 223444, 2004. (In Russ.)

Table 4

**CMU-1 carbon fiber specification**

| No. | Composite Limits |
|---|---|
| 1 | Tensile limit $\sigma_{раст}$= 1,020 MPa |
| 2 | Compression limit $\sigma_{сжат}$= 400 MPa |
| 3 | Bending limit $\sigma_{изг}$= 1,100 MPa |
| 4 | Shear limit $\sigma_{сдвиг}$= 30 MPa |
| 5 | Young's modulus of tensile $E_{раст}$= $180\times10^{-3}$ MPa |
| 6 | Young's modulus of bending $E_{изг}$= $145\times10^{-3}$ MPa |
| 7 | Young's modulus of shear $E_{сдвиг}$= $3.5\times10^{-3}$ MPa |

For testing, CMU-1 was placed in a tensile testing machine, having previously installed AE GT-300 sensors on CM. CMU-1 was loaded using the HSC. The loading results are shown in Figure 5 (a, b, c):

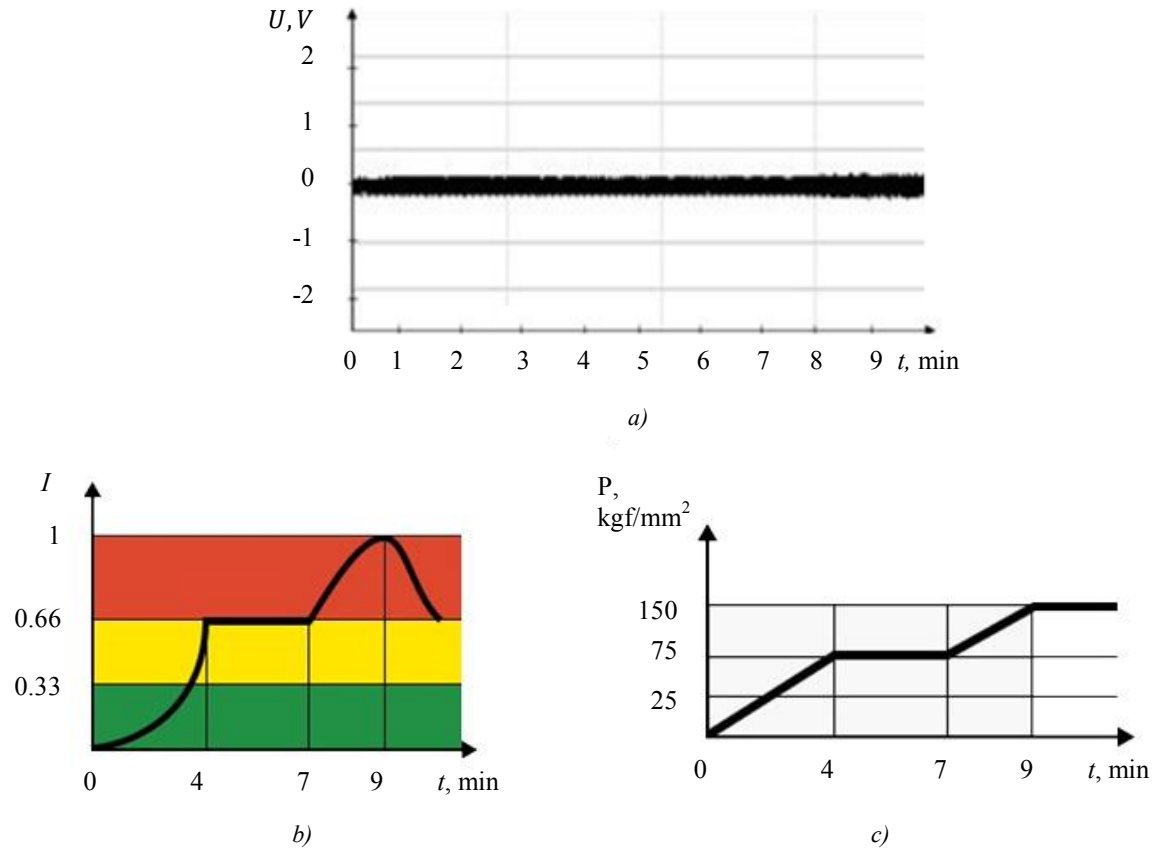


Fig. 5. CMU-1 loading results: *a*) oscillogram of AE CMU-1 signals; *b*) mode of APC operation; *c*) loading dynamics projection of RM-1 CM CMU-1

Figure 5 *a* shows the oscillogram of CMU-1 AE signals. The maximum value of the AE OC amplitude corresponds to the destruction of the OC matrix and fibers ($U_{max} = 0.25$ V).

Figure 5 *b* shows the HSC operation mode. Three zones are highlighted here — red, yellow, and green. The red zone is characterized by the presence of pronounced CMU-1 defects. The numerical value of the invariant ranges from 0.66 to 1 at t = 7–9 min. This indicates a critically active defect — the stage of destruction. The yellow zone is the zone of the active defect and the stage of crack formation (I=0.33–0.66; t = 4–7 min). Green is a benign zone that characterizes the stage of microcracks (I=0–0.33; t = 9–4 min) [12, 13].

Figure 5 *c* shows the projection of the loading dynamics of RM-1 CM CMU-1. Due to an increase in the load ($P = 25{,}75{,}150$ kgf/mm$^2$) the value of the invariant and amplitude of the AE CMU-1 increases.

**Discussion and Conclusions.** The use of CM is a promising method of assessing the technical condition under designing various aircraft and UAVs. One of the fundamental advantages of CM is the lightening of the structure mass

http://vestnik-donstu.ru

in comparison to traditional materials. Monitoring and evaluation of the technical condition of aircraft and UAVs should be carried out by advanced NDT methods that can identify various kinds of defects at an early stage of their development. The acoustic emission method meets these requirements. In the future, it is possible to install a prototype of a hardware and software complex on the fifth-generation multipurpose fighter Su-57 to diagnose the design of the aircraft in flight. This acoustic emission system will provide identifying defects that occur in the structural elements of the aircraft at a small stage of their development. The experimentally developed sample of the hardware and software complex enables to quickly register in real time the developing defects of aviation materials used in the design of aircraft and unmanned aerial vehicles.

**References**

1. Wheaton J, Scala E, eds. Fiber composite materials: trans. from English. Moscow: Metallurgiya; 2011. 240 p. (In Russ.)

2. Grigorovich VK, Sheftel EN. Dispersionnoe uprochnenie tugoplavkikh metallov. Moscow: Nauka; 1980. 303 p. (In Russ.)

3. Ermolenko IN, Ul'yanova TM. Voloknistye vysokotemperaturnye keramicheskie materialy. Minsk: Nauka i tekhnika; 1991. 125 p. (In Russ.)

4. Stepanova LN, Chaplygin VN, Lebedev EYu. Ispol'zovanie metoda akusticheskoi ehmissii pri tsiklicheskikh ispytaniyakh kompozitsionnykh ehlementov aviatsionnykh konstruktsii. Testing. Diagnostics. 2004;12:53. (In Russ.)

5. Builo SI. Diagnostika stadii razrusheniya materialov po vosstanovlennym parametram potoka aktov akusticheskoi ehmissii. Testing. Diagnostics. 2000;10:10–15. (In Russ.)

6. Chui Ch. Vvedenie v veivlety. Moscow: Mir; 2001. 412 p. (In Russ.)

7. Muravin B, Mark F. Carlo. Guide for Development of Acoustic Emission Applications for Examination of Metal Structure. Journal of Acoustic Emission. 2011;29:142–148.

8. Gangtie Zheng, Backle MA, Kister G, et al. Blind deconvolution of acoustic emission signals for damage identification in composites. AIAA Journal. 2001;39:1198–1205. https://doi.org/10.2514/2.1435

9. Skalskyi VR, Koval PM. Some methodological aspects of application of acoustic emission. Lviv: Spolom; 2007. 336 p.

10. Maochen Ge. Analysis of Source Location Algorithms, Part I: Overview and non-iterative methods. Journal of Acoustic Emission. 2003;21:14–28.

11. Barat V, Grishin D, Rostovtsev M. Detection of AE signals against background friction noise. Journal of Acoustic Emission. 2011;29.:133–141.

12. Popov AV, Kondrashin EA. Strength testing method for the load-bearing elements of construction based on numerical-temporal estimating of acoustic emission processes characteristics. Testing. Diagnostics. 2008;7:45–46. (In Russ.)

13. Popov AV, Zhumay VE. Strength characteristics of construction definition based on acoustic emissive processes amplitude invariants. Testing. Diagnostics. 2008;10:29–31. (In Russ.)

Received 28.09.2021
Revised 18.10.2021
Accepted 18.10.2021

*About the Authors:*

**Popov, Alexei V.**, professor of the Department of Restoration of Combat Aviation Equipment, Military Educational and Scientific Center of the Air Force "N.E. Zhukovsky and Y.A. Gagarin Air Force Academy" (153, Krasnoznamennaya St., Voronezh, 394052, RF), Dr.Sci. (Eng.), professor, ORCID, irinacherepanova2007@mail.ru

**Samuylov, Alexandr O.,** adjunct of the Department of Restoration of Combat Aviation Equipment, Military Educational and Scientific Center of the Air Force "N.E. Zhukovsky and Y.A. Gagarin Air Force Academy" (153, Krasnoznamennaya St., Voronezh, 394052, RF), ORCID, slavka2.0@mail.ru

**Cherepanov, Ivan S.,** military student of the Faculty of Aircraft, Military Educational and Scientific Center of the Air Force "N.E. Zhukovsky and Y.A. Gagarin Air Force Academy" (153, Krasnoznamennaya St., Voronezh, 394052, RF), ORCID, veselova.27@icloud.com

*Claimed contributorship*

I. S. Cherepanov: basic concept formulation; research objectives and tasks; computational analysis; text preparation; formulation of conclusions. A. V. Popov, A. O. Samuylov: academic advising; analysis of the research results; the text revision; correction of the conclusions.

*All authors have read and approved the final manuscript.*

# MACHINE BUILDING AND MACHINE SCIENCE

UDC 621.22 https://doi.org/10.23947/2687-1653-2021-21-4-337-345

## Synchronization in multi-motor hydromechanical systems

**A. T. Rybak**[1], **A. V. Ivanovskaya**[2], **P. P. Batura**[1], **A. Yu.Pelipenko**[1]

[1] Don State Technical University (Rostov-on-Don, Russian Federation)

[2] Kerch State Maritime Technological University (KGMTU) (Kerch, Russian Federation)

✉2130373@mail.ru

***Introduction.*** The paper submits the analysis of existing design solutions of flow dividers used to synchronize hydraulic drives of working bodies of technological and mobile machines. The market demands for multithreaded throttle flow dividers without valves with the controlled division ratio, such as multi-axle vehicle chassis, are identified. The objective of the work was to analyze the possibility and rationale for developing a throttle four-way flow divider without valves with sensing elements of the Venturi tube type. The solution should provide the synchronicity of movement (rotation) of more than three working bodies of technological and mobile machines.

***Materials and Methods.*** A patent search for the designs of hydraulic flow dividers is carried out, and systems that require the division of the hydraulic fluid flow into more than two executive bodies are considered. An upgrade option, which allows dividing the flow into four branches, is proposed for the design of a three-channel throttle flow divider without valves.

***Results.*** The urgency of developing a multithreaded throttle flow divider without valves for application in industrial and mobile machines is validated. Two types of four-flow dividers are considered, their weaknesses are indicated. It is noted that the development of a multithreaded throttle flow divider based on the designs created in 1989 and 1991 will reduce the number of hydraulic pumps and get rid of the series connection of double-flow dividers. In this way, it is possible to reduce pressure losses in the hydraulic system and implement adaptive control of hydraulic motors of multi-motor mobile machines. The possibility to obtain a divider/combiner into four flows by adding an outlet chamber connected to the membrane chamber through a channel entering the Venturi nozzle on the basis of a three-flow throttle divider is shown. The principle of operation of such equipment is described.

***Discussion and Conclusions.*** The principles of construction of throttle flow dividers without valves are considered. An upgrade option is proposed to increase the number of division channels from three to four. However, to validate the operability of this design, a numerical analysis of the various modes of operation of the divider is required — calculation of the reduced volumetric stiffness of its working cavities. The information obtained can be used to modernize the hydraulic units of technological and mobile machines, increase their reliability, manufacturability, and efficiency. The issues that need to be solved in further research are identified.

***Keywords:*** throttle flow divider, Venturi tube, hydraulic transmission, multi-axle chassis, transport platform, synchronization.

***For citation:*** A. T. Rybak, A. V. Ivanovskaya, P. P. Batura, A. Yu. Pelipenko. Synchronization in multi-motor hydromechanical systems. Advanced Engineering Research, 2021, vol. 21, no. 4, pp. 337–345. https://doi.org/10.23947/2687-1653-2021-21-4-337-345

*© Rybak A. T., Ivanovskaya A. V., Batura P. P., Pelipenko A. Yu., 2021*

**Introduction.** The condition of absolute synchronization is compliance with the proportionality of linear and angular displacements of hydraulic motors and all time derivatives of them. It is often required to synchronize:

— homogeneous linear or rotational movements of two or more hydraulic drives,

— one engine with the turn of the second.

In machine tool and mechanical engineering, when synchronizing drives, it is critical to consider the position synchronization errors. The paper discusses ways of synchronizing hydraulic motors in multi-motor systems with a flow divider, as well as examples of the application of such systems in industry. In addition, the use of a multithreaded throttle flow divider without valves as a synchronizing device of a multiaxial wheel coupling of a hydraulic transport platform is discussed.

Fundamental works on hydromechanical systems have been known since antiquity. The earliest surviving one is Archimedes' treatise “On Floating Bodies”. Today, the use of complex multi-level and branched hydraulic systems is sufficiently investigated, but the issue of control and regulation in a hydraulic drive to increase its efficiency and reduce the size of the system remains relevant[1, 2] [1–4].

The category of complex hydraulic systems includes those where one hydraulic pump feeds two or more independent hydraulic motors. At the same time, regardless of the load on the output links, the synchronicity of their movements must be provided. The required synchronization accuracy determines the selection of its method. The simplest one is the provision of rigid mechanical coupling of hydraulic motors. However, for systems with a complex arrangement of executive bodies in space, it is not applicable. The most common methods are:

— by shaft-coupled hydraulic motors or hydraulic pumps (volumetric synchronization);

— through series connection of cavities of hydraulic motors;

— by hydraulic tracking systems with distributors and hydrotachometers;

— by hydromechanical and electrohydraulic tracking systems.

The most practicable and simple means of synchronization in mobile machines and technological equipment are throttle dividers and flow dividers/combiners[3, 4] [5–8]. A hydraulic flow divider separates one working fluid flow into two or more. In this case, the specified ratio is taken into account, and it is required to provide synchronous (coordinated) movement of the output links regardless of their load. The flow divider/combiner acts similarly to the divider, but in the opposite direction. It is easily integrated into the hydraulic system, and it is cheap and easy to operate. A flow divider/combiner provides synchronization in a wide range of speeds of movement of output links of hydraulic motors.

In the classical design of the throttle divider, spool-and-sleeve valves are used as a shut-off-and-regulating element [5]. This causes the characteristic disadvantages of such dividers. Specifically, the high cost of precision spool-and-sleeve valves is due to the complexity of manufacturing, and a large share of such high-precision operations as honing, grinding, electrical discharge machining. Selective assembly and fine-tuning of spool-and-sleeve valves makes them practically non-repairable, which also increases their operational cost. The above also indicates the susceptibility of the system to the quality of hydraulic fluid, which is subject to very high requirements [6].

[1] Urekin VS, Istomina YV. Development of hydraulic automatic control system drives of technological equipment. In: Proc. II All-Russian Sci.-Tech. Conference. Penza: Mezhotraslevoi nauch.-inf. Tsentr; 2016. P. 259–262. (In Russ.)

[2] Lazuta IV, Lazuta EF. Nonlinear correlation of the relay automatic control system of the hydraulic drive. In: Proc. National Sci.-Pract. Conference: Education. Transport. Innovation. Omsk: SiBADI; 2018. P. 64–69. (In Russ.)

[3] Yatsukhin YuA. Issledovanie gidravlicheskoi sistemy sinkhronizatsii dvizheniya rabochikh organov sel'skokhozyaistvennykh mashin: Cand.Sci. (Eng.), diss., author’s abstract. Rostov-on-Don; 1972. 25 p. (In Russ.)

[4] Rybak AT. Izyskanie ratsional'nogo tipa zaporno-reguliruyushchego ehlementa drossel'nogo delitelya potokov gidroprivodov sinkhronnykh mekhanizmov sel'skokhozyaistvennykh mashin: Cand.Sci. (Eng.), diss., author’s abstract. Rostov-on-Don; 1989. 23 p. (In Russ.)

There are known attempts to design dividers without spool-and-sleeve valves [5, 6, 7, 8]. The possibilities of improving the characteristics of spool dividers were investigated. It should be noted that the listed designs of flow dividers provide synchronization of only two actuators, and this significantly narrows the scope of their application. The objective of this study is to search for a promising design of a multithreaded throttle divider that meets the requirements of the operation of mobile machines.

**Materials and Methods**

**Multi-motor hydromechanical systems.** Hydraulic systems are known, which include more than two working bodies (both reversible and non-reversible). Depending on the operating conditions, they require constant or short-term synchronicity of movement with a constant or variable speed ratio. Such systems, in particular, include:

— travel hydraulic drives of mobile machines,

— pulling presses for large sheet metal,

— stamping machines for dimensional parts,

— groups of hydraulic jacks for lifting the building footings,

—rudder folding hydraulic drives in aerospace engineering,

— positioning systems of the radio reflector petals.

The application of well-known throttle flow dividers without valves in such systems undoubtedly improves operational characteristics. At the same time, the number of synchronized working bodies is limited to two per one flow divider. This limitation stimulates designers to use sequential cascading of flow dividers. As a result, pressure losses (up to 30 %) increase at the output of the division cascades, and the synchronization error of each divider is summed up. It is also important to increase the volume occupied by hydraulic equipment. In general, this approach is technically unjustified and financially costly.

In this regard, it is worth noting the diaphragm flow divider design [9]. It can be used in reversible hydraulic systems in which it is required to dynamically change the ratio of execution speeds. In addition, this design enables to create a divider into 3, 4 or more independent flows based on it [10].

We consider the application of a throttle flow divider without valves using the example of a hydrostatic wheel drive transmission of multi-axle transport chassis.

To design transmission systems of modern all-wheel-drive vehicles, as a rule, a locked and differential circuit is used. The locked transmission provides a rigid connection of the drive wheels. The differential one is characterized by the branching of one incoming power flow between the drive axles and wheels through a special differential node. There are also combined transmission schemes in which one part of the wheels is connected by a differential coupling, and the other is locked (e.g., locking of several differentials). For transmission systems, forced adjustment of:

— the power supplied to one or more wheels,

— one axle independently of the others,

is not possible.

The presence of a hydraulic drive chassis in the transmission system enables to individually supply power to the wheels and provides stepless regulation in a wide range of values. The hydraulic drive design is compact, resistant to external atmospheric influences. In addition, the hydraulic drive, as a rule, has a large range of regulation, which is important for an off-road vehicle. Another advantage of the hydro-volume wheel drive is the capability to quickly

[5] Kirikov RP, Sherman EB, Kuzik VL, et al. Flow divider. USSR Patent, no. 1041773, 1983. (In Russ.)
[6] Flow divider: France Patent no. 1566897, 1970. (In Russ.).
[7] Rybak AT, Yatsukhin YuA, Negodov VN, et al. Throttle flow divider. USSR a. c. 1151725, 1985. (In Russ.).
[8] Flow divider: US Patent no. 10578221, 2020.
[9] Yatsukhin YuA, Kolosov LP, Rybak AT. Throttle flow divider. USSR Patent no. 1670191, 1991. (In Russ.).
[10] Rybak AT, Yatsukhin YuA, Antonenko VI. Multithreaded flow divider/combiner. USSR Patent no. 1742530, 1992. (In Russ.).

reverse. This is important when swinging over obstacles. The hydrostatic wheel drive provides continuous movement at minimum speed with high tractive effort, which also increases the vehicle's off-road performance.

The hydraulic scheme of the undercarriage for one axis of such a machine is generally shown in Fig. 1.

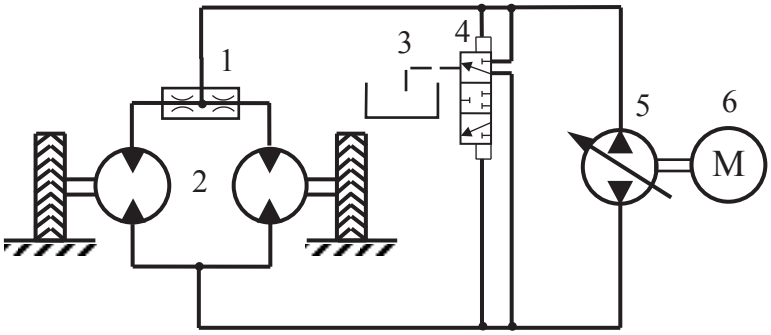


Fig. 1. Hydraulic diagram of one wheel axle of a mobile transport machine

Consider the system of hydrostatic transmission. The internal combustion engine 6 transmits torque to the reversible hydraulic pump 5, which is connected by pipelines and the hydraulic distributor 4 with a flow divider 1 and hydraulic motors 2. The shafts of the hydraulic motors are connected to the drive wheels. Often, axial-piston or radial-piston hydraulic motors are structurally connected to the wheel. This arrangement forms a single "hydraulic motor — wheel" node. Under the engine operation, the hydraulic pump provides the hydraulic motors of the drive wheels with hydrodynamic fluid pressure, which is further converted into mechanical work. Depending on the design of the hydraulic units, the operating pressure in the system is in the range of 25–50 MPa. The operation of the "hydraulic motor — wheel" unit increases the passability of the chassis as a result of a continuous flow of power and a smooth change in torque.

Scheuerle and Kamag (Germany) produce modular hydraulic transport platforms: medium — FlatCombi K22, and heavy self-propelled — InterCombi K25 (Fig. 2).

Fig. 2. Two connected 6-axis self-propelled InterCombi K25 modules from Kamag (Germany)

The modules of the medium series with a width of 2,750 and 3,000 mm are designed for a load of 23 and 25 tons per axle at speeds up to 10 km/h. Heavy series modules are equipped with 2–6-wheel axles. The width of the platform is 3,000 and 3,100 mm, the load on one axle is 36–45 tons. Self-propelled modules are driven by PowerBooster power plants. Options for combining them are as follows:

— one platform on which a bridge structure is laid,

— two turntable trolleys.

http://vestnik-donstu.ru

In the domestic engineering industry, it is possible to distinguish a promising design of a multiaxial, fully hydraulic chassis developed by the Central Research and Development Automotive and Automotive Engine Institute "NAMI". This is "Gidrokhod-49061"[11], a three-axle vehicle (Fig. 3).

Fig. 3. "Gidrokhod-49061", NAMI vehicle

The design of this machine implements the idea of a ""flexible wheel drive", which provides an individual hydraulic pump for each of three wheel axles. The conveyor is built on the basis of ZIL-4906 chassis. Equipping the chassis with a hydrostatic transmission enables to implement all possible types of wheel transmissions: locked, differential, with independent control, as well as their combinations. The industry is interested in developing the production of volumetric-hydraulic wheeled cross-country chassis, which stimulates new research in this area.

Flow dividers are widely used in hydraulic transmission circuits to provide differential locking, which increases the passability of obstacles. The flow divider ensures that both synchronized wheels will always generate traction, even if one of them is on soft or slippery ground. But for synchronization and flow control in a 4- and 6-axis design, several dividers must be connected in series, and with a variable division ratio according to the control signal.

**Research Results.** The considered four-threaded dividers can be attributed to one of two types. In the first case, we are talking about units with a spool. This is a cascade of three flow dividers in one housing. An example is the Poclain FD-M4[12] flow divider (France). Figure 4 shows its physical form and hydraulic circuit.

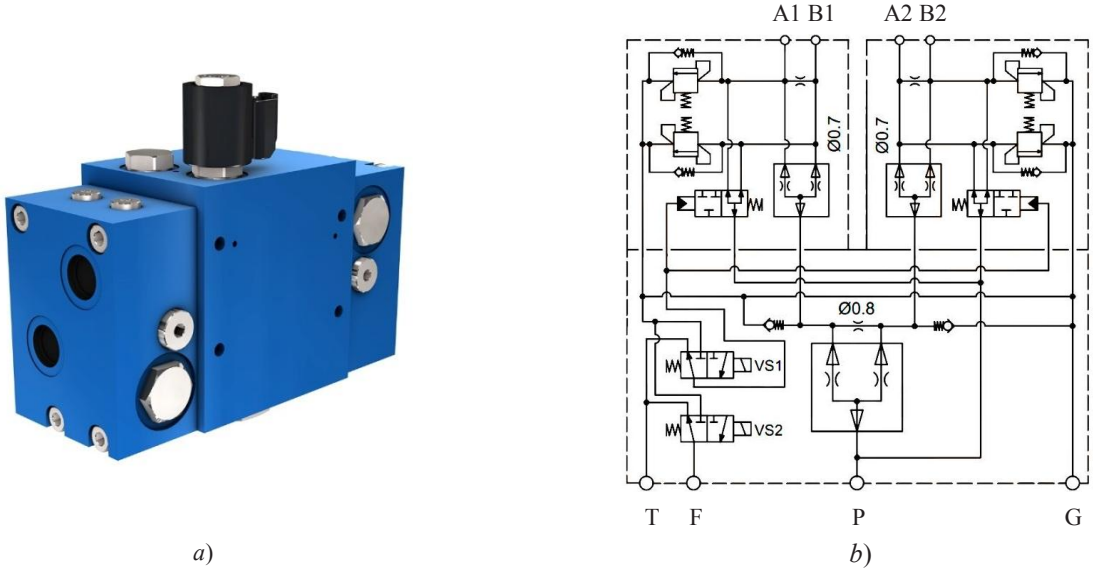


*a*) *b*)

Fig. 4. Four-way flow divider Poclain FD-4M: *a*) appearance, *b*) hydraulic circuit diagram

[11] Prochko EI. Metody postroeniya sistem silovykh gidroob"emnykh privodov koles polnoprivodnykh avtomobilei: Cand.Sci. (Eng.), diss., author's abstract. Moscow; 2007. 20 p. (In Russ.)

[12] POCLAIN Hydraulics product catalog. POCLAIN Hydraulics. URL: https://www.poclainhydraulics.com/_upload/ressources/media/pdf/B33971Z.pdf (accessed 18.01.2021).

In designs of the second type, it is not possible to change the division ratio by an external control signal. This limits the scope of application of dividers in controlled multi-motor hydraulic systems. The development of a multi-way throttle flow divider based on the designs created in 1989 and 1991[13, 14], will reduce the number of hydraulic pumps and get rid of the serial connection of two-flow dividers (respectively, reduce pressure losses in the hydraulic system), as well as implement adaptive control of hydraulic motors of multi-motor mobile machines [7].

Thus, e.g., it is possible to obtain a divider/combiner into four flows (Fig. 5) by adding the outlet chamber 16 connected to the membrane chamber 10 through a channel entering the Venturi tube nozzle 3. In this case, the left chambers 15, 16 and right chambers 17, 18 can be connected by a movable plunger 13 between chambers 16 and 17.

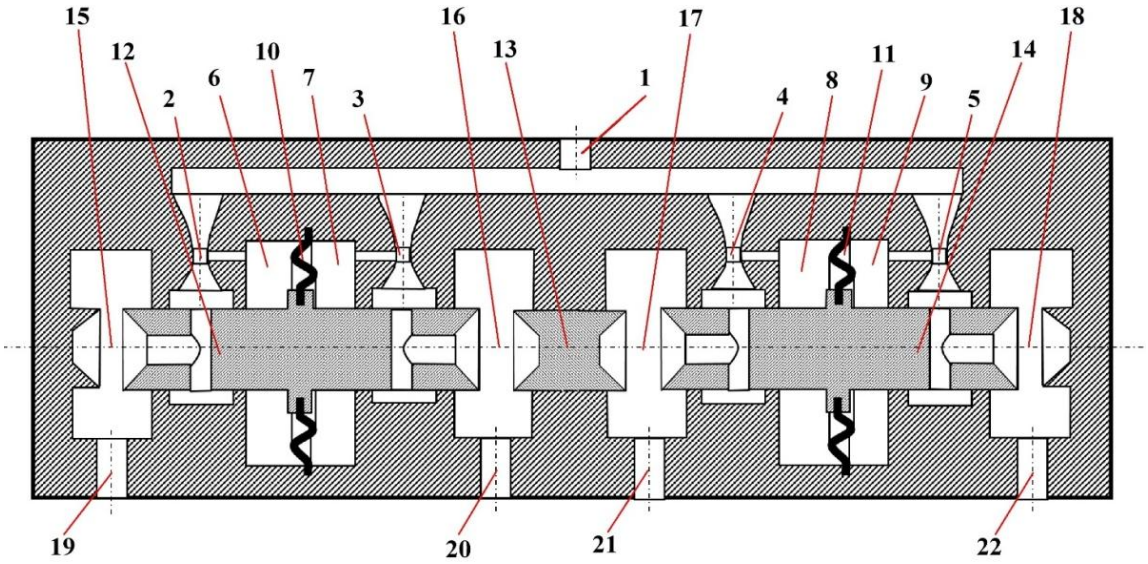


Fig. 5. Four-flow divider with sensitive elements of the Venturi tube type

We describe the principle of operation of a flow divider/combiner with sensitive elements in the form of Venturi tubes. During the flow division, the working fluid is directed to the input of the divider/combiner 1. Then the flows are divided between the sensing elements 2, 3, 4 and 5. They are made in the form of Venturi tubes, and their necks are connected to adjacent working chambers 6, 7, 8 and 9. In this case, chambers 6, 7 and 8, 9 are the executive elements of the structure. They are separated from each other by membranes 10 and 11 and are rigidly fixed in the body of movable plungers 12 and 14. The movable plunger 13 provides connection between the left and right parts of the divider. After the Venturi tubes, the fluid flows pass through the axial and radial bores of plungers 12 and 13, and then fall on the variable resistances 15, 16 and 17, 18 and to the output channels 19, 20 and 21, 22.

Assume that hydraulic motors on all branches are under the same load. Accordingly, the flows in the branches are the same, and, therefore, the flows through the corresponding Venturi tubes are the same. In the necks of the Venturi tubes there will be the same high-speed pressures, so the pressures in the control chambers will also be equal. The pressure on the walls of the membrane elements of the actuators will be the same on both sides, and this will bring them into a balanced state.

If the load increases (e.g., on a hydraulic motor connected to the outlet channel 19), the flow rate in the corresponding branch and the Venturi tube 2 connected to it will decrease. As a result, the high-speed pressure in its neck will decrease, which means that the pressure in it will increase. In turn, this will cause an increase in pressure in the working chamber 6. As a result, the equilibrium of the membrane 10 is disturbed, and it will shift to the right. Plunger 12 will also move to the right, narrowing the free area of the variable resistances 16 and 17, which are connected to the resistance 16 through the movable plunger 13. As a result, the flow in the corresponding branches and

[13] Yatsukhin YuA, Kolosov LP, Rybak AT, et al. Throttle flow divider. USSR Patent no. 1670191, 1991. (In Russ.)
[14] Rybak AT, Yatsukhin YuA, Antonenko VI. Multithreaded flow divider/combiner. USSR Patent no. 1742530, 1992. (In Russ.)

http://vestnik-donstu.ru

Venturi tubes 3 and 4 will decrease. Just as before, plunger 14 will start moving to the right and reduce the free area of the variable resistance 18. This process will continue until the flows are balanced in all branches of the divider.

In the summation mode, the flows for combining are fed to the output channels of the divider/combiner, and its workflow is reversed.

It is worth noting that even at the development stage, it is required to know the reliability and functional properties of the proposed design of the divider/combiner. The best ways to obtain the required data are modeling and numerical experiments[15] [9–13].

**Discussion and Conclusions.** The widespread application of multi-motor branched hydraulic systems in the industrial and mobile equipment often involves the synchronization of their actuators. Depending on the operating conditions and functional requirements, solutions based on complex designs of adjustable volumetric hydraulic machines or throttle flow dividers are used [5–8]. In cases where it is needed to use the matching mechanism for a short time, the most economical way of synchronization, in our opinion, is to apply a throttle flow divider. The considered hydraulic machines (Fig. 2, 3) fully correspond to the concept of a multi-motor hydraulic system. The application of throttle flow dividers in the design of the driving wheel axles of such machines will provide the implementation of a differential circuit without a mechanical transmission. This will increase the off-road performance and enable to effectively control the hydraulic drives of the wheelset.

There are no multi-way throttling controllable flow dividers on the market. This indicates the demand for their development.

Further work on the design of the four-flow divider/combiner described in the paper will be aimed at creating a mathematical model. Its basis will be the fundamentals of the theory of volumetric rigidity[16, 17, 18] [14–16]. This will revise the physical dimensions of the elements of the divider/combiner and calculate the permissible operating modes.

**References**

1. Simanin NA, Konovalov VV, Rodionov YuV. Adaptive control of the hydraulic drive of the metal cutting machine. Transactions of TSTU. 2017;23:338–347. (In Russ.) https://doi.org/10.17277/vestnik.2017.02

2. Korolev VA, Korobova IL, Stazhkov SM, et al. Hydraulic stabilization of loaded high speed pneumatic drives. Mechatronics, Automation and Robotics. 2019;4:34–38. (In Russ.) https://doi.org/10.26160/2541-8637-2019-4-34-38

3. Selivanov AM. The principle of combined speed control output unit hydraulic drive and its modern implementation. Aerospace MAI Journal. 2011;18:147–151. (In Russ.)

4. Sunarchin RA, Mashkov MA, Matrosov AV. Instability and self-oscillations in electro-hydraulic servo drive. Dynamics and Vibroacoustics. 2018;4:16–25. (In Russ.) https://doi.org/10.18287/2409-4579-2018-4-3-16-25

5. Skritskiy VYa, Rokshevskiy VA. Sinkhronizatsiya ispolnitel'nykh organov gidrofitsirovannykh mashin i mekhanizmov. Moscow: Mashinostroenie; 1973. 140 p. (In Russ.)

6. Rybak AT. Drossel'nye deliteli i deliteli-summatory potokov sinkhronnykh gidrosistem mobil'nykh mashin i tekhnologicheskogo oborudovaniya. Vestnik of DSTU. 2005;5:179–188. (In Russ.)

[15] Rybak AT. Modelirovanie gidravlicheskikh sistem na osnove teorii ob"emnoi zhestkosti. In: Proc. Int. Sci.-Pract. Conf. Divnomorskoe: DSTU-Print; 2017. P. 234–242. (In Russ.)

[16] Mirnyi VI. Povyshenie ehffektivnosti bystrodeistvuyushchego gidravlicheskogo privoda vozvratno-postupatel'nogo dvizheniya: Cand.Sci. (Eng.), diss., author's abstract. Rostov-on-Don; 2008. 21 p. (In Russ.)

[17] Zatolokin SA. Sovershenstvovanie teorii i metodov proektirovaniya gidromekhanicheskikh sistem s nasosno-akkumulyatornym istochnikom raskhoda postoyannogo davleniya: Cand.Sci. (Eng.), diss., author's abstract. Rostov-on-Don; 2009. 18 p. (In Russ.)

[18] Ust'yantsev M. V. Povyshenie ehffektivnosti privoda stenda ispytanii gidromashin vrashchatel'nogo deistviya: Cand.Sci. (Eng.), diss., author's abstract. Rostov-on-Don; 2012. 18 p. (In Russ.)

7. Rybak AT. Drossel'nye deliteli i deliteli-summatory potokov dlya razvetvlennykh gidravlicheskikh sistem. Vestnik of DSTU. 2005;5:28–35. (In Russ.)

8. Korobkin VA, Kotlobai AYa, Kotlobai AA, et al. On perspective directions pertaining to development of hydraulic units for construction and road machinery drives. Science and Technique. 2012;6:71–76. (In Russ.)

9. Kobzev K, Vyalov S, Rybak A. Learning the basics of a battery pack control system. E3S Web of Conferences. 2020;164:13006. https://doi.org/10.1051/e3sconf/202016413006

10. Khinikadze T, Pershin V, Karagodskaya Y. Simulation of the hydraulic system of a device with self-adaptation by power and kinematic parameters on the working body. IOP Conference Series: Materials Science and Engineering. 2020;1001:012061. http://dx.doi.org/10.1088/1757-899X/1001/1/012061

11. Ivanovskaya AV, Bogatyreva EV, Popov VV. Obosnovanie primeneniya gidravlicheskogo privoda, chuvstvitel'nogo k izmeneniyu nagruzki. Bulletin of the Kerch State Marine Technological University. 2018;1:62–68. (In Russ.)

12. Pilipenko SS, Baiguzin MR, Potapenkov AP. Hydraulic transmission-multiplier drive with dosing modules. Steel in Translation. 2016;46:705–710.

13. Yong Sang, Weiqi Sun, Fuhai Duan, et al. Bidirectional synchronization control for an electrohydraulic servo loading system. Mechatronics. 2019;62:102254. http://dx.doi.org/10.1016/j.mechatronics.2019.102254

14. Vanin VA, Kolodin AN, Rodina AA. Stepper hydraulic motor with pneumatic (jet) control system in machines with hydromechanical forming links. Journal of Physics: Conference Series. 2019;1278:012019. http://dx.doi.org/10.1088/1742-6596/1278/1/012019

15. Jarov VP, Rybak AT, Zatolokin SA, et al. Reduced volumetric rigidity of hydraulic systems. Vestnik of DSTU. 2008;8:177–185. (In Russ.)

16. Pershin VA, Khinkadze TA. Technique of functional unification of adaptive hydraulic drive module capable of load stabilization on the working body of mobile machines. Vestnik of DSTU. 2018;18:3:319−326. http://dx.doi.org/10.23947/1992-5980-2018-18-3-318-325 (In Russ.)

Received 04.10.2021
Revised 08.11.2021
Accepted 08.11.2021

*About the Authors:*

**Rybak, Alexander T.,** professor of the Tool Engineering and Biomedical Engineering Department, Don State Technical University (1, Gagarin sq., Rostov-on-Don, 344003, RF), Dr.Sci. (Eng.), professor, Scopus, Researcher, ORCID, 2130373@mail.ru

**Ivanovskaya, Aleksandra V.,** associate professor of the Ship Power Plants Department, Kerch State Maritime Technological University (82, Ordzhonikidze St., Kerch, 298309, Republic of Crimea), Cand.Sci. (Eng.), associate professor, Scopus, Researcher, ORCID, invkerch@yandex.ru

**Batura, Pavel P.,** postgraduate of the Tool Engineering and Biomedical Engineering Department, Don State Technical University (1, Gagarin sq., Rostov-on-Don, 344003, RF), ORCID, stalker-ghost77@mail.ru

**Pelipenko, Aleksei Yu.,** postgraduate of the Hydraulics, Hydropneumoautomatics and Heat Management Department, Don State Technical University (1, Gagarin sq., Rostov-on-Don, 344000, RF), Scopus, ORCID, pelipenko16a@mail.ru

*Claimed contributorship*

A. T. Rybak: academic advising; analysis of the research results; the text revision; correction of the conclusions. A. V. Ivanovskaya: consultations on the research topic. P. P. Batura: basic concept formulation; research objectives and tasks setting; literature analysis; text preparation; formulation of conclusions. A. Yu. Pelipenko: the text revision.

*All authors have read and approved the final manuscript*.

# INFORMATION TECHNOLOGY, COMPUTER SCIENCE, AND MANAGEMENT

UDC 910.31 https://doi.org/10.23947/2687-1653-2021-21-4-346-363

## Machine Learning and data mining tools applied for databases of low number of records

**Hubert Anysz**
Warsaw University of Technology (Warsaw, Poland)
✉ h.anysz@il.pw.edu.pl

The use of data mining and machine learning tools is becoming increasingly common. Their usefulness is mainly noticeable in the case of large datasets, when information to be found or new relationships are extracted from information noise. The development of these tools means that datasets with much fewer records are being explored, usually associated with specific phenomena. This specificity most often causes the impossibility of increasing the number of cases, and that can facilitate the search for dependences in the phenomena under study. The paper discusses the features of applying the selected tools to a small set of data. Attempts have been made to present methods of data preparation, methods for calculating the performance of tools, taking into account the specifics of databases with a small number of records. The techniques selected by the author are proposed, which helped to break the deadlock in calculations, i.e., to get results much worse than expected. The need to apply methods to improve the accuracy of forecasts and the accuracy of classification was caused by a small amount of analysed data. This paper is not a review of popular methods of machine learning and data mining; nevertheless, the collected and presented material will help the reader to shorten the path to obtaining satisfactory results when using the described computational methods.

***Keywords:*** machine learning, data exploration, artificial neural networks, association analysis, automatic classification

***For citation:*** Hubert Anysz. Machine Learning and data mining tools applied for databases of low number of records. Advanced Engineering Research, 2021, vol. 21, no. 4, pp. 346–363. https://doi.org/10.23947/2687-1653-2021-21-4-346-363

© *Hubert Anysz, 2021*

**Introduction.** In the era of universal Internet access, more and more devices interact with each other or with centralized databases. Advertisers outperform each other in the effectiveness of personalized ads. This makes the group of tools known as artificial intelligence develop rapidly. The amount of data that needs to be processed to obtain the necessary information is huge, so the number of publications on algorithms that provide fast extraction of information from information noise is very large. Most often, you have to deal with information overload. Scientists from different fields of knowledge are familiar with the problems associated with data analysis. Often, collecting data on the phenomena under study requires expensive devices, installations, and tests. The study itself can also be lengthy. This means that research databases on the causes and consequences of the analyzed phenomena can often contain only a few dozen or a few hundred records. The advantages of machine learning and data mining tools, including the ability to search for significant dependences between multidimensional input and output data, enable researchers to use these tools to determine previously undetected relationships of the processes and phenomena under study. Insufficient number of records in the created database describing any phenomenon may reduce the value of the obtained analysis results. The paper presents the author's developments in which machine learning and data mining tools were used to study materials and analyze processes when the amount of input data was large compared to the number of tests performed (i.e., records in the database). The collected application examples have been expanded to include data preparation techniques and methods for evaluating the accuracy of predictions and classification to make it easier and faster to achieve expected results for people who are about to use machine learning tools to analyze their own research.

**Analysis of phenomena described by many variables**. Any researcher will certainly face the following questions: what input values to take for analysis as affecting the phenomenon under study, and what parameters to

measure at the output. The statistical approach to research can be very useful, but it has a significant drawback, which is that only one pair of functions can be analyzed. In this case, it is worth, of course, to determine what statistics is. According to [1], statistics is the science of methods of conducting a statistical survey and methods of analyzing its results. The subject of a statistical survey is a separate set of objects, which is called a statistical community (population), or several statistical communities. Statistics can be divided into three main parts: descriptive statistics, random values distribution, and statistical inference (Fig. 1) [2].

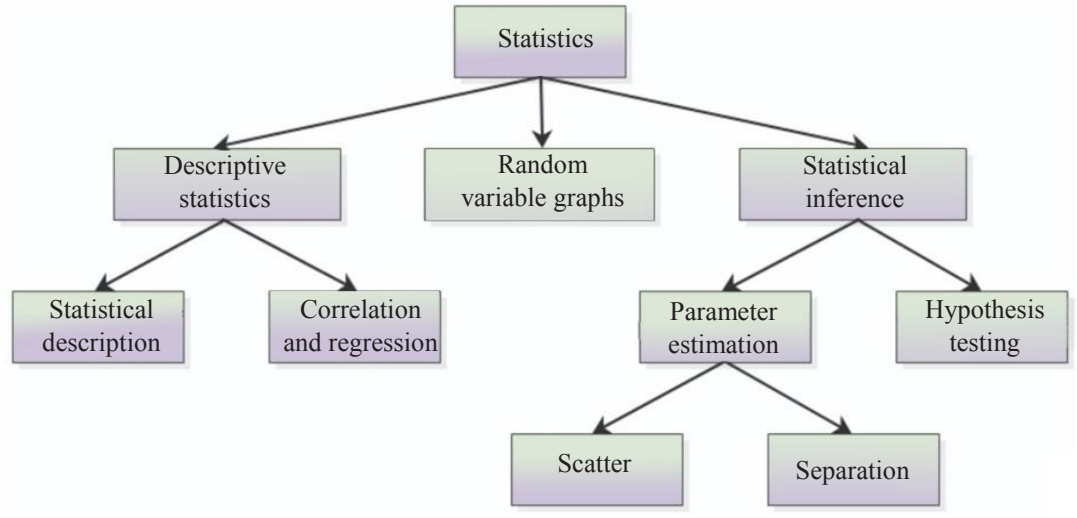


Fig. 1. Statistical control [2]

In case when the result of the process is influenced by many variables, to find such combinations of values of input variables that significantly affect the variability of output data through statistical methods is a challenge. And the most demanded is how to effectively manage a process or phenomenon to get the desired result at the output. Using data mining tools, it is much easier to find relationships between multidimensional input and output data. Data mining is very precisely defined by the very title of book [3] — "Discovering Knowledge in Data". There is a definition of data mining, formulated in 2001, as the analysis of (often huge) sets of observational data to discover unexpected relationships and generalize the data in an original way so that they are understandable and useful to their owner [4–5]. For these needs, methods and algorithms are being developed, thanks to which the search for the above compounds is faster and more efficient. Data mining methods can be divided into:

— association detection (association rules);
— classification and prediction;
— grouping;
— sequence and time series analysis;
— detection of characteristics;
— text and semi-structured data mining;
— study of content posted on the Internet;
— study of graphs and social networks;
— intelligent analysis of multimedia and spatial data;
— outliers detection [6].

On this basis, methods commonly called artificial intelligence have been developed, through which the most frequently selected data mining tasks are performed. Despite the development of information technology and the increasing processing power of computers, it is still almost unfeasible to test all possible combinations of multidimensional input and output of a complex system [7]. The more complex the problem is and the mechanisms controlling it are unknown, the more justified the application of artificial intelligence methods is (Fig. 2).

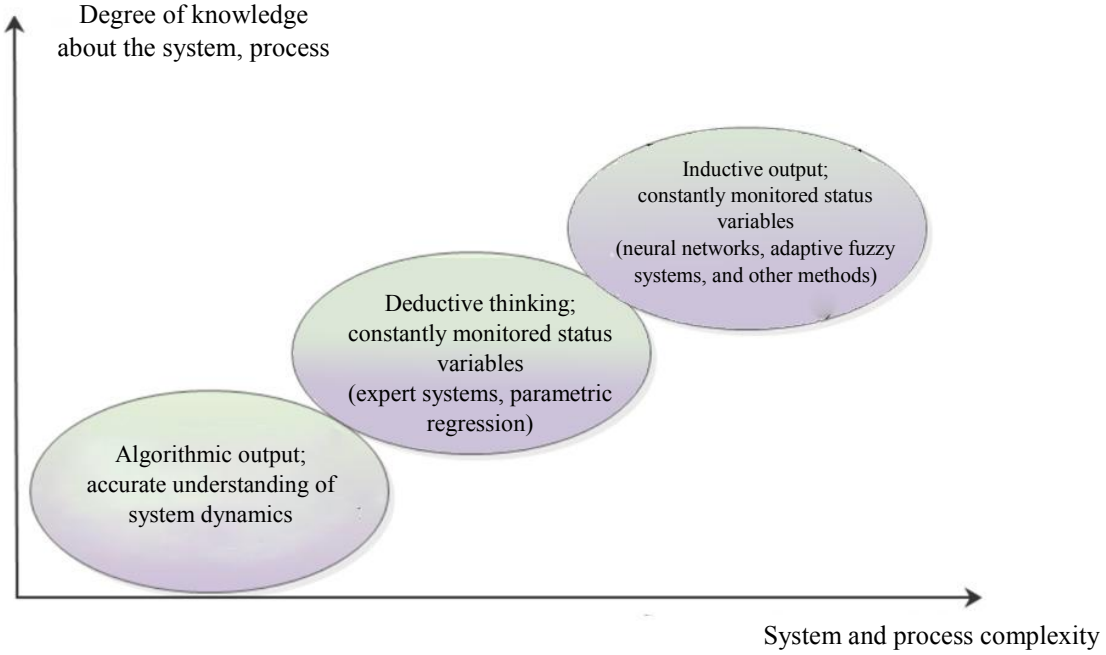


Fig. 2. Proposed conditions for application of artificial intelligence methods [7]

There are many methods and techniques of artificial intelligence (including artificial neural networks, the K-nearest neighbor method, random forest, decision trees), and they are still being developed[1]. Popularity, which can be read as the usefulness of applications of one of the artificial intelligence tools — artificial neural networks — is very noticeable, e.g., based on [8]. Instead of a strict search for possible combinations, metaheuristics is used. If you want to apply the aforementioned tools, you should decide whether to use specialized software or create it yourself through publicly available modules (so-called "engines") that implement artificial intelligence algorithms. Regardless of the decision taken, the basis will be the data that are analyzed.

**Data preparation.** The following stages of data preparation for analysis can be distinguished:

— data cleansing;

— data integration;

— data selection;

— data consolidation and transformation [6].

Such preparation should be performed regardless of the database size. Their proper preparation is even more important for small datasets than for large ones. An example is a comparison of two datasets: one with 10,000 records, and the other with 100 records, where 5 % of the records relate to a recurring phenomenon (repeatability has not yet been detected). When two records contain erroneous data, then in the first case, we can find repeatability in 4.8 % of cases instead of 5.0 %. In the second case, the repeatability is detected only in 3.0 %. The difference is significant.

**Data cleansing and integration.** When clearing data, records containing incomplete data are mostly deleted from the database. In large databases, deletion, e.g., of 2 records will not significantly affect the results obtained at subsequent stages. With a small number of datasets, the loss of even one record can significantly affect the analysis results obtained. For this reason, the missing values cannot be replaced, e.g., by the average for the entire population (one of the data augmentation methods) or its part (similar to the description in the record to be deleted), as is done for large databases. The reason is the same as described above — replacing one missing feature in the description of the phenomenon can significantly change the results if a small dataset is analyzed. However, records deleted in the process should not be permanently deleted. At subsequent stages, it may turn out that this feature will not be taken into account in the finally adopted model, and the initially deleted record will contain complete data — this will be useful for analysis.

The second important stage of data cleansing is a statistical analysis of each characteristic (columns in the database) separately and its correlation with the output data. It is recommended to present statistics of the major characteristics of the analyzed process (number of records, arithmetic mean, median, minimum and maximum values, standard deviation, quartiles of characteristic values) also for the function or functions describing the output data. "Box-and-whisker" plots are very easy-to-follow (Fig. 3).

http://vestnik-donstu.ru



[1] StatSoft. Internetowy Podręcznik Statystyki. URL: https://www.statsoft.pl/textbook/stathome.html (accessed: July 2020).

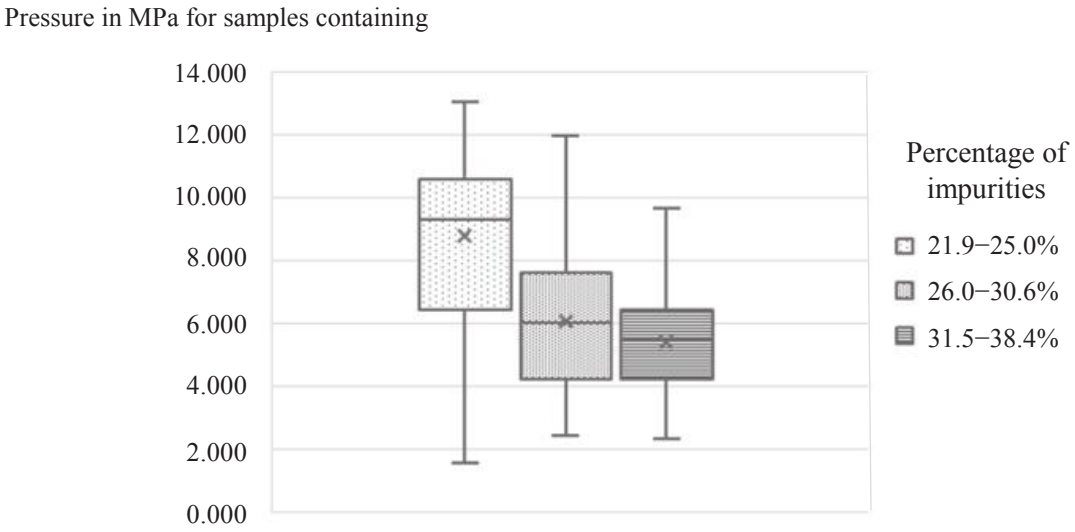


Fig. 3. Example of a "box-and-whisker" type diagram [9]

On such a chart, it is easy to read, e.g., that for 50 % of samples with 21.9–25.0 % clay content with dust, the strength was above 9 MPa, but the minimum strength for this type of samples was below 2 MPa. For such samples, the strength was below 6.5 MPa. The analysis of basic statistics can facilitate the decision to exclude from the analysis the records (i.e., samples or investigated phenomena) for which the measured values are incompatible with all other cases. Significant discrepancy may be the result of an erroneous measurement or the fact that the measurement was affected by another factor that was not taken into account at all (it was not taken into account, it was not measured in any of the cases). For these reasons, all records rejected from the database should be described, and the reasons for rejection should also be indicated [10].

Another case. You have discovered, e.g., that a decision to reject a record can be made only after all or part of the calculations have been performed. This is discussed in paper [11]: on the basis of sets of 95 accelerations of a standardized hammer (hitting the tested steel element), measured every 0.01 ms using artificial neural networks, an attempt was made to assign the tested steel element to one of nine classes (Fig. 4–5).

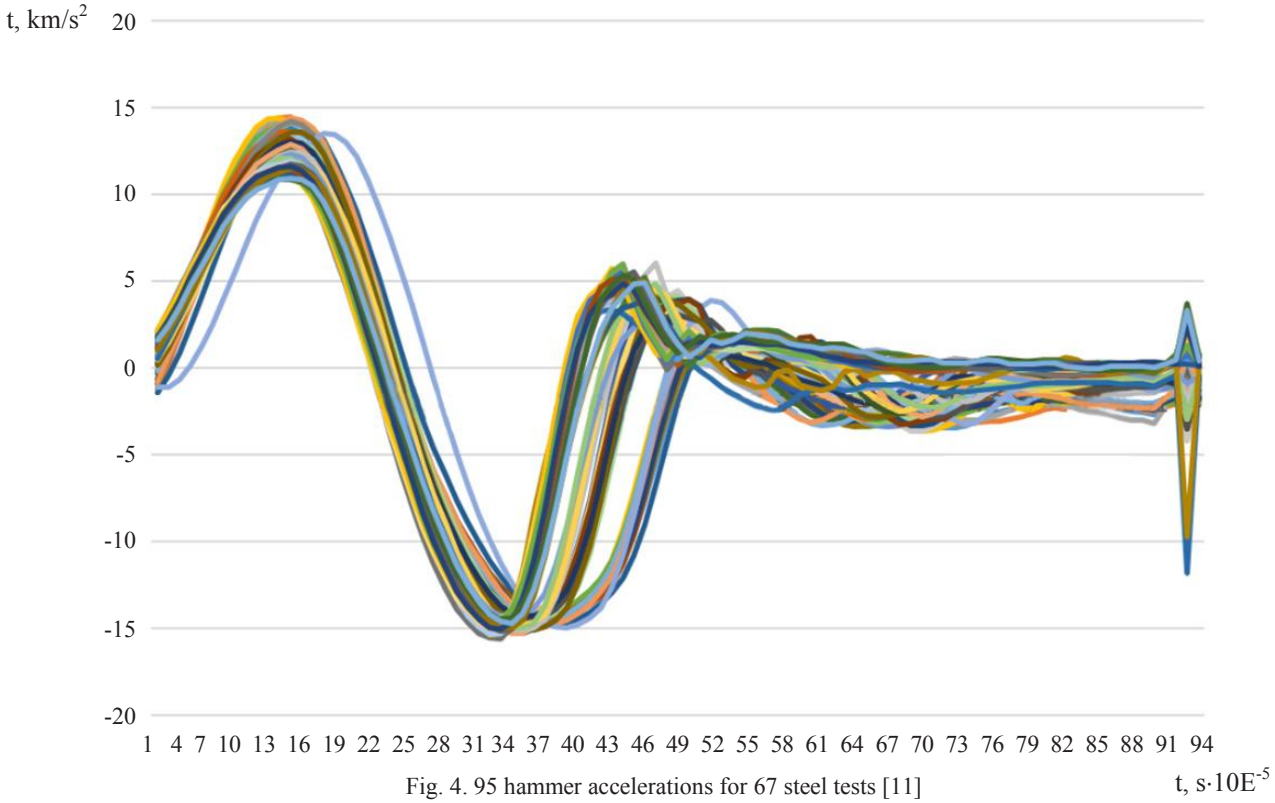


Fig. 4. 95 hammer accelerations for 67 steel tests [11]

Analyzing the accelerations in Figure 4, we can say that one of the tests in the time range from 0.01 to 0.31 ms lags behind the others, but still behaves like other samples. Only the preliminary classification into four groups of steel grades showed that after 0.31 ms in test No. 29, results were obtained that show a sharply deviating nature of the results also after 0.31 ms (Fig. 5). In Test No. 29, a steel sample was examined, for which, in all other tests, acceleration changed the sign from negative to positive between 0.424 and 0.450 ms. For Test No. 29, the acceleration sign changed within 0.460–0.495 ms, i.e., in a time suitable for another group of steel grades. Only this conclusion allowed us to justify the deviation from the analyses of Test No. 29 well enough. Consequently, the initially obtained classification accuracy was increased to nine grades of steel according to the results of 67 tests, equal to 80 %, to 95 % (after excluding Test No. 29 and reusing artificial neural networks).

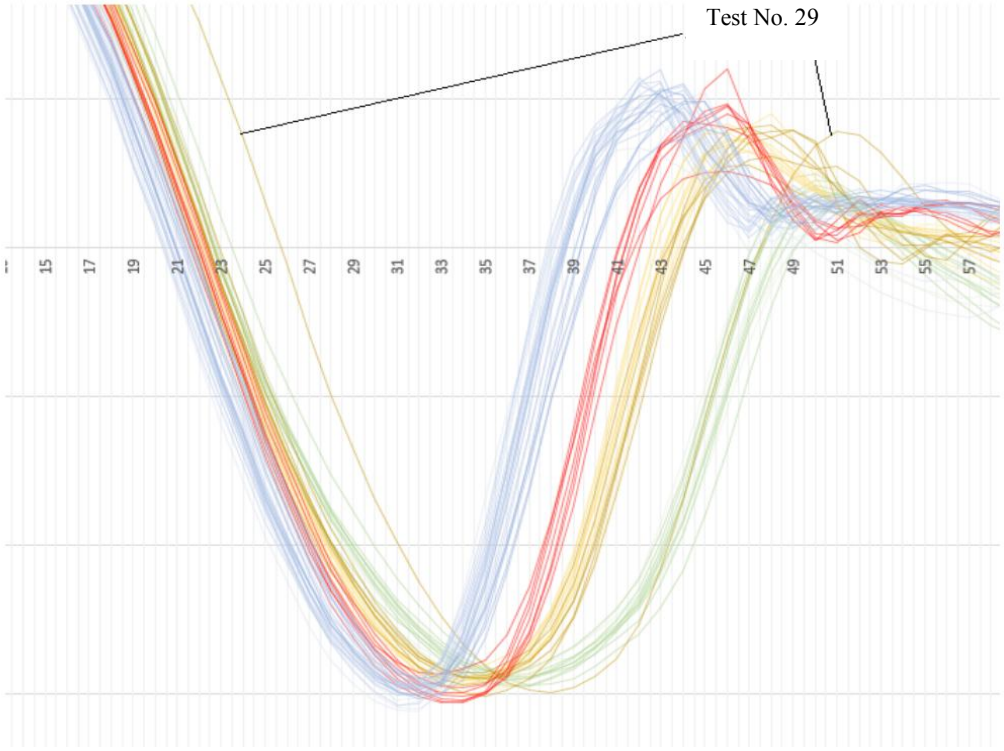


Fig. 5. Fragment of the diagram from Fig. 4 with a preliminary classification into four groups of steel classes and outlier Test No. 29 also after 0.31 ms [11]

Data integration is combining data on the same phenomenon from different sources into one database. An example of integration is presented in [12], which predicts a delay in the construction of sections of expressways and motorways in Poland. The independent variables on whose basis forecasts were made are data on the constructed facilities (prescribed by the Access to Information Act of the General Directorate for National Roads and Highways), data on enterprises implementing these facilities (collected in the Registration court), the Internet, the business intelligence agency, macroeconomic data (with a source in the publications of the Central Statistical Office). The dependent variable value (required for "training" an artificial neural network) is the number of days for which the completion of each of the analyzed road investments is postponed; it was searched for in publications in the press and on the Internet. The collected information was used for integrating the data on the implementation of 128 construction projects into the database. In Poland, 156 sections of expressways and motorways were built in 2009-2013, but it was almost impossible to get complete information on them. After analyzing this construction progress, those cases were rejected when unexpected violations occurred (e.g., in the form of protests by environmentalists, they were not taken into account in the analyses as an independent variable). This reduced the number of cases by 28, but provided the completeness and integrity of the database — the basis of the calculation.

**Data selection.** In large datasets, their size is a significant problem — a large number of records causes inefficient and long software performance. In databases with small record sizes, the search software for I/O relationships may not be sufficient to find those relationships. It happens that the phenomenon under study can be described by many parameters, but there are few cases (records) in the database with the described parameters of the phenomenon. Thus, the data selection means the need to choose only a few independent variables on whose basis the classification or prediction of the output value will be performed using artificial intelligence (also known as machine learning). When selecting independent variables, the following may be useful:

— study of the mutual correlation of linear independent variables, as well as the correlation with the values at the output;

— analysis of the main components;

— empirical search for the optimal set of independent variables.

**Correlation research.** The study of Pearson's linear correlation between pairs of independent variables and between each of them and the dependent variable can be presented in the form of a table with numbers, as well as graphically, in the form of so-called "heat maps" (pairs of independent variables) [13]. The variables are most strongly correlated positively, and the intense blue color in Figure 6 shows the lowest value of the Pearson coefficient. A strong positive or negative correlation read from the heat map does not oblige to delete a variable that is highly correlated with another; this is just an assumption, because it strongly positively correlates with zn2 (the correlation coefficient between them is 0.88), and at the same time zn5 does not correlate with the output (denoted as wy, the correlation coefficient is 0.03).

| | zn1 | zn2 | zn3 | zn4 | zn5 | wy |
|---|---|---|---|---|---|---|
| zn1 | **1.00** | **0.11** | **-0.58** | **0.17** | **0.77** | **0.90** |
| zn2 | **0.11** | **1.00** | **0.03** | **-0.30** | **0.88** | **0.35** |
| zn3 | **-0.58** | **0.03** | **1.00** | **0.30** | **0.52** | **-0.34** |
| zn4 | **0.17** | **-0.90** | **0.80** | **1.00** | **0.41** | **0.70** |
| zn5 | **0.77** | **0.88** | **0.52** | **0.41** | **1.00** | **0.03** |
| wy | **0.90** | **0.35** | **0.34** | **0.70** | **0.03** | **1.00** |

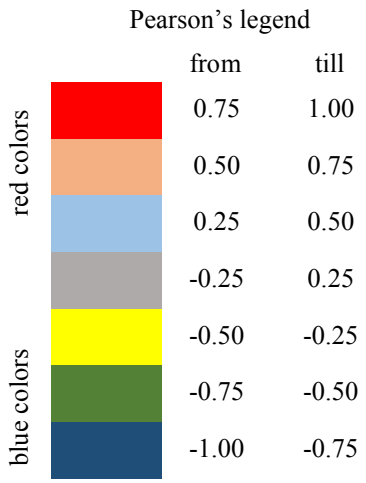


Fig. 6. Approximate "heat map" of independent variables from n1 to n5 and output data

Although linear correlation is computed, and the actual relationship between the independent variables (or the independent variable and the output-dependent variable) may not be linear, calculating these linear correlations often suggests which variables should not be included (if there is a need to reduce them). Such a check was made, among others, in [9, 12]. In [12], the number of dependent variables was reduced, and in [9], a new variable was accepted for analysis as the sum of the values of two strongly positively correlated independent variables (this was also technically justified). A variable that has a strong negative correlation with another independent variable can also be removed from the database.

**Principal component analysis.** Principal component analysis (PCA) is performed for independent variables — the output value is not taken into account[2] . As a result, we obtain a rating showing which of the independent variables most affects the variability of sets of independent variables. Each of the independent variables can measure multidimensional space. Independent variables are interconnected, they form sets (records in the database describing the phenomenon). The PCA result is the answer to the question which of the independent variables is most responsible for the fact that the distances (in multidimensional space) between points (sets of independent variables described in the records — coordinates of points) are the largest. The variables that have the least impact on the data scattering are those that can be removed from the analysis in an attempt to reduce the number of independent variables. Examples of the effective application of the principal component analysis to improve the performance of machine learning tools can be easily found, e.g., in [14–16]. However, it should be borne in mind that PCA does not consider the value of the dependent variable. Thus, there is no certainty that it is the independent variable that also has the greatest impact on the predicted value (the dependent variable) that causes the greatest variability in the datasets.

[2] StatSoft. Internetowy Podręcznik Statystyki. URL: https://www.statsoft.pl/textbook/stathome.html (accessed: July 2020).

**Empirical research.** Both the correlation study and the principal component analysis do not give absolute confidence whether the selection of independent variables was optimal. Optimal here means the most accurate prediction or the maximum possible proportion of accurate classifications for the database and the selected machine learning tool. Artificial intelligence tools are most often applied when their user suspects that there is a connection between input and output (between sets of independent variables and the effect of their joint occurrence — a dependent variable). When these dependences cannot be described strictly (by a function of many variables), when the studied processes and phenomena are complex (Fig. 2), then using machine learning tools may be the only way to find out about it. So, it is hard to expect that any auxiliary tool will accurately indicate which of the dependent variables should be used to "train" artificial intelligence. Hence, one of the methods of searching for the optimal set of input data (dependent variables) is the empirical verification of the results of an artificial intelligence tool on various sets of dependent variables. There are two main modes of action: forward and backward. "Forward" means selecting two dependent variables based on which the results of the prediction or classification are the best. It is sometimes very easy to choose the first one, but it is difficult to imagine a prediction of delays without specifying the planned duration [12, 17]. To select the second variable, we check the operation of the tool on each created pair of dependent variables (they are sometimes called predictors) [18]. When the best pair of predictors is selected, one of the remaining predictors is added sequentially. This is done until adding some not-yet-used independent variable improves the results. In the backward procedure, the first step is to use all independent variables, and then remove sequentially only one, checking which predictor was removed, the accuracy of prediction and classification increased the most. The procedure continues until the removal of any of the predictors does not improve the results.

**Data consolidation and transformation.** The consolidation and transformation of data is so that it can be used by the selected data mining tool [6]. The most common form of data transformation is their standardization, i.e., such a transformation of the values of independent variables and dependent variable, in which they take values from the same range. Data standardization is the result of the need to provide each of the independent variables with a "level playing field" that will be included in the machine learning model. In [12], the formula is given:

$$dla\ 1 \le i \le\ k \qquad a_{1i} = \frac{a_{0i}}{max_k(a_{0i})} \tag{1}$$

where $k$ — number of records in the database;

$a_{0i}$ — i-th element of variable *a* before standardization;

$a_{1i}$ — $i$-th element of variable *a* after standardization.

The second widely used type of data standardization is the so-called standardization "to zero mean and standard deviation of one" defined from the following formula:

$$a_{1i} = \frac{a_{0i} - \overline{a_0}}{\sigma_a} \tag{2}$$

where $\overline{a_0}$ — arithmetic mean of variable *a* before standardization;

$a_{0i}$ — i-th element of variable *a* before standardization;

$a_{1i}$ — i-th element of variable *a* after standardization;

$\sigma_{0a}$ — standard deviation of variable *a* before standardization [7].

Other types of standardization, also nonlinear, can be found, e.g., in [19]. However, it should be remembered that the type of data standardization can change the results obtained through machine learning [20]. Thus, the type of data standardization can be one of the parameters that the tool adjusts to get the best results.

Binarization can be the second data transformation process. It means converting the numeric values of a variable into only two values (e.g., 0 and 1) according to the following formula [22]:

$$a_{1i} = \begin{cases} a_{0i} \le p \to 0 \\ a_{0i} > p \to 1 \end{cases} \tag{3}$$

http://vestnik-donstu.ru

where $a_{0i}$ — i-th element of variable *a* before binarization,

$a_{1i}$ — i-th element of variable *a* after binarization,

$p$ — user-selected parameter.

Data binarization is especially useful when searching for rules applying market basket analysis (also known as association analysis)[3] . This type of analysis was created to investigate the contents of shopping carts to increase sales. Computer programs with the market basket analysis module work most effectively if the variables are binary (this product was present in the shopping carts or not). Many scientific problems can be formulated, whose very essence is binary, but in most cases, the description of the phenomenon includes numbers that are converted into binary form for the application of the market basket analysis [21–22]. Such transformation can also be performed for a variable that may belong to several disjoint subsets. Then, two dichotomous subsets (which are the sums of the original subsets) are created from the primary subsets. Then, if $a_{0i}$ belongs to one of them, then $a_{1i}$ is 0, if the other is 1.

**Error measurements.** So far, the author has used general terms such as "accuracy of predictions", "correctness of classification", which can be called the quality or effectiveness of artificial intelligence tools. However, if we analyze ways to improve the quality of their work, it is required to identify errors in the results of machine learning tools and the results of data mining.

**Prediction errors.** Machine learning tools mainly serve two purposes: to predict values (regression) and to carry out automatic classification. Using the same commonly accepted error measures facilitates understanding of work, but also makes it easier to assess the value of the prediction. It is assumed that the absolute value of the error is analyzed. Therefore, the absolute error (AE) [7, 18] can be defined as

$$AE = \left|\hat{b} - b\right| \tag{4}$$

where $\hat{b}$ — predicted value;

$b$ — actual observed value.

Relative error expressed as absolute percentage error (APE), is defined as

$$APE = \left|\frac{\hat{b}-b}{b}\right| * 100\% \tag{5}$$

To be able to evaluate the quality of predictions made through an artificial intelligence tool (e.g., an artificial neural network), some data is not used in the "learning" process. After building the model, this dataset called a test sample is entered, and the machine makes predictions. So, the predicted values are a dozen, a few dozen or more. Then, to assess the quality of predictions, you can calculate the mean absolute percentage error (MAPE):

$$MAPE = \frac{\sum_{i=1}^{n}\left(\left|\frac{\hat{b}_i-b_i}{b_i}\right|*100\%\right)}{n} \tag{6}$$

where *n* — size of the validation sample.

The most common error measure (check test) is the mean square error (MSE), defined as

$$MSE = \frac{\sum_{i=1}^{n}(\hat{b}_i-b_i)^2}{n} \tag{7}$$

When solving regression problems, most machine learning tools, through the use of heuristic algorithms, search for input and output display that minimizes MSE. When specifying the quality of the predictions received, the most common are MSE or MAPE (or both). It should be noted that in case of MAPE, it does not matter whether this error is calculated for standardized or real values — MAPE is the same. This is not the case with MSE. This error most often has different values for standardized predictions and for predictions converted to true values (without standardization). Hence, it is required to specify for which values the MSE were calculated. Comparing the accuracy of predictions (different processes, phenomena with different instruments) based on MSE is feasible if MSE is calculated

[3] StatSoft. Internetowy Podręcznik Statystyki. URL: https://www.statsoft.pl/textbook/stathome.html (accessed: July 2020).

for standardized values. On the other hand, from the point of view of practical application, MAPE or the maximum value of AE is more important. The usefulness of the predictions obtained is also an important issue [24]. Predicting indirect construction costs with an average relative error of 6 % can be considered accurate and useful, but the same 6 % MAPE for stock market predictions makes them useless [24]. Thus, the size of the error obtained in the predictions should also be assessed from the point of view of usefulness for decision-makers using predictions.

**Classification accuracy measures.** When using machine learning tools for automatic classification, assignment of a case to the wrong class can be assessed in two ways. First, just as a mistake. However, the mere information that the tool correctly classifies 90 % of cases may not be enough. If there are multiple classes assigned to separate cases (described in the database) (e.g., 8), it may happen that for 5 classes, the classification is 100 % correct, and 10% of the errors are attributed to the other 3 classes. Hence, the quality of the classification results is assessed by the so-called error matrix (Table 1).

Table 1

Results of classification of tender procedures by validation sample [25]

| | **Class: free from collusion** | **Class: suspicion of collusion** | **Class: collusion is highly likely** | **Total: for all classes** |
|---|---|---|---|---|
| Validation sample size | 52 | 14 | 4 | 70 |
| Number of correct classifications | 50 | 10 | 3 | 63 |
| Number of misclassifications | 2 | 4 | 1 | 7 |
| Share of correct classifications in % | 96.15 | 71.43 | 75.00 | 90.00 |
| Share of misclassifications in % | 3.85 | 28.57 | 25.00 | 10.00 |

Significant differences in the classification accuracy of individual subsets may contribute to the further search for an even more accurate classification model. The error matrix may also contain information to which incorrect class this record from the validation sample was incorrectly assigned. This affects the forecasting inference. Analyzing the example from Table 1 with the following assumptions:

— 2 misclassified records from the “free from collusion” class assigned to the “suspicion of collusion” class by the automatic classifier;

— 4 misclassified cases from the “suspicion of collusion” class were assigned to the “highly likely collusion” class by the automatic classifier;

— 1 misclassified case from the “highly likely” class was assigned to the “suspicion of collusion” class by the automatic classifier,

it can be stated that as long as the classifier does not assign this procedure to the “free from collusion” class, one can be sure that this production is not related to collusion. All cases assigned to this class were correctly classified by the automatic classifier (despite the classification accuracy of less than 100%). This effect was used, e.g., in [11]. Thus, it is worth analyzing which classes this case was automatically assigned to.

The classification error in medical applications is the division of errors into only two classes, where it is just as important not to administer medications to a healthy person as not to refuse treatment to a really sick person (mistaking him healthy) (Fig. 7).

| | | Class assigned by the classifier | |
|---|---|---|---|
| | | positive | negative |
| Sorted class | positive | Number of positive correct, defined as TP | Number of positive incorrect, defined as FN |
| | negative | Number of negative incorrect, defined as FN | Number of negative correct, defined as TN |

Fig. 7. Classification error matrix into two classes; gray background indicates correct classification[4] [26]

For *n* classified cases, the following equality holds:

$$n = TP + FP + TN + FN \tag{8}$$

To interpret the error matrix in the form shown in Figure 7, the concepts of accuracy, precision, sensitivity, specificity, are used; they are determined from the following equations[5] [26]:

$$accuracy = \frac{TP+TN}{n} \tag{9}$$

$$precision = \frac{TP}{TP+FP} \tag{10}$$

$$sensitivity = \frac{TP}{TP+FN} \tag{11}$$

$$specificity = \frac{TN}{FP+TN} \tag{12}$$

However, it should be remembered that the above indicators are applicable only if the tool classifies but two classes.

**Determination of the significance of the discovered association rules.** Through the market basket analysis (one of the mining tools), rules are discovered in the data that can be written as

$$b \rightarrow h \tag{13}$$

where *b* — predecessor;

*h* — successor of the rule.

This rule reads as follows: if there was a predecessor, then there was a successor. Both the predecessor and the successor may consist of several variables, but most often the rules are sought in which the predecessor is described by many variables, and the successor — by one (e.g., if the pressure dropped in the morning and the temperature at noon exceeded 30, then there was a thunderstorm in the afternoon). Such a rule (as in the example above) does not always work. Consequently, the quality measures of the discovered rules are not error measures, but three parameters (proportions) [6, 9], through which it can be easily determined that the rule will be checked in case of violation of the predecessor [3, 4, 6]:

— support — marked as *sup*

— confidence — marked as *conf*;

— marked as *lift*

[4] PQStat Statystyczne Oprogramowanie Obliczeniowe. Available from: https://pqstat.pl/?mod_f=diagnoza (assessed: July 2020). (In Polish)
[5] PQStat Statystyczne Oprogramowanie Obliczeniowe. Id.

Support is defined as follows:

$$sup(b \to h) = \frac{n(b \to h)}{N} \quad (14)$$

where $n(b \to h)$ — the number of cases in which the occurrence of a predecessor was accompanied by the occurrence of a successor;

$N$ — the number of all cases in the database.

On the other hand, the validity of the rule is determined as follows:

$$conf(b \to h) = \frac{n(b \to h)}{n(b)} \quad (15)$$

where $n(b)$ — the number of cases in which the occurrence of a predecessor was noted.

Equally important is a lift of the rule. If its value is less than 1, it means that the found rule does not explain the occurrence of a successor. Lift is defined as follows:

$$lift(b \to h) = \frac{conf(b \to h)}{P(h)} \quad (16)$$

where $P(h)$ — the likelihood of a successor (independent form the predecessor occurracne).

For a better understanding of the assessment of the quality of the association rules discovered, there is an example in which 10 observations were made in 12 processes for the occurrence of a predecessor and a successor (Fig. 8). For the rule "if a predecessor, then a successor ", support, confidence and lift (for each of the processes) were calculated (Table 2).

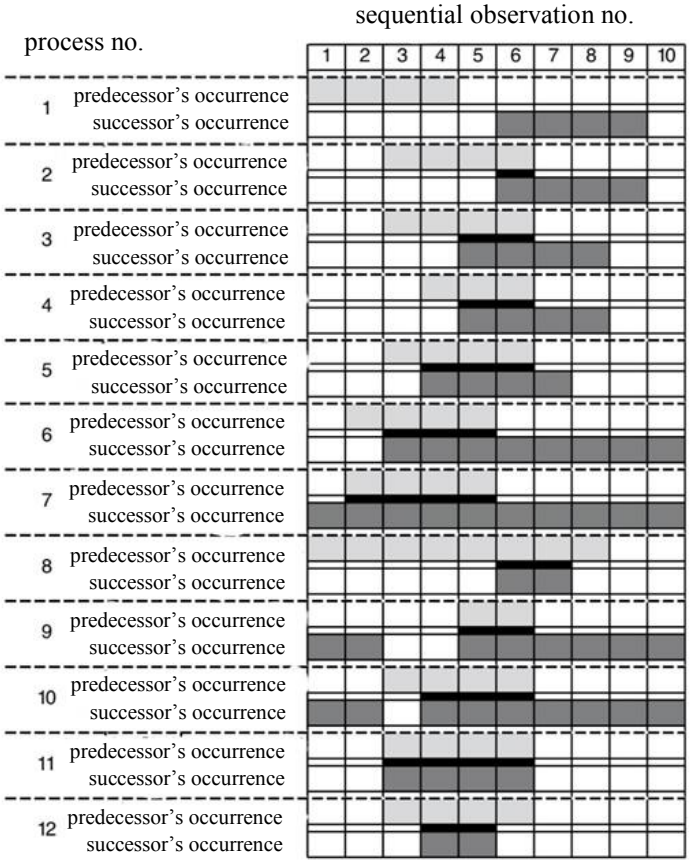


Fig. 8. Observing the occurrence of predecessor and successor in 12 processes

Source: own development

Comparing processes 5 and 6, it should be noted that a high degree of reliability of the rules is not always important. In process 6, a successor is almost always present, and the discovered rule does not explain the occurrence of the successor (*lift*<1). This does not apply to process 8. Lift indicates the importance of the rule, while its confidence is

http://vestnik-donstu.ru

low. However, every observation of the successor is accompanied by an observation of the predecessor. In case of process 8, therefore, it is worth clarifying the predecessor (e.g., by adding another variable). In that event, probably, another parameter (not yet included in the predecessor) affects the presence of a successor (in process 8).

Table 2

Rule evaluation using *sup*, *conf*, and *lift* for the processes in Figure 8

| Process no. | Support ($Sup$) | Confidence ($Conf$) | Increment ($Lift$) |
|---|---|---|---|
| 1 | 0.00 | 0.00 | 0.00 |
| 2 | 0.10 | 0.25 | 0.63 |
| 3 | 0.20 | 0.50 | 1.25 |
| 4 | 0.20 | 0.67 | 1.67 |
| 5 | 0.30 | 0.75 | 1.88 |
| 6 | 0.30 | 0.75 | 0.94 |
| 7 | 0.40 | 1.00 | 1.00 |
| 8 | 0.20 | 0.25 | 1.25 |
| 9 | 0.20 | 1.00 | 1.25 |
| 10 | 0.30 | 0.75 | 0.83 |
| 11 | 0.40 | 1.00 | 2.50 |
| 12 | 0.20 | 0.50 | 2.50 |

**Important aspects of applying selected tools of artificial intelligence and data mining to small databases**

**The number of records in the database and complexity of the tool.** In statistics, it is most often assumed that a small sample size is less than 30 cases, but it can be found that the limit beyond which we cannot talk about a small sample is 100 [27−28]. Artificial intelligence tools need complete data sets (inputs and outputs) to be able to find the most accurate way to transform one into another. The more complex the problem, the more data sets (records in the database) are required. In deep learning, when a tool is taught not with sets of numbers, but with files (graphics, audio, text), thousands of data sets are needed. In [29], more than 4,000 standardized images were used to predict compressive strength. In other studies, there were few samples (e.g., in [11] there were only 66). There is an indication that for artificial neural networks, the number of connections between neurons should be 10 times less than the number of records in the database [30]. Small databases require more computational testing and finer tuning of the tools used. However, the rule that the more complex the problem and its model, the more data sets are required to train the tool, remains valid. The application of complex models (e.g., artificial neural networks with more than one hidden layer and many neurons in hidden layers) in small databases most often causes errors (prediction or classification), much greater than in models with less complexity of the tool itself. Hence the popularity of the methods of reducing the number of independent variables described in Section 3. When the number of datasets is too small, reducing the number of independent variables most often increases the accuracy of forecasts and classification.

**Type of inference and quality of prediction and classification.** Paper [30] suggests that artificial neural networks can more accurately determine whether, e.g., the predicted value will be greater than the value given by the network user. Referring to the requirement of the prediction usefulness [23], if the predictions obtained are not accurate enough (i.e., the prediction errors are too large), it is possible to decide whether an accurate value is required. When, e.g., predicting the strength of a material, it is possible, instead of a prediction, only to report that the strength will not be lower than the estimated strength specified by the user. It is the same with the classification problem. Automatic classification of steel into 9 grades based on a total of 66 entries in the database did not enable to obtain the classification accuracy above 80 % [11]. Then, one classification process was replaced by the eighth, as a result of which the steel test results were divided into two dichotomous subgroups, as shown in Fig. 9.

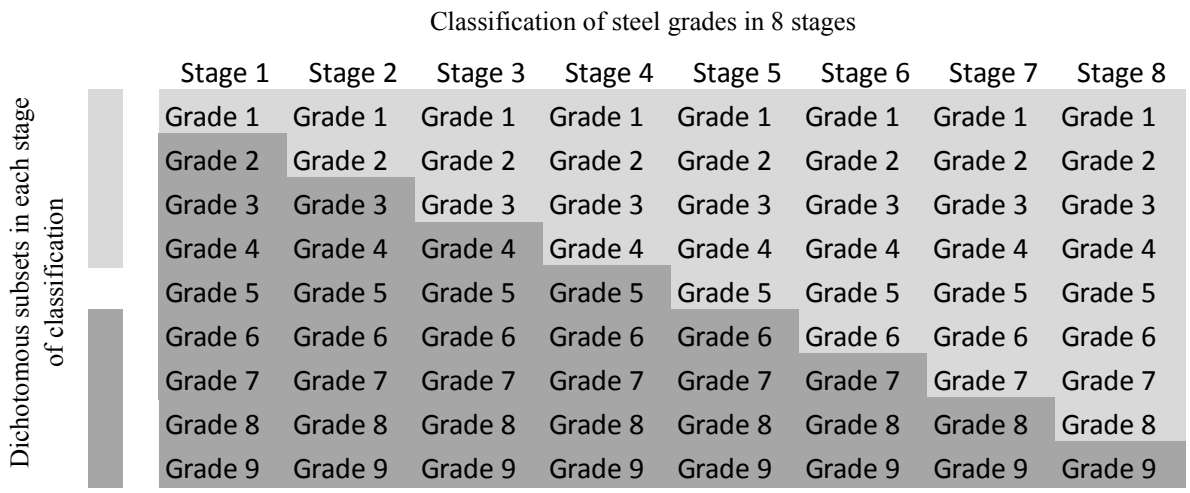


Fig. 9. Eight-stage classification process into 2 dichotomous subsets (at each stage of classification) [11]

Automatic classification of only two subsets was carried out using a simpler model (with complexity corresponding to the number of steel tests, i.e., 66). The process used eight times provided an increase in the classification accuracy from 80 to 95 %. In [12], out of the originally selected 12 predictors, only 6 remain. This made it possible to make a sufficiently small error prediction for the model to be useful. Computer programs enable to predict, e.g., 2 dependent variables at the same time; but for the above reasons, better results (smaller errors) are obtained when predicting 2 dependent variables separately, using 2 models, although the results are obtained on the same dataset.

**Output modification.** Let us consider the case when at the initial stage of calculations, sufficiently accurate predictions or classifications are not obtained. In addition to the actions related to data and complexity in the machine learning tool used above, we can consider the possibility of searching for another dependent variable, the one on whose basis it will be possible to calculate a strictly dependent variable that needs to be found. With a small number of records in the database, this can simplify the model, which, in turn, can increase the accuracy of predictions. This effect was used in [31], where an artificial neural network prediction is only part of the mixture design process. Another procedure that can reduce prediction errors is the prediction of a relative value (instead of an absolute value). When optimizing the operation in [12], the predicted delay expressed in days was replaced by a delay expressed as a proportion of the number of days of delay to the planned number of days of the construction. In this case, it did not reduce the errors in the predictions. Another possibility to change the type of output (i.e., the predicted dependent variable) is to replace one number with several values of membership functions calculated on the basis of fuzzy set theory [32]. In [17], instead of the number of days of the construction delay at the output of an artificial neural network, 3 values of the set membership function were used: low delay, medium delay and long delay. After clarifying the predicted values, it turned out that the prediction errors were less than when predicting the number of days of delay [12]. The same was done in [33] through predicting the values of the membership function at the first stage of calculations, and only at the second stage, based on these predictions, the cases were divided into 3 subsets. However, in this case, the direct application of an artificial neural network as a classifier caused an increase in the classification accuracy.

**Hybrid tools.** With a small number of cases in the database, the machine learning tool used cannot be very complex since there are too few cases to successfully train the model. Hybrid models can be a remedy for too big a prediction error or too low classification accuracy. Instead of one complex tool, two simpler ones are used. In the above example [17], the application of fuzzy set theory actually adds 2 elements to the model that can be properly “tuned”. The diagram of the model is shown in Figure 10.

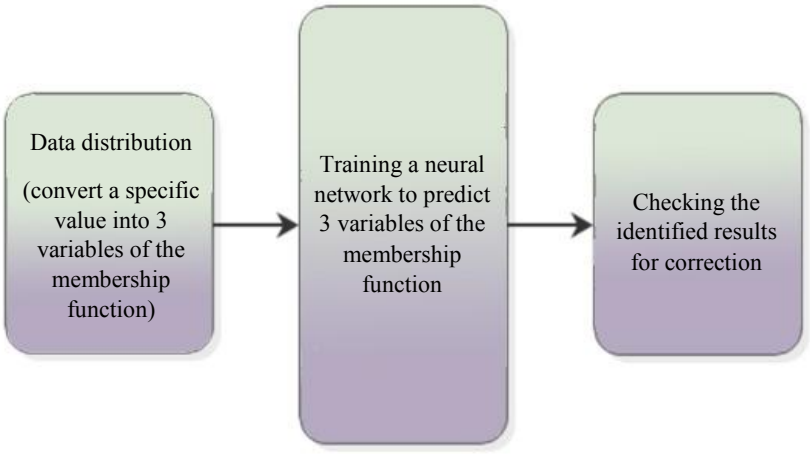


Fig. 10. Three modules of the neuro-fuzzy model [17]

The first module is the conversion of exact numbers into the values of three membership functions. The second is to configure the network to predict these three values with the least error, and the third is to increase the accuracy of the obtained forecasts to exact numbers. Operations in each of these three modules can be performed differently, so, 3 tools can be used to model the dependent variable, and not just the artificial neural network itself. There is variety of examples when hybrid models, i.e., those in which more than one tool, are used together and make more accurate predictions than models with one tool [34–30]. Therefore, when analyzing research results, it is worth considering the possibility of using machine learning tools together with other mathematical tools.

**Separation of the validation subset.** To train artificial neural networks, from an existing database, three subsets are allocated, containing both independent and dependent variables: training, testing and validation. The training subset is used to train the tool. This process continues until the MSE stops decreasing in the test sample, then the network learning process stops. Further training of the network could lead to a better agreement of the tool with the training data, but the possibilities of generalization would be lost (the MSE errors for the test and test samples would be much higher) [30]. This effect, called artificial neural network overfitting, is schematically shown in Figure 12.

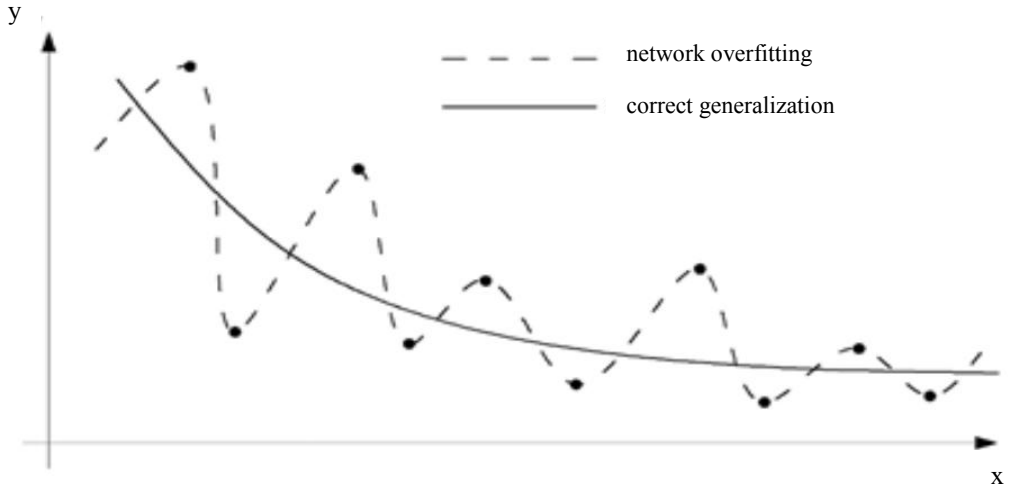


Fig. 12. Schematic of artificial neural network overfitting and correctly found trend [32–33]

A validation subset is used to assess the quality of predictions or classification. These sets of independent variables and the dependent variable do not see the network in the learning process. Therefore, predictions (or classifications) are made for a test subset, and the errors described in the previous sections can be calculated through comparing to the known dependent variables. It is critical to specify which subset the calculated error belongs to. One of the methods of assessing whether the tool is not overfitted is to compare errors (most often MSE) for the above three subsets, they should be at a similar level. Explicitly lower MSE for the training subset may indicate overfitting, and

explicitly higher MSE may indicate a tool imperfection. Explicitly lower MSE for the test and validation sample implies the need to select other parameters of the artificial neural network or other dependent variables (or even another tool).

For large databases, a random division of data into three subsets is appropriate. There are suggestions in the literature that the proportions of the size of these subsets should be in the range of 60:20:20–70:15:15 (trainer: test: check) [36–37]. For small databases, random selection is only appropriate when different ranges of the dependent variable (or class for classification) are equally numerically represented. Most often, this condition is not met. Then it would be good to provide such a balanced representation in all 3 subsets. This controlled data separation was used in [11, 25]. In [11], out of 66 tests of steel, one brand (5 tests) was the least numerous, and the brand with 12 tests was the most numerous. With a random selection of tests for subsets, it could happen that not a single test of any steel grade was included in the training subgroup, which would undoubtedly prevent its automatic recognition. In [25], out of 249 analyzed cases, only 9, according to the authors, should be classified as "highly likely collusion". After partitioning the dataset into subsets, 4 of these procedures were assigned to the training one, 1 — to the test one, and 4 — to the validation one. With this procedure, 3 out of 4 procedures in the validation set can be correctly classified.

In the Polish and English-language literature, you can find examples of the authors using only the concepts of a training dataset, a test dataset. This probably happens for two reasons. Some computer programs completely (without user intervention) control whether the tool is overfitted. Then, only the validation set is extracted (either by specifying its quantity or percentage in the total data, or through selecting the records to be used for validation). In this case, a validation subset is often called a test subset. The second reason is that some machine learning tools (e.g., classification trees, C&RT trees[6]) are protected from overfitting in a different way than MSE control for a test sample. The quality of these tools can be checked using a test subset (just like a validation subset — without participating in the learning process of the tool). Usually, already when reading papers on machine learning, it comes out whether two or three subsets of data have been allocated, so the different nomenclature of the set used to assess the quality of work is not a problem.

**Model quality check.** Databases with a small number of records used to build a model based on machine learning make the model less stable (i.e., give significantly different errors) when replacing records between subsets (training, testing, and validation). To see if the constructed model works well with only a certain separation of data into subsets, it should be run on randomized subsets. Using suggestions on the proportion of data separation, they can be divided into 5–7 subsets, and as many model building processes should be performed as possible, so that training will take place at each iteration. This model quality check is called cross-validation (in English, cross-validation datasets are called "convolutions"). The MSE or MAPE errors are then averaged. If, however, errors in any dataset deviate significantly from the average value, you should seek the reason for this.

Regardless of the size of the database, error estimation should also be viewed through the prism of the usefulness of the results. Predictions with relatively large errors, phenomena that cannot be accurately described, can be very useful and considered important. On the other hand, predictions with the same MSE or MAPE of another phenomenon may not give any new information on the phenomenon being studied. Thus, in addition to numerical values of prediction accuracy or classification accuracy, it is important to refer to the phenomenon under study itself.

It is also critical to check whether another model has been built for the previously studied phenomenon. If so, then a link to these previous studies (regarding the level of errors obtained there) will also validate the quality of the new patented solution. If such models have not been created before, you can check the quality of the new solution through comparing the results to a much simpler model (e.g., based on Microsoft Excel with Solver add-in).

There is a question to which there is no clear answer yet: does a small number of datasets mean that the predictions, classifications and association rules obtained are irrelevant (precisely because of their small number)?

For example, a complex and strict rule with the following indexes: $sup = 0.01,\ conf = 1,\ lift = 100$ for a database with 10,000 records means that every time a particular predecessor occurs 100 times, the specified predecessor

http://vestnik-donstu.ru



[6] StatSoft. Internetowy Podręcznik Statystyki. URL: https://www.statsoft.pl/textbook/stathome.html (accessed: July 2020).

is always (sic!) the next one. The same rule for a database of 100 records means that there was only one unique case when the specified predecessor took place. In one case, you cannot talk about a rule, but you can talk about a case (randomness). However, even for a small database (e.g., with 100 records), a 100 % confidence rule supported by 3 cases may already indicate repeatability (provided that the increment for this rule is greater than one).

There are small databases, usually because they are small in themselves, because the preparation of larger ones is expensive and very time-consuming. Moreover, they can also be a consequence of the nature of the phenomenon (e.g., a limited number of objects constructed by the same company). In reality, these databases cannot be expanded (several times or several dozen times). Analyzing such databases under the conditions described in this chapter, may cause the emergence of new, as yet unrecognized dependences. Constructed, properly functioning models may not be directly applicable to other similar phenomena, but they can effectively indicate methods for finding common relationships in cases where the number of datasets is much larger. Unique association rules or unexpected automatic classifications may also indicate areas on which further research of the described phenomena should be focused.

**Summary.** The problems and issues discussed in the paper related to the search for relationships between multidimensional input and output data are presented in a small number of cases. This work, therefore, cannot be a comprehensive subject overview. The length of the paper and the author's limited experience in applying machine learning and data mining methods do not allow describing most of the methods used. Calculation problems (mainly on small databases) contained in the works mentioned in the text and their solutions are systematized in such a way that the sequence of actions is observed: from database preparation to calculations, to discussion of the results. It is not possible to clearly state how many records in the database may indicate a "small" or "large" database. However, it can be said that at least several dozen records are required for the effective use of machine learning or data mining tools. Through applying appropriate procedures (input data development, model building), these tools can be used for successful modeling and studying phenomena described in only a few dozen cases. Based on the calculations carried out, it is possible to draw a reliable conclusion.

**References**

1. Lissowski G, Haman J, Jasiński M. Podstawy statystyki dla socjologów. Opis statystyczny. Tom 1. Warszawa: Wydawnictwo Naukowe Scholar; 2011. 223 p. (In Polish).

2. Stanisławek J. Podstawy statystyki: opis statystyczny, korelacja i regresja, rozkłady zmiennej losowej, wnioskowanie statystyczne. Warszawa: Oficyna Wydawnicza Politechniki Warszawskiej; 2010. 212 p. (In Polish).

3. Larose DT, Larose CD. Discovering Knowledge in Data: An Introduction to Data Mining. 2nd ed. Hoboken, NJ, USA: Wiley-IEEE Press; 2016. 309 p.

4. Larose DT. Metody I modele eksploracji danych. Warszaw: PWN; 2012. 337 p. (In Polish).

5. Hand D, Mannila H, Smyth P. Principles of Data Mining. Cambridge, MA, USA: MIT Press; 2001. 322 p.

6. Morzy T. Eksploracja danych. Metody i algorytmy. Warszawa: PWN; 2013. 533 p. (In Polish).

7. Bartkiewicz W. Sztuczne sieci neuronowe. W: Zieliński JS. (red), Inteligentne systemy w zarządzaniu. Teoria i praktyka. Warszawa: PWN; 2000. 348 p. (In Polish).

8. Rutkowski L. Metody i techniki sztucznej inteligencji. Warszawa: PWN; 2012. 449 p. (In Polish).

9. Doroshenko A. Applying Artificial Neural Networks In Construction. In: Proceedings of 2nd International Symposium on ARFEE 2019. 2020;143:01029. https://doi.org/10.1051/e3sconf/202014301029

10. Anysz H, Brzozowski Ł, Kretowicz W, et al. Feature Importance of Stabilised Rammed Earth Components Affecting the Compressive Strength Calculated with Explainable Artificial Intelligence Tools. Materials. 2020;13:2317. https://doi.org/10.3390/ma13102317

11. Beskopylny A, Lyapin A, Anysz H, et al. Artificial Neural Networks in Classification of Steel Grades Based on Non-Destructive Tests. Materials. 2020;13:2445. https://doi.org/10.3390/ma13112445

12. Anysz H. Wykorzystanie sztucznych sieci neuronowych do oceny możliwości wystąpienia opóźnień w realizacji kontraktów budowlanych. Warszawa: Oficyna Wydawnicza Politechniki Warszawskiej; 2017. 280 p. (In Polish).

13. Rabiej M. Statystyka z programem Statistica. Poland: Helion, Gliwice; 2012. 344 p. (In Polish).

14. Mrówczyńska M, Sztubecki J, Greinert A. Compression of results of geodetic displacement measurements using the PCA method and neural networks. Measurement. 2020;158:107693. https://doi.org/10.1016/j.measurement.2020.107693

15. Mohamad-Saleh J, Hoyle BS. Improved Neural Network Performance Using Principal Component Analysis on Matlab. International Journal of the Computer, the Internet and Management. 2008;16:1–8.

16. Juszczyk M. Application of PCA-based data compression in the ANN-supported conceptual cost estimation of residential buildings. AIP Conference Proceedings. 2016;1738:200007. https://doi.org/10.1063/1.4951979

17. Anysz H, Ibadov N. Neuro-fuzzy predictions of construction site completion dates. Technical Transactions. Civil Engineering. 2017;6:51–58. https://doi.org/10.4467/2353737XCT.17.086.6562

18. Rogalska M. Wieloczynnikowe modele w prognozowaniu czasu procesów budowlanych. Lublin: Politechniki Lubelskiej; 2016. 154 p. (In Polish).

19. Kaftanowicz M, Krzemiński M. Multiple-criteria analysis of plasterboard systems. Procedia Engineering. 2015;111:351–355. https://doi.org/10.1016/j.proeng.2015.07.102

20. Anysz H, Zbiciak A, Ibadov I. The influence of input data standardization method on prediction accuracy of artificial neural networks. Procedia Engineering. 2016;153:66−70. https://doi.org/10.1016/j.proeng.2016.08.081

21. Nicał A, Anysz H. The quality management in precast concrete production and delivery processes supported by association analysis. International Journal of Environmental Science and Technology. 2020;17:577-590. https://doi.org/10.1007/s13762-019-02597-9

22. Anysz H, Buczkowski B. The association analysis for risk evaluation of significant delay occurrence in the completion date of construction project. International Journal of Environmental Science and Technology. 2019;16:5396–5374. https://doi.org/10.1007/s13762-018-1892-7

23. Zeliaś A, Pawełek B, Wanat S. Prognozowanie ekonomiczne. Teoria, przykłady, zadania. Warszawa: PWN; 2013. 380 p. (In Polish).

24. Juszczyk M, Leśniak A. Modelling Construction Site Cost Index Based on Neural Network Ensembles. Symmetry. 2019;11:411. https://doi.org/10.3390/sym11030411

25. Anysz H, Foremny A, Kulejewski J. Comparison of ANN Classifier to the Neuro-Fuzzy System for Collusion Detection in the Tender Procedures of Road Construction Sector. IOP Conference Series: Materials Science and Engineering 2019;471:112064. https://doi.org/10.1088/1757-899X/471/11/112064

26. Piegorsch WW. Confusion Matrix. In: Wiley StatsRef: Statistics Reference Online. 2020. P. 1-4 (accessed: July 2020) https://doi.org/10.1002/9781118445112.stat08244

27. Kot SM, Jakubowski J, Sokołowski A. Statystyka. Warszawa: DIFIN; 2011. 528 p. (In Polish).

28. Aczel AD, Saunderpandian J. Statystyka w zarządzaniu. Warszawa: PWN; 2000. 977 p. (In Polish).

29. Narloch P, Hassanat A, Trawneh AS, et al. Predicting Compressive Strength of Cement-Stabilized Rammed Earth Based on SEM Images Using Computer Vision and Deep Learning. Applied Sciences. 2019;9:5131. https://doi.org/10.3390/app9235131

30. Tadeusiewicz R. Sieci neuronowe. Kraków: Akademicka Oficyna Wydawnicza; 1993. 130 p. (In Polish).

31. Anysz H, Narloch P. Designing the Composition of Cement Stabilized Rammed Earth Using Artificial Neural Networks. Materials. 2019;12:1396. https://doi.org/10.3390/ma12091396

32. Zadeh LA. Fuzzy Sets. Information and Control. 1965;8:338–353. https://doi.org/10.1016/S0019-9958(65)90241-X

33. Yagang Zhang, Guifang Pan. A hybrid prediction model for forecasting wind energy resources. Environmental Science and Pollution Research. 2020;27:19428–19446. https://doi.org/10.1007/s11356-020-08452-6

34. Eugene EA, Xian Gao, Dowling AW. Learning and Optimization with Bayesian Hybrid Models. 2020 American Control Conference (ACC). IEEE; 2020. https://doi.org/10.23919/ACC45564.2020.9148007

35. Hagan MT, Demuth HB, Beale MH, et al. Neural Network Design. Martin Hagan: Lexington, KY, USA; 2014. 1012 p.

36. Osowski S. Sieci neuronowe do przetwarzania informacji. Warszawa: Oficyna Wydawnicza PW; 2006. 419 p. (In Polish).

Received 01.10.2021
Revised 25.10.2021
Accepted 26.10.2021

*About the Author:*

**Hubert Anysz,** assistant professor, Faculty of Civil Engineering, Warsaw University of Technology (1, Pl. Politechniki, Warsaw, 00-661, Poland), PhD, Scopus, Researcher, ORCID, h.anysz@il.pw.edu.pl

*The author has read and approved the final manuscript.*

# INFORMATION TECHNOLOGY, COMPUTER SCIENCE, AND MANAGEMENT

UDC 625.7/.8 https://doi.org/10.23947/2687-1653-2021-21-4-364-375

## Evaluation of the elastic modulus of pavement layers using different types of neural networks models

**M. M. M. Elshamy** [1, 2], **A. N. Tiraturyan** [1], **E. V. Uglova** [1] ✉

[1] Don State Technical University (Rostov-on-Don, Russian Federation)

[2] Al-Azhar University (Cairo, Arab Republic of Egypt)

✉ uglova.ev@yandex.ru

***Introduction.*** This paper studies the capability of different types of artificial neural networks (ANN) to predict the modulus of elasticity of pavement layers for flexible asphalt pavement under operating conditions. The falling weight deflectometer (FWD) was selected to simulate the dynamic traffic loads and measure the flexural bowls on the road surface to obtain the database of ANN models.

***Materials and Methods.*** Artificial networks types (the feedforward backpropagation, layer-recurrent, cascade back-propagation, and Elman backpropagation) are developed to define the optimal ANN model using Matlab software. To appreciate the efficiency of every model, we used the constructed ANN models for predicting the elastic modulus values for 25 new pavement sections that were not used in the process of training, validation, or testing to ensure its suitability. The efficiency measures such as mean absolute error (MAE), the coefficient of multiple determinations $R^2$, Root Mean Square Error (RMSE), Mean Absolute Percent Error (MAPE) values were obtained for all models results.

***Results.*** Based on the performance parameters, it was concluded that among these algorithms, the feed-forward model has a better performance compared to the other three ANN types. The results of the best four models were compared to each other and to the actual data obtained to determine the best method.

***Discussion and Conclusions.*** The differences between the results of the four best models for the four types of algorithms used were very small, as they showed the closeness between them and the actual values. The research results confirm the possibility of ANN-based models to evaluate the elastic modulus of pavement layers speedily and reliably for using it in the structural assessment of (NDT) flexible pavement data at the appropriate time.

***Keywords:*** asphalt pavements, artificial neural networks (ANN), falling weight deflectometer (FWD), backpropagation network, nondestructive test (NDT).

***For citation:*** M. M. M. Elshamy, A. N. Tiraturyan, E. V. Uglova. Evaluation of the elastic modulus of pavement layers using different types of neural networks models. Advanced Engineering Research, 2021, vol. 21, no. 4, p. 364–375. https://doi.org/10.23947/2687-1653-2021-21-4-364-375

*© Elshamy M. M. M., Tiraturyan A. N., Uglova E. V., 2021*

**Introduction.** All pavement roads will deteriorate over time, regardless of how well designed or constructed [1]. Deterioration of the pavement is affected by traffic volume, climate condition, building quality, layers thickness and the efficiency of earlier rehabilitation and treatment plan. Usually, the pavement condition stays good in the first 50−75 % of service life and the processes of deterioration progress slowly. The degradation processes make rapid progress once the pavement status is decreased [2, 3]. Proper maintenance or repair activities may slow down or reset degradation processes if utilized at a suitable time.

The structural condition of pavements can be evaluated using non-destructive surface deflection testing; impulse load devices such as Falling Weight Deflectometer (FWD) and Heavy Weight Deflectometer (HWD). It is the most frequently used measuring instrument for this objective. Based on the measured pavement responses in deflection tests, material layer modules can be estimated using back-calculation [4, 5].

The FWD load tests simulate traffic characteristics such as type, volume, and time of vehicle loading correctly. These devices apply an impulse load (P) through a mass in free fall on a circular plate with a cylindrical rubber buffer mounted under the falling weight system [6, 7]. The device records the vertical pavement deformation using different sensors located at various distances from the centre of the loading circle [8, 9], as shown in Figure 1. The maximum displacement is known as the peak deflection, which occurs under the loading point. Traditional methods use the highest values of FWD deflections to back-calculate linear elastic modulus for each layer of pavement [10].

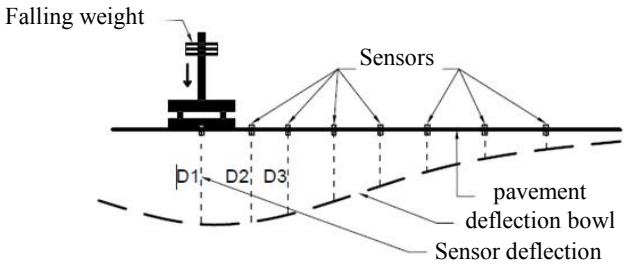


Fig. 1. Pavement deflection according to FWD testing

During the past few years, it has been observed that the pavement administrations use new and different methods of collecting and processing data for road maintenance [11]. Due to the rapid development of information technology and artificial intelligence, there have been multiple opportunities for implementation in developing pavements management systems.

More effective ways to address the problem of specifying (complex, non-linear, multivariate) parameters should be considered. ANN is one of the artificial intelligence techniques that provide solutions to classification and regression problems. It is known as one of the best techniques for data mining tasks. It has a framework for different machine learning algorithms to perform together with data inputs. ANN learns how to predict the output from a set of attributes. The algorithm learns to forecast during the training process, which must include data with a large domain, to avoid a problem of falling the expected data outside that range, which affects the validity of the results [12]. In addition, the frequency of sampling should be sufficient to learn correctly. It has been observed from a lot of research that ANN provided good accuracy in pavement performance prediction. The goal of ANN is to find solutions to problems in a similar manner that a human brain does [13].

In 2004, the authors submitted a formulation for the reverse calculation of the pavement layer modules using artificial neural networks (ANN). The research has shown that the proposed ANN method needs considerably less time computed than other methods such as layered elastic theory, equivalent layer thickness (ELT), and finite-element methods, respectively. The ANN is used in simulation at a high rate because it can learn complex nonlinear relationships [14].

Halil Ceylanet and the contributing authors (2008) developed back-calculation models based on artificial neural networks (ANNs) for predicting the elastic modulus of the Portland cement concrete (PCC) layer and the coefficient of subgrade reaction for the pavement foundation. ANN-based models have been trained to estimate the layer modules with deflective basin data (FWD) and the pavement structure thickness. The research indicates that the ANN models can predict the rigid module of paving layers with high precision [15].

More studies were conducted on the development of more accurate and effective models with algorithms of optimization and hybrid systems [16–19].

G. Beltrán and the contributing authors (2014) collected data from field tests to recalculate layer models by artificial neural network models. The results proved the efficiency of the ANN models in calculating the pavements parameters [20].

Maoyun Li and Hao Wang built a model for calculating the elasticity modulus for flexible pavement layers using both the genetic algorithm and the artificial neural network system based on the falling weight deflectometer data. The results of the ANN-GA model showed reasonable accuracy with the data registered in the LTPP test database, where there were no big differences between the predicted values of the elastic modulus for the asphalt surface layer and the registered in the LTPP data [21].

In this investigation, several analyses were performed to define the best possible architecture along with learning rules and the type of the ANN model to increase the forecasting capabilities of ANNs. The used database includes wide ranges of deflection values obtained from impact load tests conducted on existing three-layer pavement systems on the roads network by the State Company Russian Highways from 2014 to 2018. It was utilized as an experimental basis for training artificial neural network models.

**Materials and Methods**

**The properties of the used sections.**

In Table 1, the acceptable limits of the pavement layer parameters used in building models are mentioned for calculating the elasticity modulus for the pavement layers (surface, base, and subgrade).

Table 1

Limits of geometries and properties of materials for pavement sections

| Material type | Layer thickness (mm) | Poisson's Ratio | Layer elastic modulus (MPa) |
|---|---|---|---|
| Asphalt Concrete | T(AC)= 190 : 220 | V = 0.35 | $E_1$= 900 : 4500 |
| Base-layer | T(B)= 350 : 460 | V = 0.35 | $E_2$= 80 : 500 |
| Subgrade-layer | T(S)= ∞ | V = 0.35 | $E_3$= 40 : 150 |

Back-calculation models based on ANNs approach.

In this work, we used the back-propagation algorithm function to solve the problem of the nonlinear function mapping, where it has high efficiency between ANN algorithms [22–25]. Furthermore, ANN networks of this type are defined as the neural networks of multilayer feed-forward. The traditional architecture of artificial neural networks is preserved in this algorithm. The structure of this algorithm consists of inputs and outputs represented by neurons, and between them, there are connections used to transfer the weights given to each cell according to its effect. The back-propagating algorithm is characterized by its ability to change the neuron weights to reduce the differences between the goals and the output values of the algorithm using the error reduction technique [26]. The final set of node biases and connection weights is known when the error rate is reduced to permissible limits [27].

The network is trained by different algorithms with the training dataset.

– Feed-Forward Model

The feed-forward network involves at least three layers (the input layer, the hidden layer, and the output layer), and it may increase to have more than one hidden layer according to the network needs. As it is clear from the name of the network, the information has one direction from the input to the hidden layer and then to the output layer, as in Figure 2.

– Layer Recurrent Model

The structures of the recurrent neural network and the feed-forward network are similar, but the recurrent neural network is unique in that there is a specific feedback loop to each layer in the network except for the last layer, as shown in Figure 3. This feedback loop permits the network to have an unlimited dynamic reaction to incoming time series data.

– Cascade Forward Network Model

The Cascade forward network is similar to a feed-forward network, with the only difference being that it includes a link from the input to each layer and from each layer to the following layers. As shown in Figure 4, the Cascade forward model produces links from the first to the second Layer, from Layer 2 to Layer 3, and from the first to the third Layer. These networks also provide input connections for all layers, where additional links can quickly improve the learning process of the network model.

– Elman Neural Network

The Elman neural network structure overrides the feed-forward network by having a layer called the context layer in addition to the input, output and hidden layers. The function of the context layer is to store the output of the hidden layer

in each finished cycle and reuse it as input to the hidden layer in the next iteration to ensure that patterns are generated over time, as shown in Figure 5. Elman networks also reduce the error rate in the outputs to the permissible limits by using the back-propagation feature, as is the case in the forward propagation network.

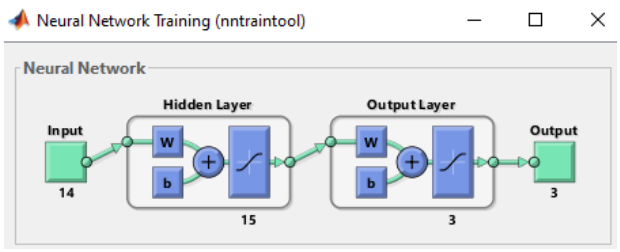


Fig. 2. Structure of feed-forward network

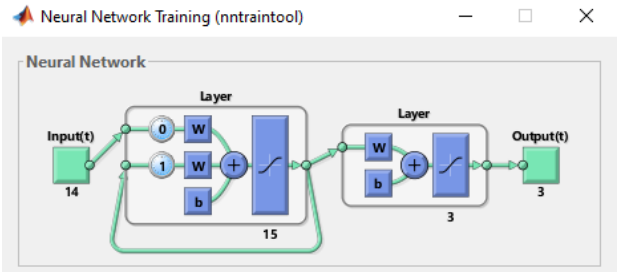


Fig. 3. Structure of layer recurrent network

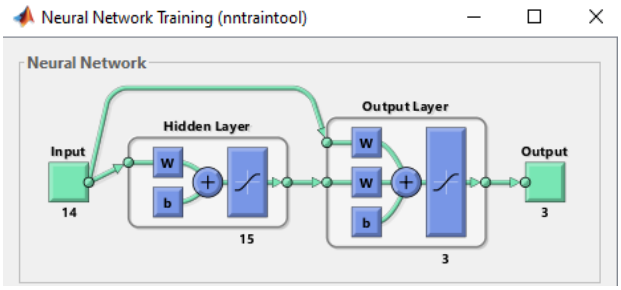


Fig. 4. Structure of cascade network

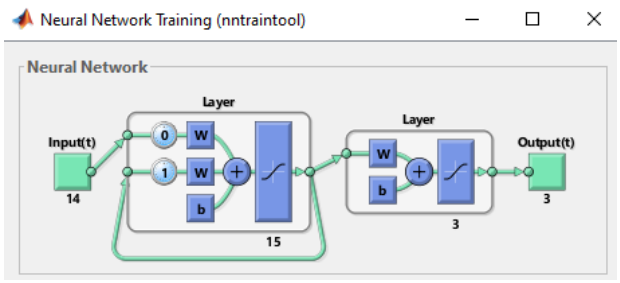


Fig. 5. Structure of Elman back-propagation network

Through the command of "nntool" in the Matlab program, we implemented the created ANN models. The data that was used in building the models belong to a group of asphalt sections of the M-4 highway of the Russian road network. The set of training data used in this study included the results of calculating the elastic moduli of the structural layers of non-rigid road pavements, carried out in a specialized software package supplied with an FWD Primax shock loading unit on 555 pavement sections, managed by the State Company Russian Highways. We used four types of artificial neural networks, which were (feed-forward, layer recurrent, cascade, and Elman) back-propagation to get the best results. Several cells were selected in the hidden layer for each type of model to study its effect on the training process. The program divided the data at random with 70 % for the training process, 15 % for verification, and 15 % for the testing process. Figure 6 shows the architecture of the artificial neural network model.

We carried out three steps to obtain the optimal number of neurons and hidden layers in ANN models: we trained the model with different hidden layers (first step), estimated the results of the performance model (second step), and compared the predicted values of the tested data to the target values (third step).

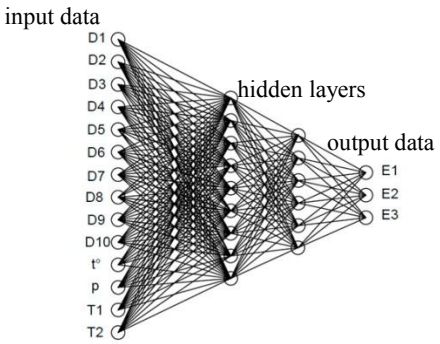


Fig. 6. Neural network architecture to determine the elastic moduli of the structural layers of the flexible pavements

D1, D2, D3 .... D10 are the results of the measured deflection values under the sensors — geophones; t° is the surface temperature of the pavement; P is the pressure on the pavement; T1 and T2 are the thickness of the layers of asphalt concrete and the thickness of the base layer of the pavement; E1, E2, and E3 – the elastic moduli of asphalt concrete layers, the base, and the subgrade, respectively.

The Models Evaluation.

The correctness of the values of the prediction results for every model is calculated using the mean absolute error (MAE), the multiple determinations coefficient $R^2$, the mean root square error (RMSE), and the mean absolute percentage error (MAPE), which are determined from the following formulas (1, 2 and 3):

$$MAE= \frac{1}{n} \sum_{t=1}^{n} \left|A_t - E_t\right| \quad (1)$$

$$RMSE= \sqrt{\frac{\sum_{t=1}^{n} (A_t - E_t)^2}{n}} \quad (2)$$

$$MARE= \frac{1}{n} \sum_{t=1}^{n} \left|\frac{A_t - E_t}{A_t}\right| *100 \quad (3)$$

Where $A_t$ is the actual value in period t; $E_t$ is the expected value in period t; and n is the number of the total period. With respect to the statistical indices, MAE, RMSE and MAPE, smaller values usually indicate higher accuracy results. In this analysis, the MAE, $R^2$, RMSE and MAPE values for every model are obtained through comparing the predicted results against the actual values.

**Results**. Four types of NNA were developed with four different neuron numbers in the hidden layers to see which one is more suitable to use in the forecasting process. The total number of ANN models generated was sixteen. All models were trained under various conditions, including 10, 15, 17, and 20 neurons in the hidden layers. The values of the following MAE, $R^2$, RMSE and MAPE indices for all models were calculated as shown in Table 2 to assess the model performance.

Table 2

Evaluation models performance

| | **Prediction E(AS) of feed-forward models** | | | | **Prediction E(AS) of cascade models** | | | | **Prediction E(AS) of Elman models** | | | | **Prediction E(AS) of layer-recurrent models** | | | |
|---|---|---|---|---|---|---|---|---|---|---|---|---|---|---|---|---|
| | 10n | 15n | 17n | 20n | 10 n | 15n | 17n | 20n | 10n | 15n | 17n | 20n | 10n | 15n | 17n | 20n |
| MAE | 2.58 | 3.24 | 5.61 | 4.9 | 41.2 | 2.48 | 5.61 | 31.8 | 1.46 | 1.81 | 1.39 | 6.45 | 4.11 | 7.66 | 4.85 | 9.27 |
| $R^2$ | 1.00 | 1.00 | 1.00 | 1.0 | 0.91 | 1.00 | 1.00 | 0.95 | 1.00 | 1.00 | 1.00 | 1.00 | 1.00 | 1.00 | 1.00 | 1.00 |
| RMSE | 3.38 | 10.3 | 10.7 | 11 | 202 | 7.78 | 10.7 | 149. | 2.05 | 6.48 | 3.20 | 26.1 | 7.15 | 16.9 | 10.5 | 25.7 |
| MARE | 0.11 | 0.15 | 0.24 | 0.26 | 1.73 | 0.12 | 0.24 | 1.34 | 0.08 | 0.08 | 0.06 | 0.27 | 0.16 | 0.34 | 0.22 | 0.47 |
| | **Prediction E(base) of feed-forward models** | | | | **Prediction E(base) of cascade models** | | | | **Prediction E(base) of Elman models** | | | | **Prediction E(base) of layer-recurrent models** | | | |
| | 10n | 15n | 17n | 20n | 10n | 15n | 17n | 20n | 10n | 15n | 17n | 20n | 10n | 15n | 17n | 20n |
| MAE | 1.11 | 0.61 | 1.39 | 1.15 | 0.55 | 0.77 | 1.39 | 1.74 | 0.89 | 0.86 | 1.02 | 1.65 | 1.37 | 1.43 | 0.87 | 1.17 |
| $R^2$ | 1.00 | 1.00 | 1.00 | 1.00 | 1.00 | 1.00 | 1.00 | 0.99 | 1.00 | 1.00 | 1.00 | 0.99 | 1.00 | 1.00 | 1.00 | 1.00 |
| RMSE | 2.10 | 2.16 | 3.58 | 2.8 | 0.82 | 2.70 | 3.58 | 6.01 | 2.14 | 3.51 | 3.34 | 6.19 | 1.80 | 2.62 | 1.19 | 3.24 |
| MARE | 0.42 | 0.19 | 0.48 | 0.4 | 0.23 | 0.24 | 0.48 | 0.52 | 0.30 | 0.25 | 0.33 | 0.51 | 0.58 | 0.55 | 0.36 | 0.38 |
| | **Prediction E(sub-grade) of feed-forward models** | | | | **Prediction E(sub-grade) of cascade models** | | | | **Prediction E(sub-grade) of Elman models** | | | | **Prediction E(sub-grade) of layer-recurrent models** | | | |
| | 10n | 15n | 17n | 20n | 10n | 15n | 17n | 20n | 10n | 15n | 17n | 20n | 10n | 15n | 17n | 20n |
| MAE | 1.82 | 0.38 | 1.81 | 4.5 | 1.51 | 2.90 | 1.81 | 2.22 | 3.34 | 0.92 | 2.90 | 4.37 | 1.74 | 1.63 | 1.89 | 2.12 |
| R2 | 0.99 | 1.00 | 0.99 | 0.87 | 0.99 | 0.96 | 0.99 | 0.95 | 0.87 | 0.99 | 0.93 | 0.86 | 0.98 | 0.99 | 1.00 | 0.97 |
| RMSE | 4.48 | 0.73 | 3.91 | 13.3 | 2.81 | 10.6 | 3.91 | 5.85 | 10.5 | 2.48 | 7.19 | 17.4 | 4.16 | 2.78 | 4.07 | 4.84 |
| MARE | 1.84 | 0.46 | 1.94 | 4.6 | 1.92 | 2.32 | 1.94 | 2.15 | 3.22 | 0.86 | 2.85 | 3.85 | 2.16 | 2.13 | 1.96 | 2.53 |

http://vestnik-donstu.ru

The best four models that express the four types of artificial neural networks were selected based on the values of the analytical parameters mentioned in the previous table for the results of the models to compare them and know the extent of their impact. Whereas, the best results were due to the models with two hidden layers and 14-15-3 structure for all developed types. All models took the maximum number of repetitions to complete the training process, which were 1000 repetitions. But they differed in the periods taken for training, as training of the models ended after (54, 157, 67, and 173) seconds for the four models, respectively, as shown in Figures (7−10). Being aware of that, the training process stops if the maximum number of repetitions or the time rate is exceeded.

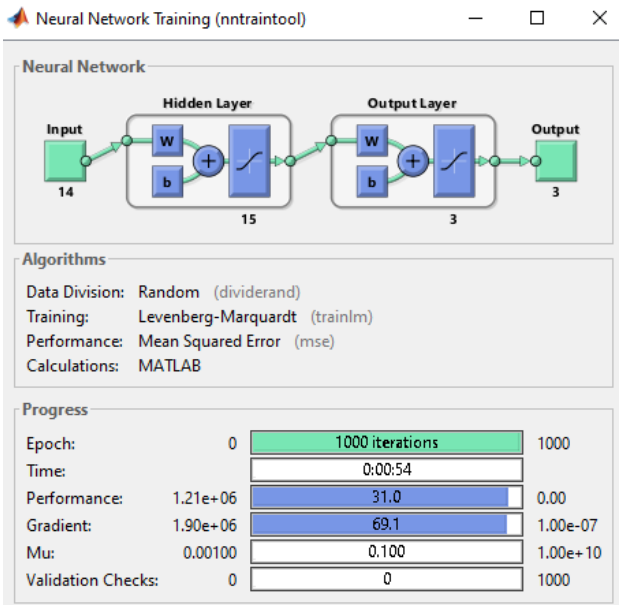


Fig. 7. Training window of feed-forward model

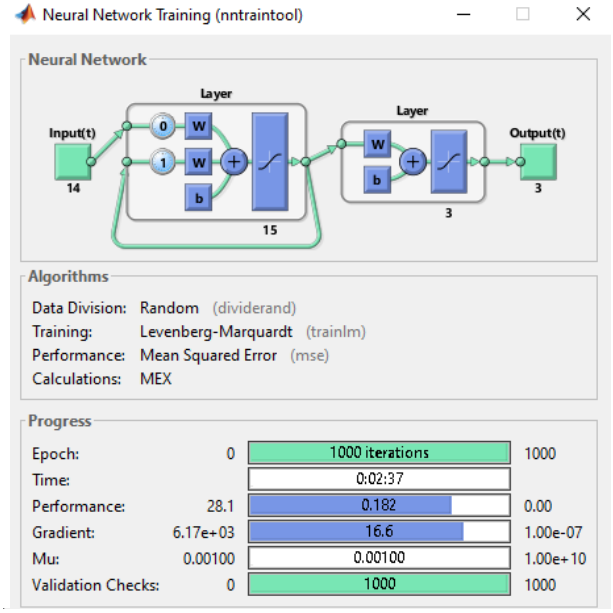


Fig. 8. Training window of layer recurrent model

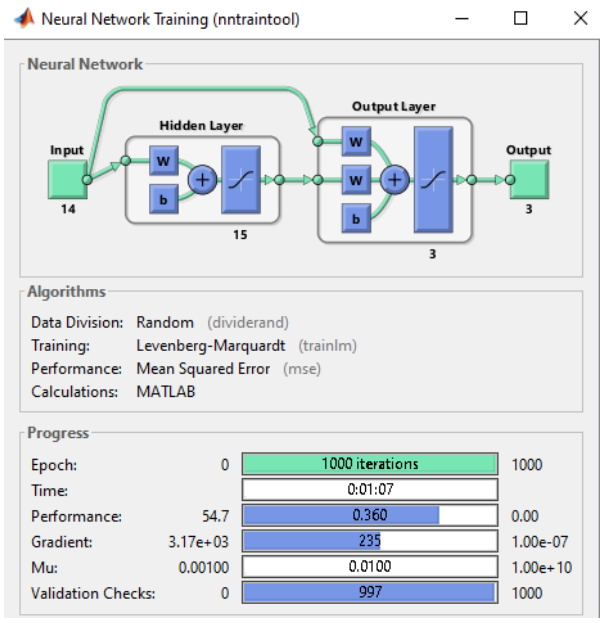


Fig. 9. Training window of cascade model

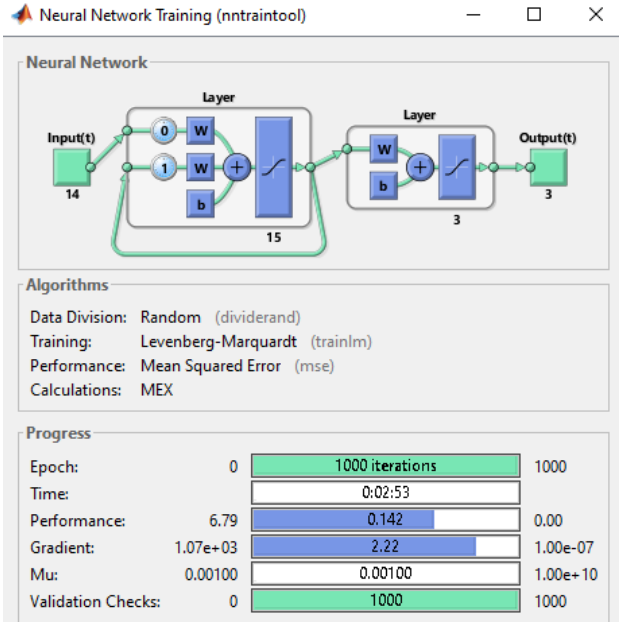


Fig. 10. Training window of Elman backpropagation

The weights and biases of all parameters were modified to decrease the error between target values and network output throughout the training phase. Each neuron weight is adjusted based on its impact on the network result. These weights and biases were evaluated during training as the weights of the inputs to the hidden layer.

Figures (11–14) illustrate the mean squared error values vs the number of iterations for the training process of the compared models, respectively. When using the feed-forward back-propagation model, the best validation performance was

16.68 at epoch 1000. Otherwise, the best validation performance for the layer recurrent, cascade and Elman back-propagation models were (11.52, 119,888 and 28,067) at epoch zero, respectively. In all of the curves, we observe the convergence of the test curves with the validation curves, which revealed that the test and validation curves are very similar.

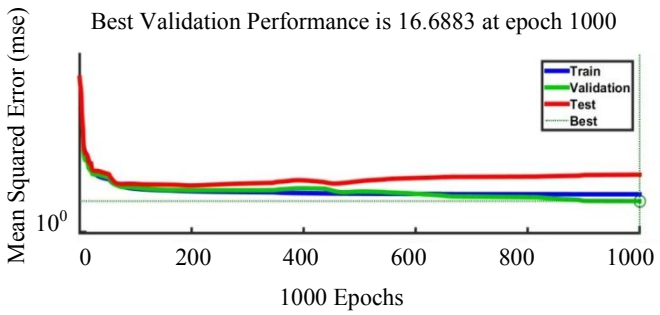


Fig. 11. Performance of feed-forward model

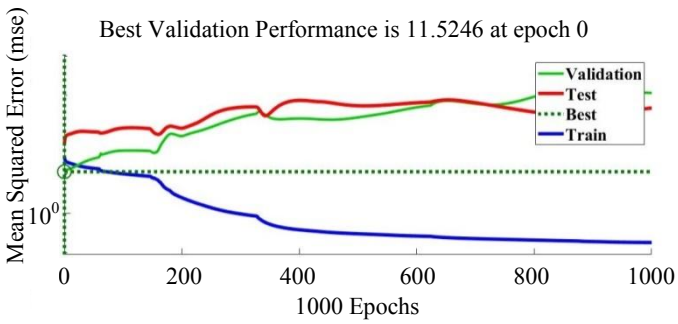


Fig. 12. Performance of layer recurrent model

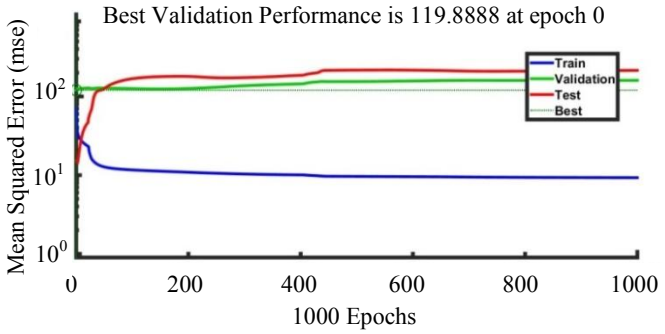


Fig. 13. Performance of cascade model performance

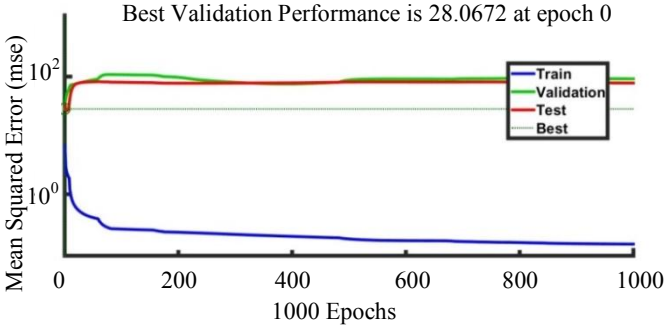


Fig. 14. Performance of Elman model

According to Figures (15 and 16), artificial neural networks are evaluated using a correlation function (R) between network result values against target data in feed-forward and cascading back-propagation models. Looking at the R-value of the models during the training, validation and testing phases, we notice a good agreement between the target values and the network results. Where we find that the slope of the line that represents the relationship between data and results is approximately equal to 1 in all stages of training, and this indicates the robustness of the models and the possibility of using them during the prediction process.

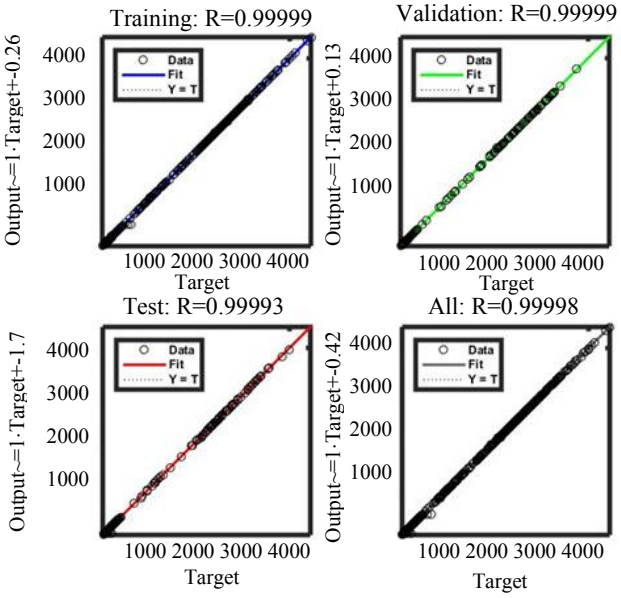


Fig. 15. Feed-forward model regression charts

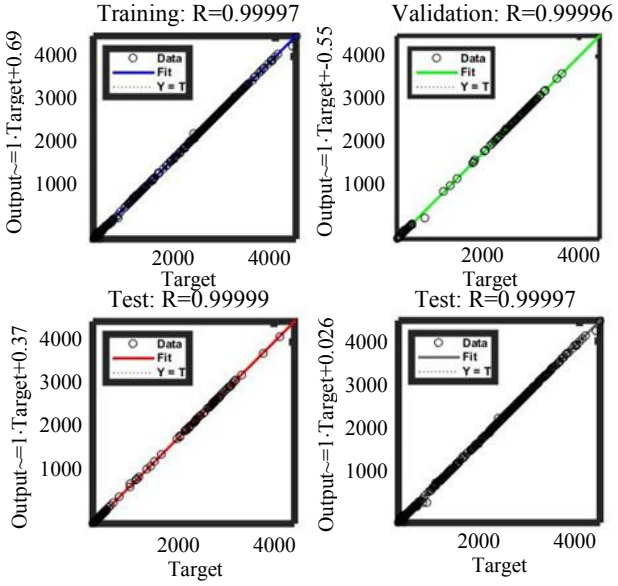


Fig. 16. Cascade backpropagation regression charts

http://vestnik-donstu.ru

At the beginning of network learning, all learning stages of training, validation, and testing, run in an open loop. Once the training phase is over, the network performance turns into a closed loop during the multi-stages of prediction.

The models that correctly represent the available data are selected during the stages of education, verification, and testing, based on the statistical parameters, as mentioned previously. It was required to determine if the models could forecast the elastic modulus for 25 segments that had not been utilized during model training and compare them to target values, along with knowing how much the network type affected its performance in terms of elastic modulus assessment. Table 3 shows the comparison of the elastic modulus target values for all layers (asphalt concrete, base, and subgrade) of 25 sections and the forecasting results values of the four ANN types (feed-forward, layer recurrent, cascade, and Elman) back-propagation models.

Table 3

The comparison of the predictions of the proposed models

| **Actual modulus of elasticity, MPa** | | | **Predicted values of feed-forward model, Mpa (15n)** | | | **Predicted values of layer recurrent model, Mpa (15n)** | | | **Predicted values of cascade backprop model, Mpa (15n)** | | | **Predicted values of Elman backprop model, Mpa (15n)** | | |
|---|---|---|---|---|---|---|---|---|---|---|---|---|---|---|
| Asphalt | Base | Sub-grade | Asphalt | Base | Sub-grade | Asphalt | Base | Sub-grade | Asphalt | Base | Sub-grade | Asphalt | Base | Sub-grade |
| 1017.0 | 208.1 | 63.1 | 1013.6 | 209.0 | 64.5 | 1024.6 | 208.0 | 67.3 | 1016.7 | 207.1 | 63.3 | 1017.7 | 209.3 | 64.5 |
| 1559.1 | 255.2 | 155.8 | 1565.1 | 254.9 | 157.8 | 1575.9 | 250.1 | 144.6 | 1565.1 | 255.8 | 151.1 | 1569.1 | 255.6 | 166.9 |
| 1226.2 | 200.7 | 88.9 | 1226.4 | 200.3 | 87.1 | 1227.7 | 201.6 | 88.1 | 1226.9 | 200.2 | 92.6 | 1222.9 | 201.0 | 93.9 |
| 2380.9 | 389.8 | 139.0 | 2431.7 | 400.5 | 137.2 | 2305.9 | 400.3 | 143.7 | 2349.2 | 407.3 | 149.8 | 2418.0 | 403.2 | 190.7 |
| 3309.2 | 329.5 | 61.9 | 3312.3 | 329.4 | 61.8 | 3302.4 | 332.5 | 62.4 | 3310.4 | 329.6 | 61.9 | 3309.9 | 329.8 | 62.2 |
| 1883.9 | 187.6 | 51.1 | 1881.0 | 187.1 | 51.0 | 1878.3 | 189.8 | 48.5 | 1885.4 | 187.7 | 51.4 | 1883.3 | 187.9 | 51.2 |
| 2104.6 | 209.6 | 45.3 | 2103.2 | 209.6 | 45.9 | 2099.3 | 209.3 | 45.1 | 2104.4 | 209.6 | 44.9 | 2104.7 | 210.0 | 44.9 |
| 2763.7 | 275.2 | 57.3 | 2761.9 | 275.1 | 57.0 | 2763.8 | 274.6 | 58.1 | 2763.4 | 275.3 | 57.3 | 2763.8 | 275.2 | 57.1 |
| 3124.2 | 311.1 | 61.2 | 3124.0 | 310.9 | 61.2 | 3120.2 | 312.3 | 60.9 | 3124.5 | 311.1 | 61.2 | 3124.0 | 311.2 | 61.5 |
| 2810.1 | 279.8 | 58.2 | 2809.8 | 279.8 | 58.2 | 2810.7 | 279.9 | 57.9 | 2810.0 | 279.8 | 58.2 | 2809.9 | 279.8 | 58.2 |
| 2733.7 | 272.2 | 60.1 | 2733.6 | 272.2 | 60.1 | 2733.3 | 271.9 | 59.1 | 2733.7 | 272.2 | 60.1 | 2733.7 | 272.1 | 60.2 |
| 2718.9 | 270.8 | 60.5 | 2718.7 | 270.5 | 60.6 | 2719.9 | 270.8 | 59.6 | 2718.8 | 270.6 | 60.5 | 2718.8 | 270.5 | 60.7 |
| 3266.2 | 325.3 | 73.0 | 3270.4 | 325.6 | 73.1 | 3254.1 | 324.4 | 71.9 | 3265.4 | 325.1 | 72.8 | 3265.8 | 325.4 | 73.1 |
| 2430.0 | 242.0 | 55.3 | 2430.4 | 242.0 | 55.3 | 2428.2 | 242.3 | 55.8 | 2429.9 | 242.1 | 55.1 | 2430.1 | 241.9 | 55.2 |
| 3671.5 | 365.6 | 69.3 | 3668.3 | 365.7 | 69.0 | 3700.0 | 365.8 | 70.5 | 3671.3 | 365.6 | 68.9 | 3666.3 | 365.0 | 69.7 |
| 2395.2 | 238.5 | 58.1 | 2395.2 | 238.6 | 58.0 | 2394.0 | 238.3 | 56.9 | 2395.1 | 238.5 | 58.1 | 2395.3 | 238.3 | 57.9 |
| 2328.7 | 231.9 | 63.2 | 2329.0 | 232.3 | 63.1 | 2327.0 | 232.5 | 62.8 | 2328.7 | 232.4 | 63.6 | 2328.2 | 232.0 | 63.3 |
| 2810.1 | 279.8 | 64.8 | 2809.8 | 279.8 | 64.7 | 2810.8 | 280.3 | 64.1 | 2809.8 | 279.8 | 64.7 | 2810.3 | 279.8 | 64.8 |
| 2350.5 | 234.1 | 60.2 | 2350.8 | 234.2 | 60.1 | 2346.3 | 233.2 | 59.1 | 2350.6 | 234.2 | 60.5 | 2350.4 | 234.1 | 60.3 |
| 2406.7 | 239.7 | 59.1 | 2406.8 | 239.7 | 59.0 | 2403.0 | 238.7 | 58.1 | 2406.8 | 239.7 | 59.1 | 2406.8 | 239.6 | 59.2 |
| 1927.2 | 191.9 | 54.8 | 1927.9 | 192.1 | 54.7 | 1929.3 | 193.7 | 56.1 | 1927.4 | 191.9 | 54.8 | 1927.2 | 192.1 | 54.8 |
| 1746.5 | 173.9 | 56.0 | 1746.0 | 173.7 | 55.8 | 1745.2 | 177.2 | 58.5 | 1746.5 | 173.9 | 56.4 | 1747.8 | 173.8 | 55.9 |
| 2149.6 | 214.1 | 55.6 | 2149.3 | 214.0 | 55.6 | 2146.1 | 213.3 | 55.7 | 2149.7 | 214.1 | 55.5 | 2149.6 | 214.3 | 55.6 |
| 1927.2 | 191.9 | 48.3 | 1927.1 | 191.8 | 48.5 | 1932.6 | 192.7 | 50.1 | 1927.8 | 191.8 | 47.8 | 1926.5 | 192.3 | 48.0 |
| 2095.8 | 208.7 | 50.5 | 2095.9 | 208.9 | 50.4 | 2095.6 | 208.6 | 51.3 | 2095.9 | 208.8 | 50.2 | 2095.7 | 209.1 | 50.2 |

A high degree of convergence can be shown between the four models when they are compared to each other and to actual data, as shown in Figure 17 (a, b, c). It is also understood from the results that the models can reduce the error

during the process of predicting the elastic modulus, where the lowest value of the coefficient of multiple determination was "$R^2$ = 0.95" for the cascade back-propagation model. However, the best performance in the prediction process, as shown in Table 2, was for the feed-forward model with a 14-15-3 structure, which had the lowest values for the statistical parameters MAE, RMSE, and MAPE, and the largest value for the coefficient of multiple determination ($R^2$) for the three pavement layers (asphalt, base, and substrate).

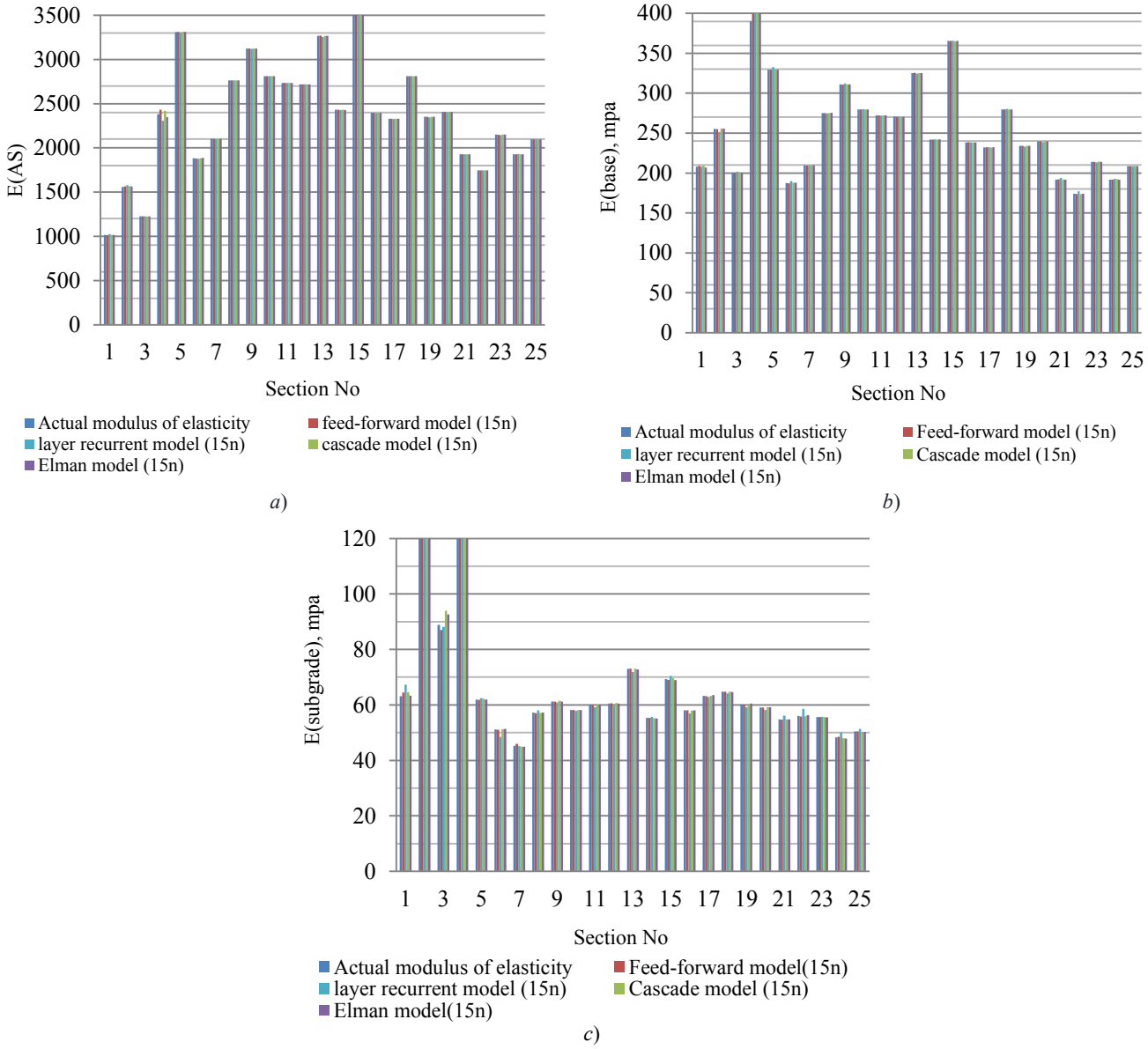


Fig. 17 (a, b, c): Illustration of the comparison between the values of the target elasticity modulus against the expected values of the developed ANN models and each other for all pavement layers

**Discussion and Conclusion.** The authors constructed sixteen models in the study. Every four models follow four different artificial neural network types (feed-forward, layer recurrent, cascade, and Elman back-propagation) to calculate the elastic modulus of the pavement layers subjected to dynamic load. The FWD test was selected to represent the dynamic load generated by the road traffic and to measure the reaction of the pavement. Matlab software was used to create ANN models utilizing deflection data from the (M4) highway in the Russian Federation Road network.

The differences between the results of the four best models for the four types of used algorithms were very small, as they showed closeness between them and the target values. The best results were for the feed-forward model with 15

neurons in the two-hidden layers to form the structure of the model 14-15-3, which produced the best values for the statistical coefficients.

There is no correlation between an increase or a decrease of neurons in the hidden layers and an improvement in models' performance. Instead, the decision is dependent on trial and error.

From the results, we find the capability of ANN models to predict the elastic modulus of flexible pavement correctly and use it in managing the pavement deteriorations.

**Acknowledgments.** Researcher Mohamed Mostafa Elshamy is funded by a scholarship under the executive program between the Arab Republic of Egypt and the Russian Federation. They have my thanks and appreciation.

**References**

1. Rukavina T, Ožbolt M. Pavement management system-data collecting. Gospodarenje prometnom infrastrukturom. Građevinski fakultet Sveučilišta u Zagrebu, Zavod za prometnice; 2009. P. 95–176.

2. Paterson WDO. Road deterioration and maintenance effects: Models for planning and management. Washington, D.C.: World Bank;1988. 454 p. http://worldcat.org/isbn/0801835909

3. Zaniewski JP, Mamlouk MS. Pavement maintenance effectiveness—Preventive maintenance treatments. Participant's Handbook. Report no. FHWA-SA-96-027, Federal Highway Administration, Washington, D.C.; 1996. 204 p. https://www.fhwa.dot.gov/pavement/pubs/013734.pdf

4. Liu GR, Xu Han. Recent progress on computational inverse techniques in non-destructive evaluation. In: Computational Fluid and Solid Mechanics 2003. Elsevier; 2003. P. 418–421. https://doi.org/10.1016/B978-008044046-0.50103-2

5. Tutumluer E, Pekcan O, Ghaboussi J. Nondestructive pavement evaluation using finite element analysis based soft computing models. NEXTRANS Center (US); 2009. 93 p.

6. Lukanen EO. Effects of buffers on falling weight deflectometer loadings and deflections (with discussion). Transportation Research Record. 1992;1355:37–51.

7. Schmalzer PN. Long-term pavement performance program manual for falling weight deflectometer measurements. MACTEC Enfineering and Consulting, Inc. United States. Federal Highway Administration (FHWA). Turner-Fairbank Highway Research Center; 2006. 79 p. https://rosap.ntl.bts.gov/view/dot/779.

8. Marecos V, et al. Evaluation of a highway pavement using non-destructive tests: Falling Weight Deflectometer and Ground Penetrating Radar. Construction and Building Materials. 2017;154:1164–1172. https://doi.org/10.1016/j.conbuildmat.2017.07.034

9. Öcal A. Backcalculation of pavement layer properties using artificial neural network based gravitational search algorithm. Middle East technical university; 2014. 181 p. http://etd.lib.metu.edu.tr/upload/12618019/index.pdf

10. Yang H Huang. Pavement analysis and design. Englewood Cliffs, NJ: Prentice-Hall; 1993. 815 p.

11. Sundin S, Braban-Ledoux C. Artificial intelligence–based decision support technologies in pavement management. Computer-Aided Civil and Infrastructure Engineering. 2002;16:143–157 https://doi.org/10.1111/0885-9507.00220

12. Ajbar A, Ali EM. Prediction of municipal water production in touristic Mecca City in Saudi Arabia using neural networks. Journal of King Saud University - Engineering Sciences. 2015;27:83–91. https://doi.org/10.1016/j.jksues.2013.01.001

13. Haykin S. Neural Networks: A Comprehensive Foundation. Upper Saddle River, N.J., Prentice Hall; 1999. 842p.

14. Saltan M, Terzi S. Backcalculation of pavement layer parameters using artificial neural networks. IJEMS. 2004;11:38−42. http://nopr.niscair.res.in/handle/123456789/9259

15. Ceylan H, Gopalakrishnan K, Bayrak MB. Neural networks based concrete airfield pavement layer moduli backcalculation. Civil Engineering and Environmental Systems. 2008;25:185–199.

https://doi.org/10.1080/10286600701838667

16. Nazzal MD, Tatari O. Evaluating the use of neural networks and genetic algorithms for prediction of subgrade resilient modulus. International Journal of Pavement Engineering. 2013;14:364–373.

17. Gopalakrishnan K, Khaitan SK. Finite element based adaptive neuro fuzzy inference technique for parameter identification of multilayered transportation structures. Transport. 2010;25:58–65. https://doi.org/10.3846/transport.2010.08

18. Gopalakrishnan K. Neural network–swarm intelligence hybrid nonlinear optimization algorithm for pavement moduli back-calculation. Journal of Transportation Engineering. 2010;136:528–536. 10.1061/(ASCE)TE.1943-5436.0000128

19. Kim D, Kim J-M, Mun S-H. Normalisation methods on neural networks for predicting pavement layer moduli. Road & Transport Research: A Journal of Australian and New Zealand Research and Practice. 2010;19:38–46.

20. Beltrán G, Romo M. Assessing artificial neural network performance in estimating the layer properties of pavements. Ingeniería e Investigación. 2014;34:11–16. http://dx.doi.org/10.15446/ing.investig.v34n2.42158

21. Li M, Wang H. Development of ANN-GA program for backcalculation of pavement moduli under FWD testing with viscoelastic and nonlinear parameters. International Journal of Pavement Engineering. 2019;20:490–498. https://doi.org/10.1080/10298436.2017.1309197

22. Ferregut C, et al. Artificial neural network-based methodologies for rational assessment of remaining life of existing pavements. University of Texas, El Paso; Texas Department of Transportation; Federal Highway Administration. 1999. 74 p.

23. Ceylan H, et al. Backcalculation of full-depth asphalt pavement layer moduli considering nonlinear stress-dependent subgrade behavior. International Journal of Pavement Engineering. 2005;6:171–182.

24. Abu-Lebdeh G, Ahmed K. A Neural Network Approach for Mechanistic Analysis of Jointed Concrete Pavement. Proceedings of the Eastern Asia Society for Transportation Studies. 2013. Vol. 9.

25. Ghanizadeh AR, Ahadi MR. Application of artificial neural networks for analysis of flexible pavements under static loading of standard axle. International Journal of Transportation Engineering. 2015;3:31–43. 10.22119/IJTE.2015.13361

26. Khalil AS, Starovoytov SV, Serpokrylov NS. The Adaptive Neuro-Fuzzy Inference System (ANFIS) Application for the Ammonium Removal from Aqueous Solution Predicting by Biochar. Materials Science Forum. 2018;931:985–990. 10.4028/www.scientific.net/MSF.931.985

27. Elshamy MMM, Tiraturyan AN. Using application of an artificial neural network system to backcalculate pavement elastic modulus. Scientific Herald of the Voronezh State University of Architecture & Civil Engineering. 2020;46:84–93.

Received 11.10.2021
Revised 29.10.2021
Accepted 01.11.2021

*About the Authors:*

**Mohamed Mostafa Mahmoud Elshamy**, PhD student of the Motorways Department, Don State Technical University (1, Gagarin sq., Rostov-on-Don, 344003, RF), assistant lecturer at the Faculty of Engineering, Al-Azhar University (11884, Arab Republic of Egypt/Egypt, Cairo, Nasr-City), Scopus, ORCID, mm.elshamy85@gmail.com

**Tiraturyan, Artem N.**, associate professor of the Motorways Department, Don State Technical University (1, Gagarin sq., Rostov-on-Don, 344003, RF), Dr.Sci. (Eng.), associate professor, Scopus, Researcher, ORCID, tiraturjan@list.ru

**Uglova**, **Evgeniya V.,** associate professor of the Motorways Department, Don State Technical University (1, Gagarin sq., Rostov-on-Don, 344003, RF), Dr.Sci. (Eng.), professor, Scopus, Researcher, ORCID, uglova.ev@yandex.ru

*Claimed contributorship*:

M. M. M. Elshamy: preparation of the text; preparation of the results and graphs; formulation of conclusions. A. N. Tiraturyan: a review of literature sources; calculations; computational analysis; analysis of the research results. E. V. Uglova: basic concept formulation; formulation of the research purpose and tasks; academic advising; text processing; correction of the conclusions.

*All authors have read and approved the final manuscript.*

# INFORMATION TECHNOLOGY, COMPUTER SCIENCE, AND MANAGEMENT

UDC 004.42 https://doi.org/10.23947/2687-1653-2021-21-4-376-383

## Software Module Development for the Parametric Generation of Truss Structure Geometry in a Two-Dimensional Setting

**S. G. Glushko**[1], **A. A. Lyapin**[1], **Yu. Yu. Shatilov**[1], **A. V. Cherpakov**[2], **R.K. Haldkar**[2,3]

[1]Don State Technical University (Rostov-on-Don, Russian Federation)
[2]Southern Federal University (Rostov-on-Don, Russian Federation)
[3]G H Raisoni College of Engineering (Nagpur, India)

✉ glsege98@gmail.com

***Introduction.*** Truss structures are widespread in construction due to a number of advantages, such as economy, versatility, and scalability. Accordingly, their modeling and calculation are urgent tasks in the design of building structures. Automatic solution to these problems causes an increase in design efficiency, calculation accuracy, and lower costs. The objective of the study is to examine the functionality and operation algorithm of the software module developed by the authors that generates the geometry of two-dimensional truss structures for subsequent modeling.

***Materials and Methods.*** Following the research of the widespread truss configurations, the classification of chords available in the software under consideration is given. The method of parameterizing a truss structure is provided. This method includes base geometric parameters of the structure such as dimensions, model construction rules, and additional features, as well as a comprehensive algorithm. The software is developed in JavaScript.

***Results.*** The software module has been integrated into a web application for calculating two-dimensional rod structures. To illustrate the functionality of the software, the examples of user interface are given as well as an example problem. The example includes configuration and calculation of an inclined truss structure. The results, such as support reactions and internal forces with axial force diagram, are provided.

***Discussion and Conclusions.*** Using this software module within the framework of the tool for calculating rod structures allows for the simplified process of modeling and calculating complex truss structures, design time, and resource reduction. The software module provides tools for specifying various types of structures, applying loads and assigning properties of a rod system, which makes it a useful instrument for design engineers.

***Keywords:*** engineering, design in construction, truss, parameterization, computing system, web development.

***For citation:*** S. G. Glushko, A. A. Lyapin, Yu. Yu. Shatilov, A. V. Cherpakov, R. K. Haldkar. Software Module Development for the Parametric Generation of Truss Structure Geometry in a Two-Dimensional Setting. Advanced Engineering Research, 2021, vol. 21, no. 4, pp. 376–383. https://doi.org/10.23947/2687-1653-2021-21-4-376-383

***Funding information:*** the research was carried out with the partial support of the Southern Federal University (grant VNGr-07 / 2020-04. IM Ministry of Education).

*Glushko S. G., Lyapin A. A., Shatilov Yu. Yu., Cherpakov A. V., Haldkar R. K., 2021*

**Introduction.** Truss structures are used in various building elements. Structural solutions of trusses are distinguished by a great variety, differing in the set of parameters for their use and optimization. In the world practice of using structures, there are more than 100 various systems differing primarily in the design of the rod interface. The basic typical structural element is a bar that has conjugate fastening with other elements at the nodes. These designs require certain approaches to the calculation and assessment of their reliability. In works [1–6], approaches to some calculation and experimental methods for assessing their reliability are highlighted. Some approaches and calculation schemes for assessing the reliability of defective structures as well as solving the problem of restoring the properties of their individual elements are covered in monographs [7–8].

Rod structures are systems consisting of linear rods connected at nodes. By the nature of the connection of elements in the nodes, systems with rigid nodes, hinged joints of all elements, and the combined ones are distinguished. From the geometric point of view, planar and spatial rod systems are distinguished.

Truss structures are a subcategory of rod systems that remain geometrically unchanged if rigid joints in nodes are replaced with hinged ones. The load is applied to truss structures only at the nodes, and only tensile-compressive forces arise in their elements [9, 10].

Truss structures are widespread as elements of buildings and structures. This popularity is due to a number of advantages [11].

Economy — lower material consumption compared to other building structures.

Versatility — the scope of application of trusses is very wide and includes bridges, roof truss systems, cranes, etc.

Scalability — truss length can vary from a few meters to several kilometers.

Due to these characteristics of trusses, their modeling and calculation are urgent tasks in the design of building structures. Automatic solution to these problems causes an increase in design efficiency and calculation accuracy and lower costs [12, 13].

The objective of the study is to examine the functionality and operation algorithm of a software module that generates the geometry of two-dimensional truss structures for subsequent modeling. This program module is a component of the SAPRUS service.

**Materials and Methods.** Since truss structures are panel structures, i.e., they consist of many sections (panels) identical or similar in geometry, it is possible to parametrically generate a model using the relative coordinates of the nodes when specifying the section. The parameters for such modeling are the total dimensions of the entire structure (height and span of the truss) and the number of sections used.

The functionality of the software module under consideration provides for the modeling of truss structures of 6 types of chords and their subtypes, depending on the lattice used (Figure 1).

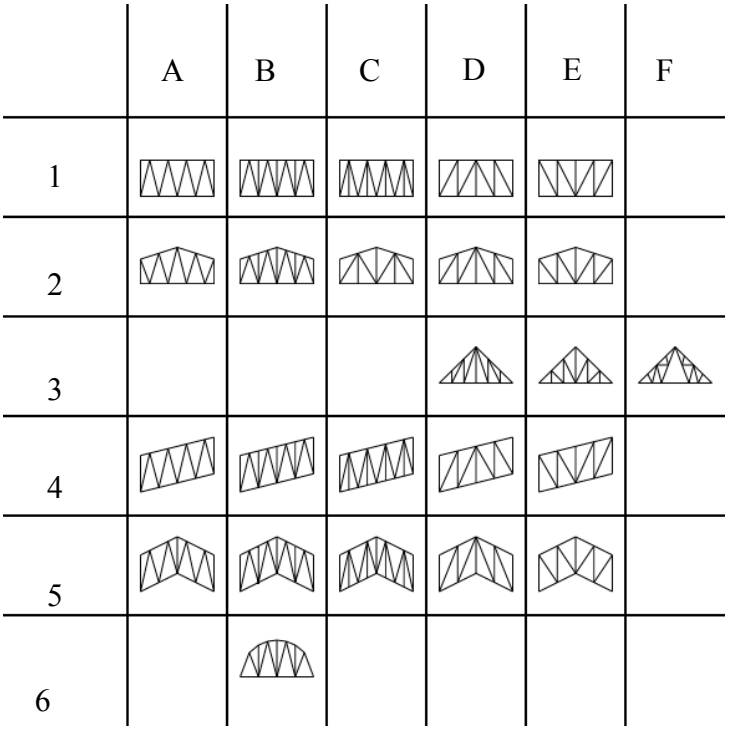


Fig. 1. Structural diagrams used in the module

Classification of the types of trusses used is the following [14, 15]:

1. rectangular with parallel chords;
2. trapezoidal;
3. triangular;
4. inclined with parallel chords;
5. inclined from both sides (arrow type);
6. polygonal.

Classification of the types of lattices used is the following:

A. triangular;
B. triangular with uprights;
C. triangular with suspensions;
D. upward diagonal brace;
E. downward diagonal brace;
F. with sub-trusses [16].

JavaScript was used as a programming language for the development of the module. In this regard, the module provides ample opportunities for the implementation of cloud computing of building structures in the web-based interface [17].

The software module is based on the object model, which is an array of objects describing each of the six types of structures. Length $l$ and height $h$ are used as parameters for all types of structures. For truss types 2, 4, 5, the height difference $dh$ is required. For each type of structure, an array of objects describing the geometry of its subtypes is given; it includes the position of nodes and bars, rules for constructing sections (parity, mirroring of structural halves, and usage of separators).

The algorithm of the software module generates, according to the specified parameters, an array of absolute coordinates of nodes of all truss rods. This data is sufficient to describe the model geometry. For a full-fledged definition of a structure model within the module, the following additional features are provided:

— supports;
— hinges;
— offset of the left node relative to the origin of coordinates on the scheme;
— loads on the upper structural nodes;
— element grouping for the convenience of subsequent processing.

The module operation algorithm is the following:

1. Calculation of nodal coordinates for the outer vertical bars of the structure if they exist for the selected structure type.
2. Calculation of the width of individual sections and the coordinates of the nodes of the central support bar of truss type 5.
3. Sequential calculation of nodal coordinates of each section and the formation of rod array.
4. Calculation of the coordinates of nodes for additional vertical bars between sections, if necessary, for the selected subtype of the structure.
5. Preliminary visualization of the structure diagram inside the module.
6. Assignment of the additional properties.
7. Data transfer for design and calculation.

After the data has been transferred, the array has to be further processed to add generated elements to the existing collections. Depending on the specific requirements of the wrapper application, this process can be vastly different. The flowchart of the algorithm used in SAPRUS service is shown in Figure 2.

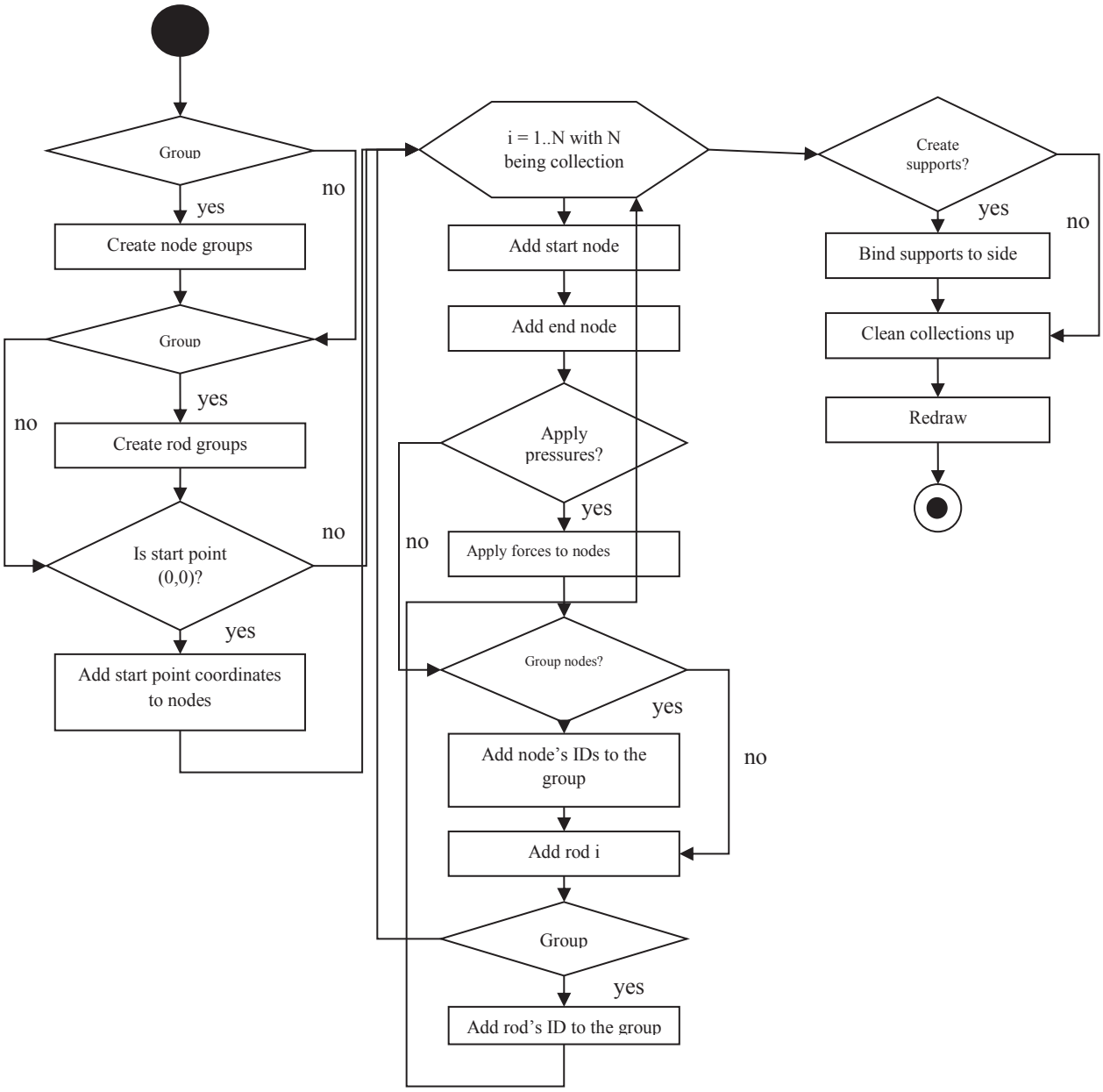


Fig. 2. Post-processing flowchart

As a result, 2 collections are created: *CollectionNodes* and *CollectionRods*. The data stored in these collections is suitable for further manipulation and calculations.

**Results**. When the module is integrated into a web application for calculating two-dimensional rod structures, the choice of the type and subtype of the scheme occurs in the graphical user interface. To enter truss dimensions as well as additional parameters, fields and switches are used. If the type of truss and parameters are changed, the preliminary design scheme is rebuilt automatically.

To illustrate the role of the module within the framework of a web application, we will demonstrate the design and calculation of an inclined structure 20 *m* long, 10 *m* high with 3 *m* offset and consisting of 5 sections (panels). In the nodes of the upper chord of this structure, concentrated forces of 5 *kN* are applied vertically, for the left and right-most nodes, this force is reduced by 50 % automatically with the Point Load Factor option. The module interface and the result structure diagram are shown in Figure 3. The structure is calculated with the finite element method [18, 19]. The resulting diagram of axial forces is shown in Figure 4.

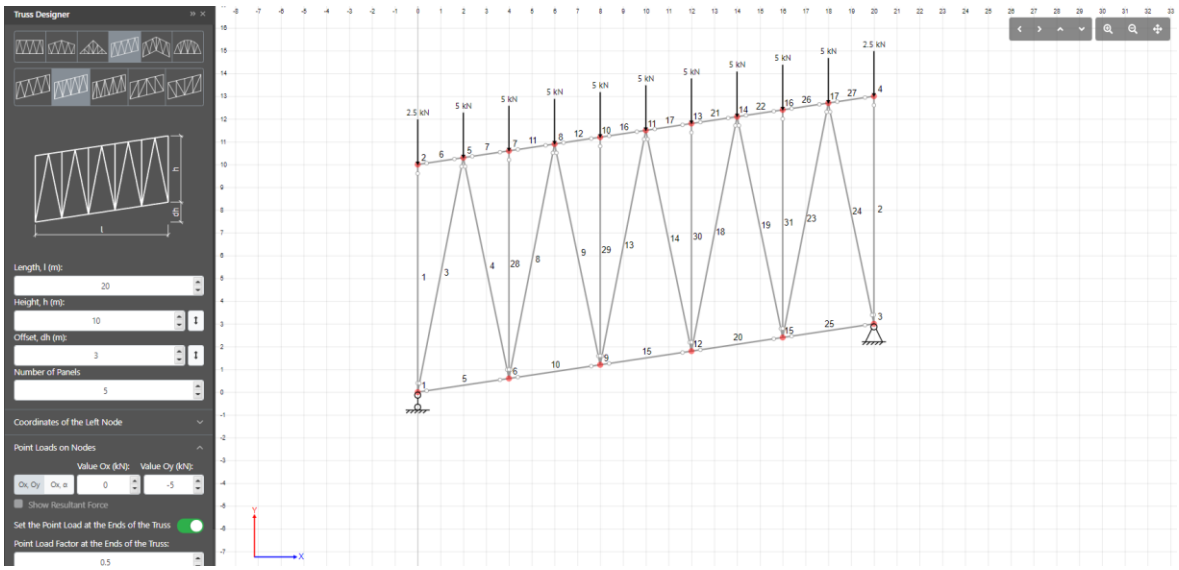


Fig. 3. Configuration window and visualization of the structure diagram

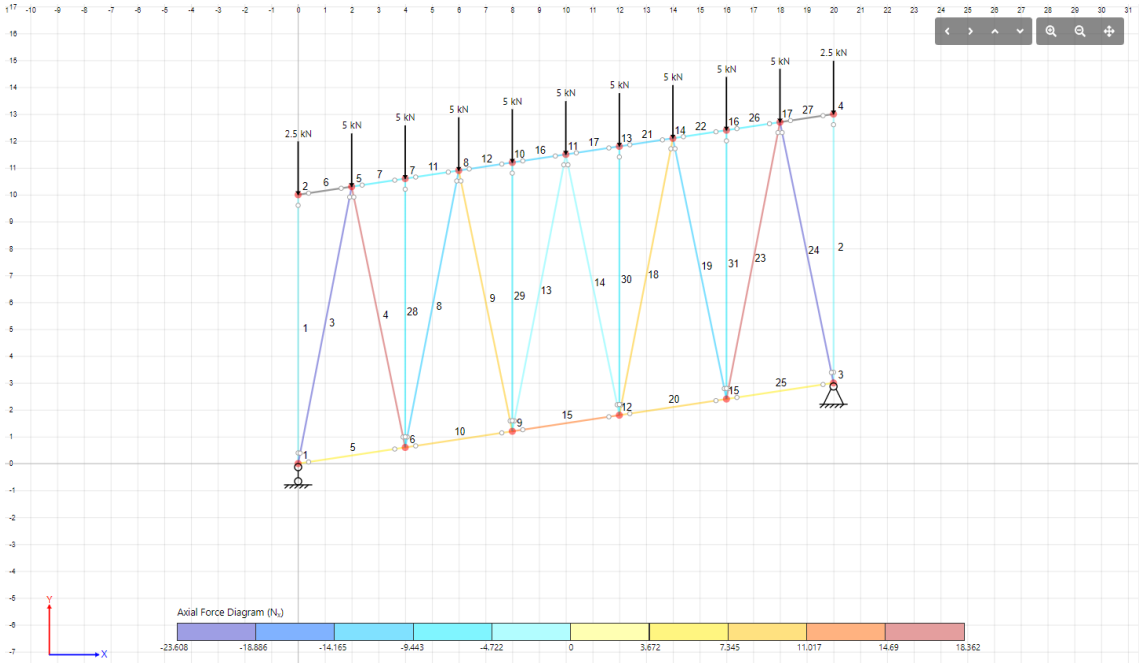


Fig. 4. Axial force diagram

The values of support reactions and internal forces of the calculated structure are presented in Tables 1 and 2, respectively. In Table 1, *R* is the vertical component of the support reaction, *H* is the horizontal component of the support reaction, *M* is the bending moment.

Table 1

Support reactions

| Node # | Support type | Values |
|---|---|---|
| 1 | Pinned hinged support | R1 = 25 (kN), H1 = 0 (kN), M1 = 0 (kN·m) |
| 18 | Fixed hinged support | R3 = 25 (kN), H3 = 0 (kN), M3 = 0 (kN·m) |

http://vestnik-donstu.ru

Table 2

Internal forces

| Rod # | \|Q, max\| (kN) | \|N, max\| (kN) | \|M, max\| (kN·m) |
|---|---|---|---|
| 1 | 0 | 2.5 | 0 |
| 2 | 0 | 2.5 | 0 |
| 3 | 0 | 23.608 | 0 |
| 4 | 0 | 17.332 | 0 |
| 5 | 0 | 4.55 | 0 |
| 6 | 0 | 0 | 0 |
| 7 | 0 | 8.089 | 0 |
| 8 | 0 | 13.115 | 0 |
| 9 | 0 | 7.428 | 0 |
| 10 | 0 | 10.617 | 0 |
| 11 | 0 | 8.089 | 0 |
| 12 | 0 | 12.134 | 0 |
| 13 | 0 | 2.623 | 0 |
| 14 | 0 | 2.476 | 0 |
| 15 | 0 | 12.64 | 0 |
| 16 | 0 | 12.134 | 0 |
| 17 | 0 | 12.134 | 0 |
| 18 | 0 | 7.869 | 0 |
| 19 | 0 | 12.38 | 0 |
| 20 | 0 | 10.617 | 0 |
| 21 | 0 | 12.134 | 0 |
| 22 | 0 | 8.089 | 0 |
| 23 | 0 | 18.362 | 0 |
| 24 | 0 | 22.284 | 0 |
| 25 | 0 | 4.55 | 0 |
| 26 | 0 | 8.089 | 0 |
| 27 | 0 | 0 | 0 |
| 28 | 0 | 5 | 0 |
| 29 | 0 | 5 | 0 |
| 30 | 0 | 5 | 0 |
| 31 | 0 | 5 | 0 |

**Discussion and Conclusions.** Using this software module within the framework of the tool for calculating rod structures allows for the simplified process of modeling and calculating complex truss structures, design time, and resource reduction. The software module provides tools for specifying various types of structures, applying loads and assigning properties of a rod system, which makes it a useful instrument for design engineers.

**References**

1. Berger M, Tusnin A. Stress redistribution in flat damaged trusses. E3S Web of Conferences. 2019;97:04033. https://doi.org/10.1051/e3sconf/20199704033

2. Rojíček J, Paška Z, Fusek M, et al. Optimization of a Truss Structure Used to Design of the Manipulator Arm from a Set of Components. Applied Sciences. 2021;11:10193. https://doi.org/10.3390/app112110193

3. Shatilov YY, Lyapin AA. Vibration-based damage detection techniques for health monitoring of construction of a multi-storey building. Materials Science Forum. 2018;931:178–183. https://doi.org/10.4028/www.scientific.net/MSF.931.178

4. Lyapin A, Shatilov Yu. Assessment of building structure using data from dynamic monitoring. IOP Conference Series: Materials Science and Engineering. 2018;365:052031. https://doi.org/10.1088/1757-899X/365/5/052031

5. Soloviev AN, Parinov IA, Cherpakov AV, et al. Experimental vibration diagnostics of the floor plate set of building construction. Lecture Notes in Mechanical Engineering. 2021. P. 255–260. https://doi.org/10.1007/978-3-030-69610-8_35

6. Soloviev AN, Parinov IA, Cherpakov AV, et al. Analysis of oscillation forms at defect identification in node of truss based on finite element modeling. Materials Physics and Mechanics. 2018;37:192-197. https://doi.org/10.18720/MPM.3722018_12

7. Lyapin AA, Parinov IA, Buravchuk NI, et al. Improving road pavement characteristics. Applications of industrial waste and finite element modelling. Springer Cham; 2021. 236 p. https://doi.org/10.1007/978-3-030-59230-1

8. Shevtsov SN, Soloviev AN, Parinov IA, et al. Piezoelectric actuators and generators for energy harvesting: Research and Development. Springer Cham; 2018. 182 p. https://doi.org/10.1007/978-3-319-75629-5

9. Smirnov VA, Gorodetsky AS. Tekhnicheskaya mekhanika. Moscow: Yurait; 2013. 423 p. (In Russ.)

10. Bakošová A, Krmela J, Handrik M. Computing of truss structure using MATLAB. Manufacturing Technology. 2020;20:279–285. https://doi.org/10.21062/mft.2020.059

11. Kopytov MM, Plyaskin AS. Prostranstvennye sterzhnevye konstrukcii pokrytij. Tomsk: TSUAB; 2019. 104 p. (In Russ.)

12. Vasilkin A. Mathematical and computer modeling in the design of steel rod structures. Journal of Physics: Conference Series. 2019;1425:012172. https://doi.org/10.1088/1742-6596/1425/1/012172

13. Fedorov SS. Principles of creation of models and technologies of high-quality designing of construction objects. Building and Reconstruction. 2018;80:94-101. (In Russ.)

14. Faibishenko VK. Metallicheskie konstruktsii. Moscow: Stroiizdat;1984. 336. (In Russ.)

15. Kirsanov MN. The choice of a lattice for the frame farm. Structural Mechanics of Engineering Constructions and Buildings. — 2017, 3: — P. 23–27. (In Russ.)

16. Kirsanov MN, Gavrilenko AB. Analytical evaluation of stiffness of the truss. Building and reconstruction. 2018;76:12–17. (In Russ.)

17. David Flanagan. JavaScript: The Definitive Guide, 7th ed. O'Reilly Media; 2020. 706 p.

18. Klaus-Jurgen Bathe. Finite Element Procedures, 2nd ed. Watertown, MA: K.J. Bathe; 2014. 1035 p.

19. Seshu P. Textbook of Finite Element Analysis, 10th edition. New Delhi: PHI Learning Private Limited; 2012. 330 p.

Received 01.11.2021
Revised 18.11.2021
Accepted 19.11.2021

*About the Authors:*

**Glushko, Sergey G.**, postgraduate student of the Information Systems in Construction Department, Don State Technical University (1, Gagarin Sq., Rostov-on-Don, 344003, RF), ORCID, glsege98@gmail.com

**Lyapin, Alexander A.**, professor of the Information Systems in Construction Department, Don State Technical University (1, Gagarin Sq., Rostov-on-Don, 344003, RF), Dr.Sci. (Eng.), professor, Scopus, Researcher, ORCID, lyapin.rnd@yandex.ru

**Shatilov, Yuri Yu.**, associate professor of the Information Systems in Construction Department, Don State Technical University (1, Gagarin Sq., Rostov-on-Don, 344003, RF), Cand.Sci. (Eng.), associate professor, Scopus, Researcher, art-web@mail.ru

**Cherpakov, Alexander V.**, Senior Research Scholar, Vorovich Research Institute for Mathematics, Mechanics, and Computer Science, Southern Federal University (8a, Milchakova St., Rostov-on-Don, 344090, RF), Cand.Sci. (Eng.), Scopus, Researcher, ORCID, alex837@yandex.ru

**Haldkar Rakesh K.,** Leading Researcher, Vorovich Research Institute for Mathematics, Mechanics, and Computer Science, Southern Federal University (8a, Milchakova St., Rostov-on-Don, 344090, RF), G H Raisoni College of Engineering, Nagpur, India (Eng.), Scopus, Researcher, ORCID, rakeshhaldkar@gmail.com

*Claimed contributorship:*

S. G. Glushko: modeling and development; text preparation; formulation of conclusions. A. A. Lyapin: academic advising; research objectives and tasks setting; the text revision. Yu. Yu. Shatilov: concept formulation; research objectives and tasks setting. A. V. Cherpakov: text preparation; formulation of conclusions; search for scientific literature. R. K. Haldkar: text preparation; formulation of conclusions; search for scientific literature.

*All authors have read and approved the final manuscript.*